Study on the Mechanism of Vapor Film Collapse in Film Boiling around a Vertical Finite-Length Cylinder

September, 2018

Department of Mechanical System Engineering
Graduate School of Engineering
Nagasaki University

Win Pa Pa Myo

Contents

Abstract

Saturated and subcooled film boiling heat transfer around a vertical finite-length cylinder has been investigated analytically to predict the local heat transfer coefficients at the bottom surface and vertical lateral surface with smooth vapor-liquid interface. Correlations of heat transfer for the vertical finite length cylinder with top and bottom horizontal surface has been already analyzed by Momoki et al.(2007) and this correlations equations for heat transfer are in good agreement with the experimental data in prediction the average heat transfer rate of the cylinders in saturated and subcooled water. In the present study, experimental observation results on vapor film collapse start from the lower corner of the silver vertical finite-length cylinder is focused to discuss with the local heat transfer characteristic and we would like to applied this correlations to estimate the local and average heat transfer rate at the corner of the horizontal bottom and vertical lateral surfaces of the cylinder. However, these correlations on local heat transfer rate at the end of the bottom surface gives infinite value and its cannot apply in discussion of film collapse start. So, to examine the local heat transfer characteristic at the corner of the bottom surface and vertical lateral surface, Shigechi et al.(1999) analysis for film boiling heat transfer on horizontal bottom surface was modified in order to get finite vapor film thickness at the end of the bottom surface to predict finite value of local heat transfer coefficient at this end. In this modification, the vapor film thickness at the end of the bottom surface can be predicted to estimate the local heat transfer rate and the prediction of the average heat transfer rate are in good agreement with the results of the previous method. Moreover, the local heat transfer coefficient at the end of the bottom surface can be predicted and discussed local heat transfer characteristic at the edge of the vertical cylinder.

The local heat transfer rate through the bottom surface and vertical lateral surface are described in terms of local Nusselt number with degree of superheat and by applying average heat transfer rate through on each surface of the cylinder, total heat transfer rate of the cylinder can be predicted and its match well with the experimental total heat transfer rate with $\pm 15\%$ .The results on local heat transfer coefficient shows the highest value at the corner of the bottom surface and vertical lateral surface and it can be confirmed the experimental results of the vapor film collapse start at the corner of silver vertical cylinder on saturated film boiling.

In order to predict and investigate the local heat transfer performance on the horizontal bottom and vertical lateral surfaces in subcooled film boiling, we apply the average heat transfer enhancement factor by the liquid subcooling to the estimated local values by the methods for saturated film boiling on each surfaces. Local heat transfer rate at the lower

end of the vertical lateral surface are found higher than any other area of the cylinder surface in subcooled film boiling and it suggests the lowest temperature at that corner to be film collapse start. Furthermore, the temperature field inside the vertical cylinder is treated as the two dimensional unsteady heat conduction problem and the boundary condition at the cylinder surfaces are given as the local heat transfer coefficient at the bottom surface and vertical lateral surface with smooth vapor-liquid interface. It was also found that the lowest temperature point is at the corner of the bottom surface and vertical lateral surface and it agrees with the vapor film collapse start at the lower corner of the vertical silver cylinder on saturated and subcooled film boiling.

List of Symbol

A	: Total heating surface of the cylinder [m^2]
$A_{r_{\text{in}}}$	: Inside wall area of the element [m^2]
$A_{r_{\text{out}}}$	: Outside wall area of the element [m^2]
A_z	: Top or bottom surface area of the element [m^2]
Bi	: Biot number [-]
c	: Specific heat of the cylinder [m^2]
$c_{A1,2,3,..}$	: Coefficient for slip and non-slip condition [-]
c_p	: Specific heat of water at constant pressure [J/(kg·K)]
$-dT/d\tau$	: Cooling rate [K/s]
D	: Diameter of the cylinder [m]
F_{A_1}	: Dimensionless parameter
F_{A_2}	: Dimensionless parameter
g	: Gravity accelaration [m/s^2]
Gr	: Grashof number [-]
h	: Local heat transfer coefficient [W/(m^2·K)]
H	: Height of cylinder [m]
J	: Dimensionless parameter [-]
J_0	: Non-dimensionless parameter for saturated liquid [-]
J_{A}	: Dimensionless parameter
J_{A_0}	: Dimensionless parameter for saturated liquid J_{A}
J_{B}	: Dimensionless parameter
J_{B_0}	: Dimensionless parameter for saturated liquid for vertical surface J_{B}
k	: Thermal conductivity [W/(m·K)]
ℓ	: Latent heat [J/kg]
L_{B_1}	: Vertical length for smooth vapor-liquid interface [m]
L_{B_2}	: Vertical length for wavy vapor-liquid interface [m]
$\dot{m}$	: Mass flowrate per unit circumference [kg/m·s]
$\dot{M}$	: Mass flowrate [kg/s]
Nu	: Nusselt number [-]
Pr	: Prandtl number [-]
q	: Average wall heat flux [kW/m^2]
Q	: Heat transfer rate [W]
r	: Radial position [-]
R	: Radius of cylinder [m]

r^* : r-R [-]

S : Total heat transfer area of the cylinder [m^2]

Sc : Dimensionless degree of liquid subcooling [-]

Sp : Dimensionless degree of superheating [-]

Sp^* : Modified dimensionless degree of superheating [-]

T : Temperature [°C]

T_{sat} : Saturated temperature [°C]

T_{w} : Wall temperature [°C]

T_{∞} : Bulk temperature [°C]

ΔT_{min} : Degree of superheating at lower limit of film boiling [K]

ΔT_{sat} : Degree of superheating($= T - T_{\mathrm{sat}}$) [K]

ΔT_{sub} : Degree of subcooling($= T_{\mathrm{sat}} - T_{\infty}$) [K]

u : Fluid velocity [m/s]

V : Volume of the cylinder [m^3]

w : Density ratio [-]

x : Vertical position along the vertical surface [mm]

y : Position normal to the bottom surface [mm]

α : Volumetric thermal expansion coefficient [1/K]

β : Dimensionless parameter [-]

δ : Vapor film thickness [m]

Δr : Radial length of the element [m]

Δz : Width of the element [m]

λ : Vapor-film unit length [m]

λ_0 : Capillary length [m]

λ_{cr} : Critical wave length [m]

μ : Dynamic viscosity [Pa·s]

ν : Kinematic viscosity [m^2/s]

ρ : Density [kg/m^3]

σ : Surface tension [N/m]

τ : Times [sec]

Φ : Dimensionless parameter [-]

Superscripts

- : Average value

$\sim$: Dimensionless

Subscripts

A : Downward facing bottom surface

B : Vertical lateral surface

B_1 : Vertical lateral surface with smooth vapor-liquid interface

B_2 : Vertical lateral surface with wavy vapor-liquid interface

C : Upward facing horizontal surface

col : Vapor film collapse point

L : Liquid at film temperature

LS : Saturated water

V : Vapor at film temperature

VS : Saturated steam

min : Lower limit of film boiling

sat : Saturated

sub : Subcooled

∞ : Bulk liquid

Chapter 1

Introduction

1.1 Film Boiling Heat Transfer

Boiling heat transfer is defined as a mode of heat transfer that occurs with a change in phase from liquid to vapor. Film boiling is the one of the several boiling regimes in pool boiling as well as in flow boiling in which the heating surface is covered by a stable vapor film formed by uniformed surface temperature and the heat transfer rate reaches a minimum. Figure 1.1 shows pool boiling regimes of A-B, natural convection; B-C, nucleate boiling; C-D, partial film boiling; D-E, stable film boiling. Film boiling regime is generally

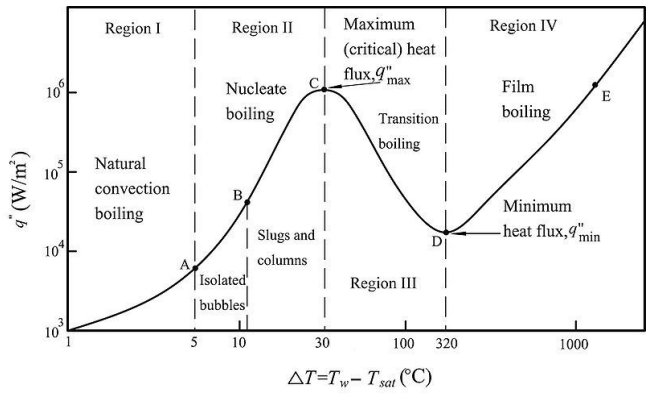

Fig. 1.1: Boiling curve

characterized during the heating or cooling process when the object is completely covered with the vapor film which leads to low heat transfer rate than others regimes. Film boiling occurs in cooling process of high temperature body such as metal quenching in manufacturing process of material, emergency core cooling of nuclear reactor and during normal operation in boiler tubes, and so on. However, the mechanism of transient film boiling heat transfer are complicated due to thermal and hydrodynamic behaviors of the

vapor and configuration of the heating surface during film boiling regime. Ther are so many research on film boiling heat transfer to investigate the minimum heat flux condition, lower limit of film boiling, film boiling heat transfer , film collapse phenomena.

Correlation of film boiling heat transfer from the single surface such as a vertical surface, a horizontal cylinder, a sphere and upward facing horizontal surface have been carried out and a lot of practical correlation of film boiling heat transfer coefficient have been proposed for the saturated and subcooled film boiling. There exist discrepancy in estimation the characteristics of the film boiling such as heat transfer coefficient, heat flux and lower limit of film boiling till now.

In our laboratory, film boiling heat transfer is studied by doing quenching experiment with the vertical cylinders with different materials and different configuration. The analysis concern with the lower limit of film boiling, average and local heat transfer performance of the cylinder, collapse mechanism of the film boiling.

Previous research on film boiling heat transfer concerned with the cooling rate of the three dimensional bodies and focus on the average heat transfer rate and the wall superheat at the lower limit of film boiling of a vertical finite-length cylinders were determined experimentally by quenching method for saturated and subcooled water at atmospheric pressure. Later, vapor film collapse mechanism or film collapse mode or stability of vapor film are area of interest in film boiling heat transfer for the safety in the cooling process of high temperature bodies. There are many experimental and theoretical studies on the film collapse mechanism or vapor film collapse behaviour on the high temperature surfaces or bodies.

1.2 Background of the Research

Since 1989, film boiling heat transfer from a horizontal circular plate facing downward have been studied by Shigechi *et al.* in our laboratory [28]. The two-dimensional, steady-state, laminar boiling heat transfer from a horizontal circular plate facing downward to a sagnant saturated liquid is studied theoretically based on that the flow of vapor beneath the circular plate is induced by the hydrostatic pressure gradient due to the change in the vapor film thickness. At 1998, a finite-size horizontal plate facing downward to a saturated liquid was analyzed with the same assuming and the resulting boundary-layer equations for the vapor flow were solved by an integral method, by taking into account the effect of the plate edge [29]. For the heat transfer on the vertical lateral surface, Bromley's solution was modified to accommodate the continuity of vapor mass flowrate around the lower corner of the vertical cylinder and the effect of horizontal bottom surface on film boiling heat transfer from a vertical cylinder is studied by Shigechi et al. [30]. In actual application, the subcooled fluid is used in cooling process, subcooled film boiling heat transfer has been studied by Momoki et al.(1995) on efect of subcooling on the film boiling heat transfer from a finite-size horizontal plate facing downward[11]. Film boiling heat transfer around a three-dimensional bodies have been studied by Shigechi *et al.* in effect of horizontal bottom surface on film boiling heat transfer from a vertical finite-length cylinder. For the vertical finite-length cylinders with different aspect ratio (L/D), film boilng heat transfer have been correlated and predicted the heat transfer rate of the cylinder in terms of boiling curve, cooling curve, cooling rate and compared with the experiment. Aspect ratio (Length to Diameter) on lower limit of film boiling for saturated water was discussed for the vertical finite-length cylinder[11].

Study of film boiling around a three-dimensional body has been analyzed by Shigechi *et al.*(1999) based on the Bromley's solution for a vertical surface to accommodate the continuity of vapor mass flow rate around the lower corner of the vertical cylinder. To predict the cooling rate of the vertical cylinder in the film boiling region, Momoki *et al.*(2003) established the correlation for the heat transfer from the surfaces of the cylinder. In this correlations, average heat transfer rate from the bottom and lower vertical surface is correlated by applying Shigechi analysis and for the vertical surface with wavy interface, heat transfer correlation for natural-convection film boiling with a wavy interface focused by Nishio and Ohtake (1992) was applied. An analytical expression for the film boiling heat transfer coefficient from a horizontal surface was derived by the Berenson (1961) and which is applied in correlation of heat transfer on the upper surface of the vertical cylinder. In 2004, Yamada *et al.* have reported a correlation of convective heat transfer for the saturated film boiling around a finite-length vertical silver cylinder, which can

correlate the experimental data within ± 20% for 18 kinds of silver cylinder.

Above mention research on pool film boiling are on saturated liquid and in actual application, to enhance cooling rate of the heating object, the liquid which is used in cooling process are subcooled condition, i.e., its temperature is lower than saturated temperature of liquid. Therefore, subcooled film boiling plays practical significance in quenching techniques. A theoretical study of subcooled film boiling on horizontal cylinders were analyzed by Nishikawa and Ito (1975). Hamill and Baumeister (1967), theoretically analyzed effect of subcooling and radiation on film boiling heat transfer from a horizontal plate. Most experimental studies on film boiling heat transfer focus on the effect of subcooling for the degree of superheat with a variety of fluid and proposed semi-empirical correlation to predict film boiling heat transfer rate. Further, Momoki *et al.*(2007) proposed the correlations of heat transfer for saturated and subcooled film boiling and these correlation equations for heat transfer and lower limit of film boiling are in good agreement with the experimental data.

Furthermore, experimental study on effect of the material thermophysical properties upon quench point in transient film boiling around a vertical cylinder have been studied with the five kinds of metal cylinder, silver, aluminum, carbonsteel (S35C and S45C), and stainless steel. This one is the initial investigation of the film collapse mechanism of the vertical cylinder, its state that the start times of the vapor film collapse based on the visual observation are about some seconds behind the time at the minimun point of the cooling rate and the collapse of the vapor film occurs at the lower corner of the silver and aluminum cylinders of high thermal conducitvity and at the upper corner of low thermal conducitivy materials such as carbon and stainless steels on saturated film boiling [10].

Most of the previous research on film boiling heat transfer of our laboratory target upon the cooling rate of the three-dimensional bodies and the lower limit of film boiling of the different materials and configuration of the vertical finite-length cylinders are experimentally determined to focus on minimum heat flux.

Later, more investigation on vapor film collapse is done with the higher speed video camera and detail examination on cooling rate near the lower limit of film boiling and observation of numbers and position of solid liquid contacts were reported as the confirmation of film collapse start point [6], [16].

1.3 Aims and Objectives

The aims of the research is to study the vapor film collapse phenomena and the local heat transfer performance during film boiling.

The objectives of the research are

(1) to investigate the film collapse behaviours around the vertical finite-length cylinder in saturated and subcooled film boiling.

(2) to predict heat transfer rate near the region of the vapor film collapse start.

(3) to predict the local heat transfer rate near the lower limit of film boiling in saturated and subcooled film boiling.

(4) to predict the surface temperature distribution of the vertical finite-length cylinder during film boiling.

(5) to discuss the local surface temperature different with the location of vapor film collapse start.

Chapter 2

Correlations of Local Heat Transfer Coefficient

2.1 Film Boiling Models

The previous authors on film boiling heat transfer have been already analyzed the film boiling around a three-dimensional body with horizontal surface such as a vertically placed cylinders. Based on the laminar film boiling heat transfer performance from a downward-facing horizontal surface, the effect of the vapor-mass flow on the film boiling heat transfer of the vertical lateral surface, the film boiling model is proposed for a vertical finite-length cylinder of diameter D and height H. The physical model for film boiling heat transfer for saturated and subcooled film boiling are shown in Fig. 2.1 (a) and (b) for the correlation of heat transfer coefficient on each regimes of the surfaces. Although vertical cylinder has three heat transfer surfaces such as downward facing horizontal surface (A), vertical surface (B) and upward facing horizontal surface (C), in consideration heat transfer regimes, vertical lateral surface is divided into two regimes as vertical lateral surface with smooth and wavy vapor liquid interface based on observation of vapor-liquid interface in experiment. From the lower end of the vertical surface to the length (L_{B1}), the vapor-liquid

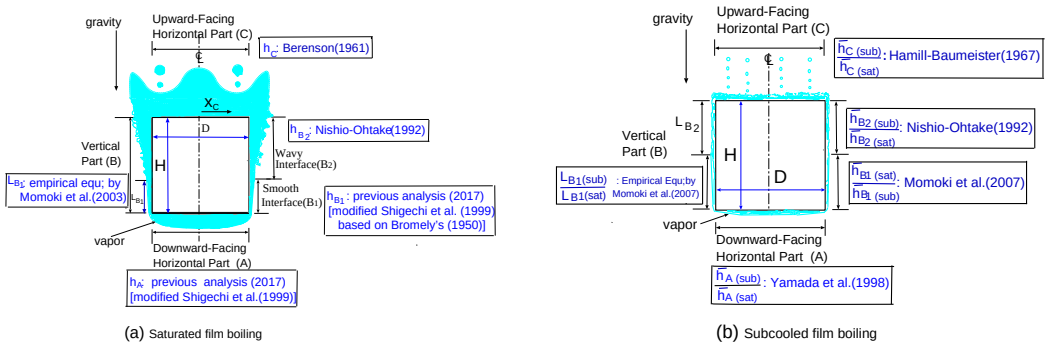

Fig. 2.1: Physical model for film boiling

interface is smooth and to be considered as laminar (B_1) and beyond this regime, the vapor-liquid interface is wavy and to be considered as turbulent (B_2). In subcooled film boiling, the length of the smooth vapor-liquid interface increased as increased in degree of liquid subcooling. The value of L_{B1} is calculated by the empirical equation based on the critical wave length [11] . Individual correlation which are applied to predict heat transfer rate on each regimes of the vertical cylinder are described in Fig. 2.1 (a) for saturated film boiling and Fig. 2.1 (b) for subcooled film boiling.

2.2 Saturated Film Boiling

Saturated film boiling heat transfer around a vertical-finite-length cylinder has been investigated analytically to predict the local heat transfer coefficients on horizontal bottom surface and vertical lateral surface with smooth vapor liquid interface. Correltions of heat transfer for the vertical cylinder with top and bottom horizontal surface has been already analyzed by Momoki et al. (2007) and this correlations equations for heat transfer are in good agreement with the experimental data for the cylinders in saturated water. In present study, this correlations are applied to estimate the local and average heat transfer rate through each surfaces of the cylinder. To predict the local heat transfer coefficient at the corner of the bottom surface and vertical lateral surface, Shigechi et al. (1999) analysis for film boiling heat transfer on horizontal bottom surface was modified in order to get finite vapor film thickness at the end of the bottom surface to predict finite value of local heat transfer coefficient at this end.

2.2.1 Prediction of heat transfer coefficient on horizontal bottom surface

The two-dimensional, steady-state, laminar film boiling heat transfer from the downward-facing horizontal plate of a finite size was already analyzed by Shigechi et al.(1989) by assuming that the flow of vapor beneath the heated plate of finite size was driven by a hydrostatic pressure gradient due to change in the thickness of vapor film. The resulting boundary-layer equations for the vapor flow were solved by an integral method, taking into account the effect of the plate edge and contribution of the radiation heat transfer. In 1999, Shigechi et al. examined the effect of the heat transfer rate on the vertical laterical surface of the three-dimensional body with horizontal bottom surface such as a vertically placed cylinder due to film boiling under the bottom surface. As the vapor produced beneath the horizontal bottom surface and results in thickening the vapor film that coats the vertical lateral surface of the body. In this work, for the heat transfer on the vertical lateral surface, Bromley's solution was modified to accomodate the continuity of vapor

mass flowrate around the corner of the vertical cylinder and the effect of vapor mass flow generated under the downward-facing horizontal surface is to decrease the film boiling heat transfer rate that would have been produced by the vertical lateral surface in the absence of the downward-facing horizontal surface [30].

However, in solving the boundary layer equations for the vapor at the bottom surface by an integral method, the resulting second order boundary value problem was solved by analytically by giving the boundary condition at r=R (which is at the end of the bottom surface, the radius R), the gradient of the vapor film thickness is -∞. In this analytical solution, the amount of heat transfer rate near the end of the bottom surface become infinity as the film thickness approach to zero at this point and the local value of heat transfer coefficient at that corner gives infinity value. Moreover, experimental study on film boiling heat transfer shows that the film collapse start from the lower corner of the vertical finite-length cylinder and the lower corner of the cylinder is the area of interest as the high heat transfer region. However, infinity value of heat transfer coefficient cannot be applied in analysing the heat transfer performance of the vertical cylinder. In order to eliminate such inconvenience to apply in prediction of local heat transfer coefficient, we modified the position of the boundary condition to be the value of local heat transfer coefficient at lower corner of the vertical cylinder finite. The following section described about the modification on the position of the boundary condition on horizontal bottom surface of the vertical finite-length cylinder.

2.2.2 Modification on the position of the boundary condition on horizontal bottom surface to predict local heat transfer coefficient at the corner

In order to predict local heat transfer coefficient at the horizontal bottom surface and vertical lateral surface with smooth vapor liquid interface, we modified the position of the boundary condition on orginal physical model and coordinate system for downward facing horizontal surface, as shown in Fig. 2.2. The following assuming are considered as

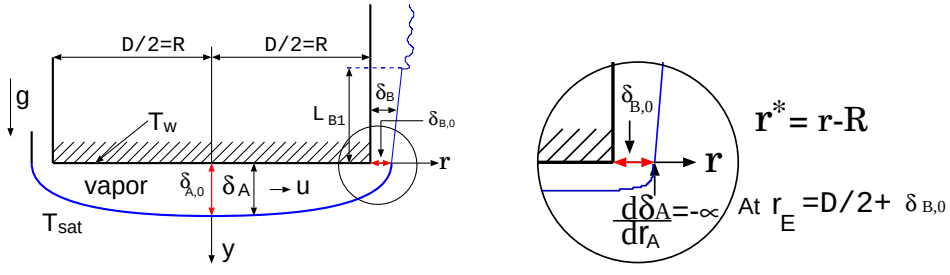

Fig. 2.2: Physical model and coordinate system for downward facing horizontal surface

previously as, two-dimensional, steady state, film boiling heat transfer from a downward facing horizontal surface with a width of D at a uniform temperature T_w to a stagnant saturated liquid at temperature T_s, the surface is covered with a stable vapor film having a maximum thickness at the center. The common assumings are also adopted as

1. The vapor film beneath the surface is treated as a laminar boundary-layer with a smooth vapor-liquid interface.

2. The effect of surface tension can be neglected and the saturation temperature of the liquid is constant.

3. Physical properties are constant.

4. Radiation heat transfer is neglectd.

So in this prediction, it was assumed that the bottom surface of the cylinder is extended to some amount of heated surface that is equal to the film thickness at the lower end of the vertical surface and the boundary condition is changed to this virtual end as the gradient of the film thickness is minus infinity at the radius $r_{\mathrm{E}} = \mathrm{D}/2 + \delta_{B,0}$. The physical model and coordinate system (r,y) are shown in Fig. 2.2 to clarify the modification.

For the horizontal bottom surface, the conservation of momentum and energy equations in y-direction for the vapor are obtained as by neglecting the inertia and convective terms,

$$-\left(\rho_{\mathrm{L}} - \rho_{\mathrm{v}}\right)\ g\frac{d\delta_A}{dr} + \mu_{\mathrm{v}}\frac{\partial^2 u}{\partial y^2} = 0 \tag{2.1}$$

$$\lambda_V \frac{\partial^2 T}{\partial y^2} = 0 \tag{2.2}$$

The boundary conditions are given at the cylinder wall, At y=0;

$$T = T_{\mathrm{W}} \colon u = 0 \tag{2.3}$$

and at the vapor-liquid interface, y=δ_A;

$$T = T_{\mathrm{sat}} \tag{2.4}$$

The velocity profile is considered as the non-slip condition at the vapor-liquid interface corresponding to Case (A-ns) and the slip condition at the vapor-liquid interface corresponding to Case (A-s). For the Case (A-ns), u =0 and for the Case (A-s), $\frac{\partial u}{\partial y} = 0$. There is one more boundary condition at the vapor-liquid interface as the rate of heat conduction through the vapor film to the interface is balanced to the rate of latent heat of vaporization and it can be expressed as :

$$-\lambda_V \frac{\partial T}{\partial y}|_{\delta_A} = \ell \frac{1}{r}\frac{d}{dr}\left[\ \int_0^{\delta_A} r\rho_{\mathrm{v}} u dy\right] \tag{2.5}$$

Solving the momentum equation, Eq.(2.1), together with the velocity boundary conditions, the equation for the velocity profile can be obtained as :

$$u = -\frac{1}{2}\left[\frac{(\rho_{\rm L}-\rho_{\rm v})\ g}{\mu_{\rm v}}{\delta_A}^2\frac{d\delta_A}{dr}\right]\ \left[c_{\rm A1}\left(\frac{y}{\delta_A}\right)\ -\left(\frac{y}{\delta_A}\right)^2\right] \tag{2.6}$$

where the numerical values of coefficient c_{A1} depends upon the boundary condition at the vapor liquid interface and for Case (A-ns), the value c_{A1} is 1 and for Case (A-s), the value of c_{A1} is 2. Also, solving energy equation of Eq.(2.2), together with temperature boundry condition, the equation for temperature profile can be obtained as :

$$T = T_{\rm w} - \Delta T_{\rm sat}\,(y/\delta_{\rm A}) \tag{2.7}$$

where $\Delta\ T_{\rm sat} \equiv T_{\rm w}$ - $T_{\rm sat}$. By applying the velocity and temperature profile equation of Eq.(2.6), and Eq.(2.7), to heat balance equation at the vapor-liquid interface, Eq.(2.5), differential equations for the vapor film thickness $\delta_{\rm A}$ is obtained as :

$$\frac{1}{r}\frac{d}{dr}\left[\ r{\delta_{\rm A}}^3\frac{d\delta_A}{dr}\right]\ = -c_{A2}\left[\frac{\nu_{\rm v}}{(\rho_{\rm L}-\rho_{\rm v})\,g}\frac{\lambda_{\rm v}\Delta T_{\rm sat}}{\ell}\right]\frac{1}{\delta_A} \tag{2.8}$$

Introducting the following dimensionless variables; $\tilde{r} \equiv r/D$, $\tilde{\delta}_{\rm A} \equiv (\delta_A/D)\,[\ {\rm Gr_A/Sp}]^{1/5}$ and dimensional parameters $\rm Gr_A$ and Sp. Here $\rm Gr_A$ is the Grashof number which is equalvalent to the $(gD^3/\nu_{\rm v}^2)\,[(\rho_{\rm l}/\rho_{\rm v})-1]$ and Sp is the dimensionless degree of superheating which is equalvalent to $c_{\rm pv}\Delta T_{\rm sat}/Pr_{\rm v}\ell$. The differential equation of the vapor film thickness is transformed to

$$\frac{1}{\tilde{r}}\frac{d}{d\tilde{r}}\left[\tilde{r}\tilde{\delta}_{\rm A}^3\frac{d\tilde{\delta}_A}{d\tilde{r}}\right]\ = -c_{A2}\left[\frac{1}{\tilde{\delta}_A}\right] \tag{2.9}$$

Defining the function $\phi \equiv \frac{d\tilde{\delta}_A}{d\tilde{r}}$ in Eq.(2.9), and the form of the differential equations is transformed to following ordinary-diferential equation.

$$\frac{d\phi}{d\tilde{r}} = -\left[\left(\frac{3}{\tilde{\delta}_A}\right)\phi^2 + \left(\frac{1}{\tilde{r}}\right)\phi + \left(\frac{c_{A2}}{\tilde{\delta}_A^4}\right)\right] \tag{2.10}$$

The value of numerical coefficient, $c_{\rm A2}$ used in Eq.(2.8), (2.9) and (2.10) corresponding to the slip and non-slip condition at the vapor liquid interface at surface (A) are described as 12 for Case (A-ns) and 3 for Case (A-s) respectively.

Applying the Runge-Kutta method to the above Eq.(2.10), with the assumption of $\tilde{\delta}_A$ at $\tilde{r} = 0$, that is $\tilde{\delta}_{\rm A,0}$ and the profile of vapor film thickness, $\int_0^{1/2}\left(\tilde{r}/\tilde{\delta}_A\right)d\tilde{r}$ and the value of $\tilde{r}_E$ = D/2+$\delta_{B,0}$ can be determined. The vapor film thickness at the lower end of the vertical surface, $\delta_{\rm B,0}$ is calculated by the following method, which is based upon the continuity of the mass of the vapor at the corner between the vertical and downward facing surface. Applying the continuity condition of the vapor mass flow rate around the

corner of the cylinder i.e at $\tilde{r} = 1/2$ and at the lower end of the vertical surface, $\tilde{x}_{\mathrm{B}}$=0.

$$\dot{M}_A|_{\tilde{r}=1/2} = \dot{M}_B|_{\tilde{x}_B=0} = \int_0^{\delta_B} \rho_{\mathrm{v}} u 2\pi \left(R + r^*\right) dr^* \tag{2.11}$$

It should be noted that compare to the radius of the cylinder, R , the value of r^* is much smaller, (i.e R >>> r^*), and (R+r^*) also approach to R and we can transform the vapor mass flow rate at the lower corner to be $\int_0^{\delta_B} \rho_{\mathrm{v}} u dr^*|_{\tilde{x}_B=0} \times 2\pi R$. The amount of generated vapor passed through the circumference of the cylinder bottom with vapor velocity, u is defined as local mass flowrate of vapor , $\dot{M}_A$ [kg/s] and it can be obtained as

$$\dot{M}_A|_{\tilde{r}_A=1/2} = 2\pi \left(\rho_{\mathrm{v}} \nu_{\mathrm{v}} D\right) \left[Gr_A Sp^4\right]^{1/5} \int_0^{1/2} \left(\tilde{r}/\tilde{\delta}_A\right) d\tilde{r} \tag{2.12}$$

Neglecting the effect of curvature of a cylinder, the vertical lateral surface of the cylinder is treated as a plane surface and by applying momentum and energy balance upon the vertical surface and specified boundary condition at the vapor liquid interface as in the analysis of the bottom surface, the velocity profile on vertical surface can be obtained as

$$u = \frac{1}{2}\left[\frac{\left(\rho_{\mathrm{L}} - \rho_{\mathrm{v}}\right) g}{\mu_{\mathrm{v}}} {\delta_{\mathrm{B}}}^2\right] \left[c_{B1}\left(\frac{r^*}{\delta_{\mathrm{B}}}\right) - \left(\frac{r^*}{\delta_{\mathrm{B}}}\right)^2\right] \tag{2.13}$$

The coefficient of the Eq.(2.13), c_{B1} depends upon the boundary condition of slip (B-s) and non-slip (B-ns) at the vapor-liquid interface of the vertical surface and the values are 1 and 2 for Case (B-ns) and Case (B-s) respectively. By substitution equation of velocity profile at the vertical surface, Eq.(2.13), into Eq.(2.11), in their respective cases, the value of δ_B can be determined by the following equations:

$$\dot{m}_B \equiv \frac{1}{c_{B2}}\left[\frac{\left(\rho_{\mathrm{L}} - \rho_{\mathrm{v}}\right)\ g}{\nu_{\mathrm{v}}}\right] {\delta_B}^3, \tag{2.14}$$

where the coefficient c_{B2}=12 for case (B-ns) and c_{B2}=3 for case (B-s). The numerical result of (δ_B) calculated from the Eq.(2.14), is the film thickness at the bottom of the vertical surface and it can be designated as $\delta_{\mathrm{B},0}$. The above procedure is looped from the assumption of the $\tilde{\delta}_{\mathrm{A},0}$ to satisfy the specified condition of Eq.(2.10), to the prediction of δ_{B} in Eq.(2.14), till the value of the $\delta_{\mathrm{B},0}$ addition to the radius of the cylinder is equivalent to the radius r_E, where the gradient of the vapor-film thickness approach to -∞. Table 2.1 shows example of the film thickness of the $\delta_{B,0}$ at degree of superheat ΔT_{sat} = 300 K predicted by above method for four cases. These numerical results are obtained by repeated assuming of the $\tilde{\delta}_{\mathrm{A},0}$ at $\tilde{r} = 0$ to satisfy the Eq. (2.10), and the resultant value of $\delta_{\mathrm{B},0}$ was rechecked by substitution in the predetermined value of $\tilde{r}_E$. When the value of r_E is equal to the radius of the cylinder plus the value of $\delta_{\mathrm{B},0}$ predicted by the continuity condition of the vapor mass flow rate around the corner , the film thickness at the bottom

Table. 2.1: Example of predicted film thickness of water at the bottom and vertical surface of the cylinder at $\Delta T_{\rm sat}$=300 K

Case	$\tilde{\delta}_{\rm A,0}$	$\tilde{r}_E$	$\int_0^{1/2}\left(\tilde{r}/\tilde{\delta}_A\right)d\tilde{r}$	$\delta_{\rm B,0}$ [mm]
Ans-Bns	1.27315	0.50524	0.12424	0.167697
Ans-Bs	1.27120	0.50331	0.12549	0.105992
As-Bns	0.96524	0.50573	0.16357	0.183795
As-Bs	0.96361	0.50360	0.16531	0.116193

of the vertical surface ($\delta_{\rm B,0}$) at respective degree of superheat is obtained. Table 5.1 in appendix shows the results of the vapor film thickness at the bottom and vertical lateral surfaces of the cylinder(D=L=32mm) at degree of superheat ΔT_{sat} = 200 to 500K during film boiling. Appendix Table 5.2 also described the vapor film thickness at the bottom and vertical lateral surface of the different diameter of the cylinder for the case Ans-Bns at ΔT_{sat} =300K.

Profile of the vapor film thickness upon the vertical surface, can be calculated by the following method. For the vertical lateral surface with smooth vapor-liquid interface , the assumption are the same as the bottom surface and the boundary equation were solved by integral method. And also the differential equation of the film thickness on vertical lateral surface can be written as:

$$\frac{d{\delta_{\rm B}}^4}{dx_{\rm B}} = c_{B3}\left[\frac{\nu_{\rm v}}{(\rho_{\rm L}-\rho_{\rm v})\,g}\frac{k_{\rm v}\Delta T_{\rm sat}}{\ell}\right] \tag{2.15}$$

Introduction the following dimensionless variables $\tilde{x}_{\rm B} \equiv x_B/L$, $\tilde{\delta}_{\rm B} \equiv (\delta_B/L)\,[\,Gr_{\rm B}/Sp]^{1/4}$ and parameters for the vertical surface, Gr_B , the differential equation for the dimensionless film thickness ($\tilde{\delta}_B$) can be defined as:

$$\frac{d\tilde{\delta}_{\rm B}^4}{d\tilde{x}_B} = c_{B3} \tag{2.16}$$

In this Eq.(2.15), and (2.16), c_{B3}=16 for Case (B-ns) and 4 for Case (B-s). Solving Eq.(2.16), together with the initial condition of $\tilde{\delta}_B$= $\tilde{\delta}_{B,0}$ at $\tilde{x}_B = 0$, the exact solution for $\tilde{\delta}_B$ is obtained with the coefficient c_{B4}=2 for Case (B-ns) and $\sqrt{2}$ for Case (B-s) as,

$$\tilde{\delta}_B = c_{B4}\left[\tilde{x}_B + \left(\tilde{\delta}_{\rm B,0}/c_{B4}\right)^4\right]^{1/4} \tag{2.17}$$

In consideration the represented length for the L is equal to L_{B1} for the vertical surface with smooth vapor-liquid interface. The value of L_{B1} is calculated by the following empirical equation based on the critical wave length, λ_{cr} and the relation is $L_{B1} = S\lambda_{cr} = S2\pi\lambda_0$. In which λ_0 is the capillary length defined by $\lambda_0 \equiv [\sigma/\,(g\,(\rho_{\rm Lsat}-\rho_{\rm vsat}))]^{1/2}$. The

value of empirical parameter S was obtained as 0.5 using observation results for saturated film boiling around a vertical cylinder of different aspect ratio with water at atmospheric pressure [14].

Finally, heat transfer coefficient and Nusselt number for the bottom surface (A) can be calculated by the following equations,

$$h_A \equiv k_{\mathrm{v}} \frac{1}{\Delta T_{\mathrm{sat}}} \left[-\frac{\partial T}{\partial y}|_0 \right] = \frac{k_{\mathrm{v}}}{\delta_A} \tag{2.18}$$

$$Nu_A \equiv \frac{h_A \cdot D}{k_{\mathrm{v}}} = \left(1/\tilde{\delta}_A \right) \left[Gr_A / Sp \right]^{1/5} \tag{2.19}$$

$$\overline{Nu}_A \equiv \frac{\overline{h}_A \cdot D}{k_{\mathrm{v}}} = \left[8 \int_0^{1/2} \left(\tilde{r}/\tilde{\delta}_A \right) d\tilde{r} \right] \left[Gr_A / Sp \right]^{1/5} \tag{2.20}$$

The Nusselt number (Nu_B and $\overline{Nu}_B$) and heat transfer coefficient (h_{B1} and $\overline{h}_{\mathrm{B1}}$) upon vertical lateral surface with smooth vapor-liquid interface (B_1) can be calculated by the following equations,

$$h_{\mathrm{B1}} \equiv k_{\mathrm{v}} \frac{1}{\Delta T_{\mathrm{sat}}} \left[-\frac{\partial T}{\partial y}|_0 \right] = \frac{k_{\mathrm{v}}}{\delta_B} \tag{2.21}$$

$$Nu_{\mathrm{B1}} = \left(1/\tilde{\delta}_B \right) \left[Gr_{\mathrm{B1}} / Sp \right]^{1/4} \tag{2.22}$$

$$\overline{Nu}_{\mathrm{B1}} \equiv \frac{\overline{h}_{B1} \cdot L_{\mathrm{B1}}}{k_{\mathrm{v}}} = \left[\int_0^1 \left(1/\tilde{\delta}_B \right) d\tilde{x}_{\mathrm{B}} \right] \left[Gr_{\mathrm{B1}} / Sp \right]^{1/4} \tag{2.23}$$

2.2.3 Vertical lateral surface and upward facing horizontal surface

As mention in section 2, the vapor-liquid interface at the upper vertical surface (B_2) and upward-facing horizontal surface (C) is wavy and considered as turbulent. It was assumed that, in this surfaces (B_2) and (C), local heat transfer rate is changed slightly with the position compare to the other surfaces and the local heat transfer coefficient is assumed as uniform. Heat transfer rate on the upper vertical surface is already analyzed by Nishio-Ohatake (1992) and upward-facing horizontal surface is analyzed by Berenson(1961)'s correlation. In this study, heat transfer rate on the upper vertical surface and upward-facing horizontal surface are estimated by the prediction method which is proposed in that analysis (Momoki et al. 2007). The heat transfer coefficient upon the vertical surface with wavy vapor-liquid interface, (B_2) can be estimated as:

$$h_{\mathrm{B_2}} = 0.740 (k_{\mathrm{V}}/\lambda) (Gr_{\mathrm{B_2}}/Sp^*)^{1/4} \tag{2.24}$$

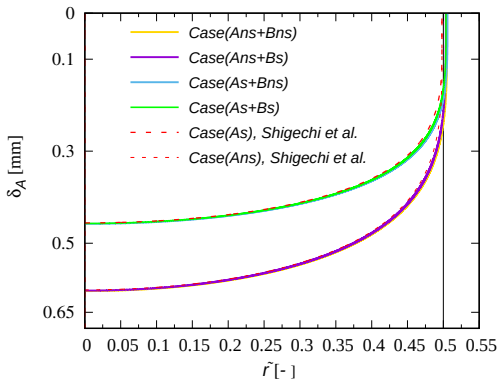

Fig. 2.3: Vapor film thickness at the end of bottom surface (water at atmospheric pressure, $\Delta\ T_{\rm sat}\ = 300$ K)

where Grashof number for this surface is considered as $Gr_{\rm B2} \equiv (g\lambda^3/\nu_{\rm V}^2)\,[(\rho_{\rm L}/\rho_{\rm V}) - 1]$, the modified dimensionless degree of superheating, $Sp^* \equiv c_{p_{\rm V}}\Delta T_{\rm sat}/\left[Pr_{\rm V}(\ell + 0.5c_{P_{\rm V}}\Delta T_{\rm sat})\right]$ and the vapor-film unit-length as $\lambda = 16.2\left[1/(Sp^{*^3}Gr_{{\rm B}_{\lambda_0}})\right]^{1/11}\lambda_0$.

for the upwarding-facing horizontal surface (C),

$$h_{\rm C} = 0.425(k_{\rm V}/\lambda_0)(Gr_{\rm C}/Sp)^{1/4} \tag{2.25}$$

where $Gr_{\rm C} \equiv (g\lambda_0^3/\nu_{\rm V}^2)\left[(\rho_{\rm L}/\rho_{\rm V}) - 1\right]$ is coincides with the calculation method of the $Gr_{{\rm B}_{\lambda_0}}$ used in to calculate the vapor-film unit-length.

2.2.4 Modification results

To predict the heat transfer coeficient upon all surfaces of the vertical-finite-length cylinder, first we modified the prediction method of the Shigechi et al. to predict the local heat transfer coefficient at the end of the bottom surface. In this modification, the value of average heat transfer rate on each surface of the cylinder is the same as predicted by Shigechi et al.'s one for all Cases and local heat transfer rate by the present method is only about 1 % smaller than predicted by the Shigechi et al.'s method except near the end of bottom surface. Furthermore, during film boiling, the calculated vapor film thickness decreased and heat transfer coefficient increased as the degree of superheat decreased as usual. Here, local heat transfer coefficient is predicted for the degree of superheat $\Delta T_{\rm sat}$= 200, 300, 400 and 500K but only described the results on $\Delta T_{\rm sat}$ = 300K with possible two cases at Fig. 2.3. For the comparison of the previous and present modification, Fig. 2.4 shows the vapor film thickness at the bottom surface and vertical lateral surface for two methods at degree of superheat, ΔT_{sat}=200 to 500K. The highest local heat transfer rate is at the corner of the bottom and vertical surface where there is the film collapse start

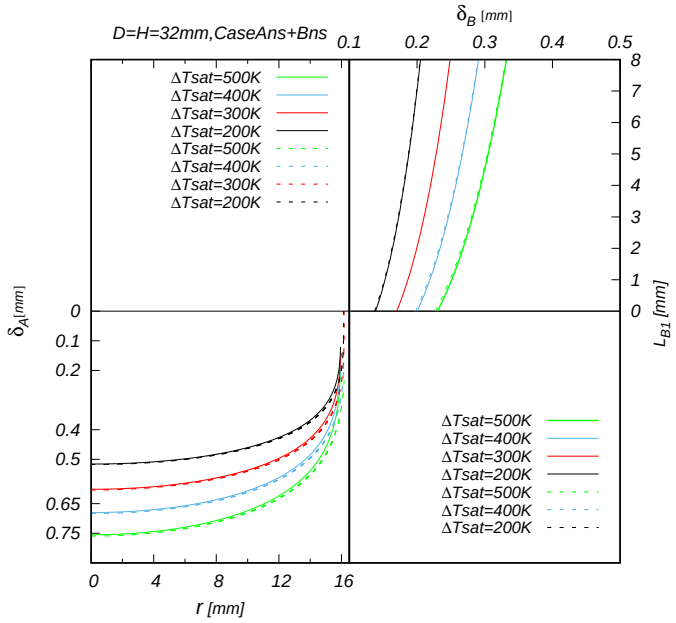

Fig. 2.4: Vapor film thickness at the end of bottom surface and vertical lateral surface

by the experimental observation.

As mention above, the author reported that the combination of the case, i.e (Ans-Bns) of the estimated average heat transfer coefficient for each regions agreed with the experimental results on cooling rate. In this comparison, the Shigechi et al. method are used for the region A and B_1. Here, we discussed the difference between the present method and the Shigechi et al. method, at first.

Figure 2.3 shows vapor film thickness distribution on downward-facing bottom surface predicted by two types of prediction methods. Vapor film thickness predicted by the boundary condition at the end of the bottom surface by Shigechi et al. are represented by dotted lines and still undertermined the vapor film thickness at that end since the gradient of the vapor film thickness is minus infinity. Present predicted results are represented by the solid lines with the boundary condition at the virtual radius, $\tilde{r}_E$, the gradient of the vapor film thickness is minus infinity and the vapor film thickness at the end of the bottom surface can be determined. While the Shigechi et al. method for the downward-facing bottom surface (A), is not affected by the vertical surface (B_1), the present method is slightly affected by slip or non-slip condition at vapor-liquid interface at the surface (B_1). Therefore, to focus on the difference between two methods, we also presents the results at dimensionless radius at $\tilde{r} = 0.5$ in this Fig. 2.3, the obtained film thickness for all cases, A-ns+B-ns, A-ns+B-s, A-s+B-ns and A-s+B-s by the present method and those for cases A-ns and A-s for the Shigechi et al. method are shown for the water at degree of superheat 300K. However, the vapor film thickness at the center of the bottom surface (δ_A at r=0) is slightly thicker than the previous one by Shigechi et al.'s but this

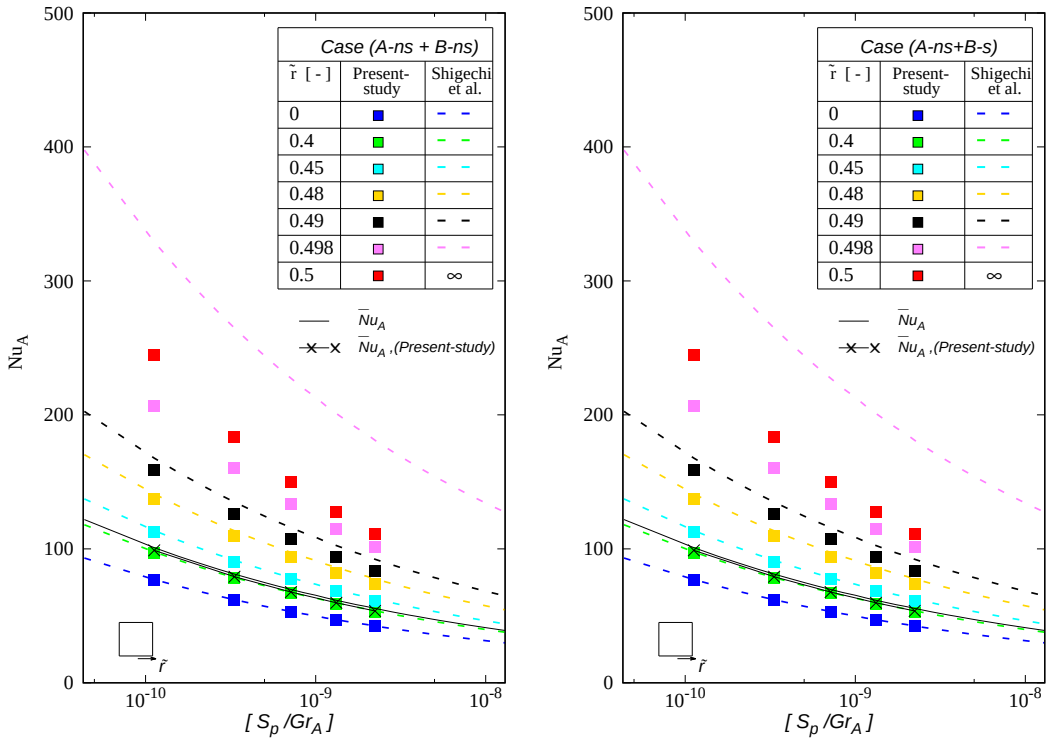

Fig. 2.5: Nusselt number on the horizontal bottom surface and degree of superheat for Case Ans

small value is not effective in prediction the heat transfer rate through the entire bottom surface. Furthermore, we can predicted the thickness of the vapor film at the end of the bottom surface with their respective cases as δ_A for Case (A-ns+B-ns) = 0.239 mm, δ_A for Case (A-ns+B-s) = 0.214 mm, δ_A for Case (A-s+B-ns) = 0.185 mm and δ_A for Case (A-s+B-s) = 0.165 mm in order of decreasing.

The result on local and average Nusselt number changed with degree of superheat upon the horizontal bottom surface are shown in Fig. 2.5 for four Cases (A-ns+B-ns), (A-ns+B-s), (A-s+B-ns) and (A-s+B-s) as the effect of the case in the region (B_1) on the heat transfer coefficient in the region (A) was small. It is clear that the value of slip condition at the vapor-liquid interface is much higher than the condition at non-slip. The local Nusselt number is described with the position of the dimensionless radius $\tilde{r} = 0$ to $\tilde{r} = 0.5$ and the results on present study are shown at degreee of superheat at $\Delta T_{\text{sat}} = 200$, 300, 400 and 500K respectively and which is defined by the ratio of dimensionless number on x-axis of the Fig. 2.5 and 2.6, as S_p/Gr_B. Here, S_p/Gr_B value of 3.3×10^{-10} represents to $\Delta T_{\text{sat}} = 200$K, 7.1×10^{-10} represents to $\Delta T_{\text{sat}} = 300$K, 1.3×10^{-9} represents to $\Delta T_{\text{sat}} = 400$K and 2.2×10^{-9} represents to $\Delta T_{\text{sat}} = 500$K respectively. As the dimensionless radius approach to 0.5, that is at the end of bottom surface, local Nusselt number is the highest on both cases and for both study. As the different of the result on local Nusselt

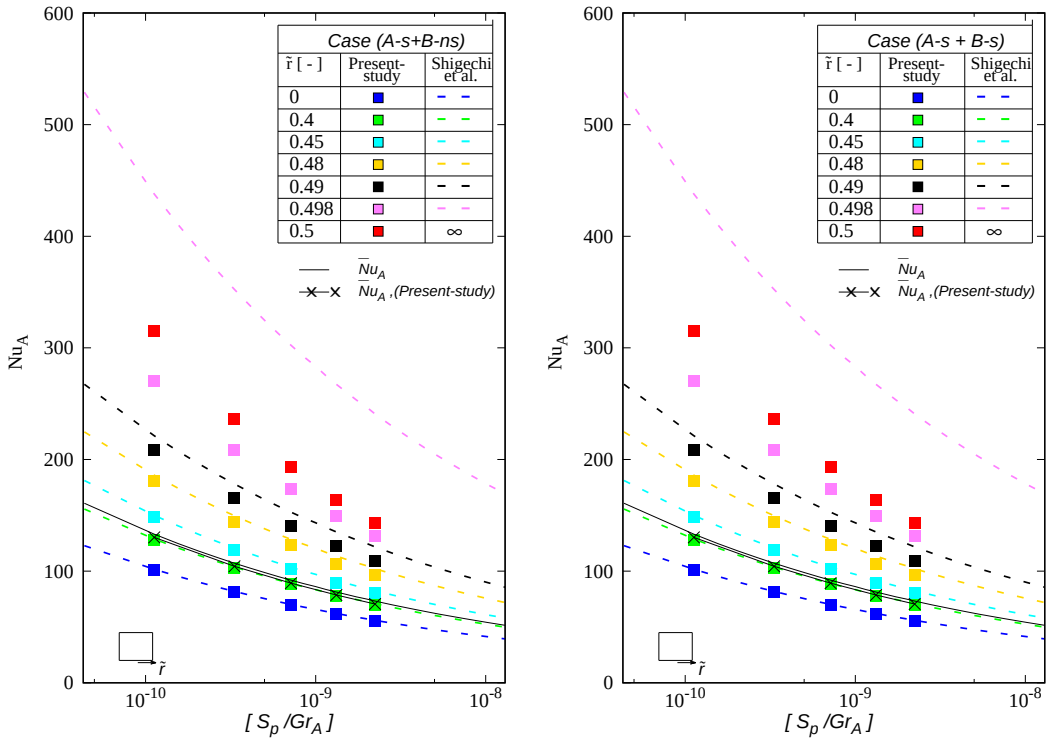

Fig. 2.6: Nusselt number on the horizontal bottom surface and degree of superheat for Case As

number predicted by Shigechi et al. method and present study start from $\tilde{r} = 0.48$ and at the end of the bottom surface, local Nusselt number predicted by the previous method apporach to infinity. At that time, local Nusselt number at the end of the bottom surface can be predicted by the present modification method. Furthermore, the average Nusselt number predicted by the present study are almost the same those of the average Nusselt number predicted by the Shigechi et al. method. At the end of the bottom surface at low degree of superheat (which is at the lower limit condition) the local Nusselt number is highest and as the degree of superheat higher, increasing rate of local Nusselt number is not reasonable amount. For all cases, the local Nusselt number predicted by the present method in the area $\tilde{r} \leq 0.48$ are almost the same to the Shigechi et al.'s method and as increasing $\tilde{r} > 0.48$, the results on local Nusselt number by the present methods are smaller than the Shigechi et al. one's.

The result of local and average Nusselt number upon the vertical surfce was shown in Fig. 2.7 to 2.8 for Case (A-ns+B-ns), (A-ns+B-s), (A-s+B-ns) and (A-s+B-s) although considered for the combination of four cases, but only for two combination Cases, (Ans+Bns) and (A-ns+Bs) are discussed as the effect of slip and non-slip condition in the bottom surface upon vertical surface is not so large. Local and average Nusselt number on vertical surface are predicted by Shigechi et al.'s method and also present method and

compared the results. As the prediction of $\delta_{B,0}$ at the lower end of the vertical surface predicted by the present study is smaller than the value of the film thickness predicted by Shigechi et al., all value predicted at the vertical lateral surface by the present study are just only about 1% greater than the Shigechi et al.'s method. Local Nusselt number upon vertical surface with smooth vapor-liquid interface are described with the value at vertical position, at the lower end of the vertical lateral surface (x_B=0) the value of local Nusselt number is the highest and as the distance x_B from the lower end of the vertical surface increased, the value of local Nusselt number decreased and finally approachs to constant value. The difference between the highest Nusselt number at x_B=0 mm and lowest Nusselt number at x_B= 9.6 mm becomes smaller as increasing degree of superheat, that is the value of S_p/Gr_B increase at x-axis for both cases. From the results on local Nusselt number upon the vertical surface, combination of non-slip condition at the bottom surface and slip condition at the vertical surface gives the highest heat transfer rate at the lower end of the vertical surface.

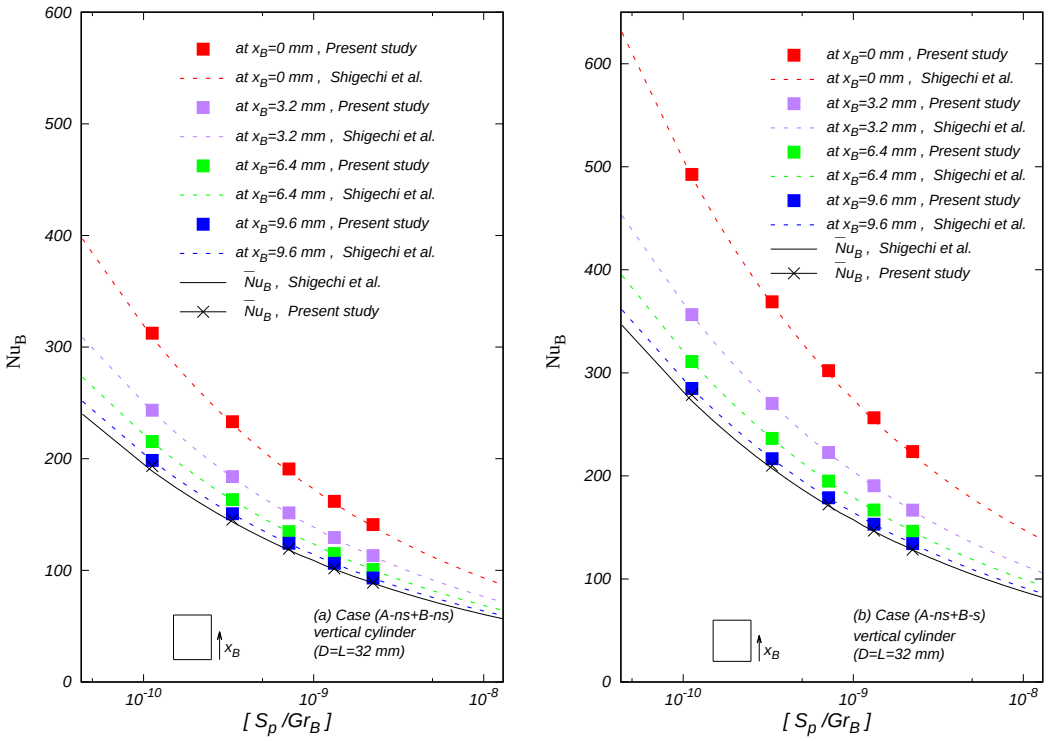

Fig. 2.7: Nusselt number on the vertical surface and degree of superheat

2.2.5 Lower limit of saturated film boiling

The lower limit of film boiling, $\Delta T_{\min}$ is important in prediction the film collapse and film boiling characteristic and it can be defined as the point where the cooling rate, $-dT/d\tau$

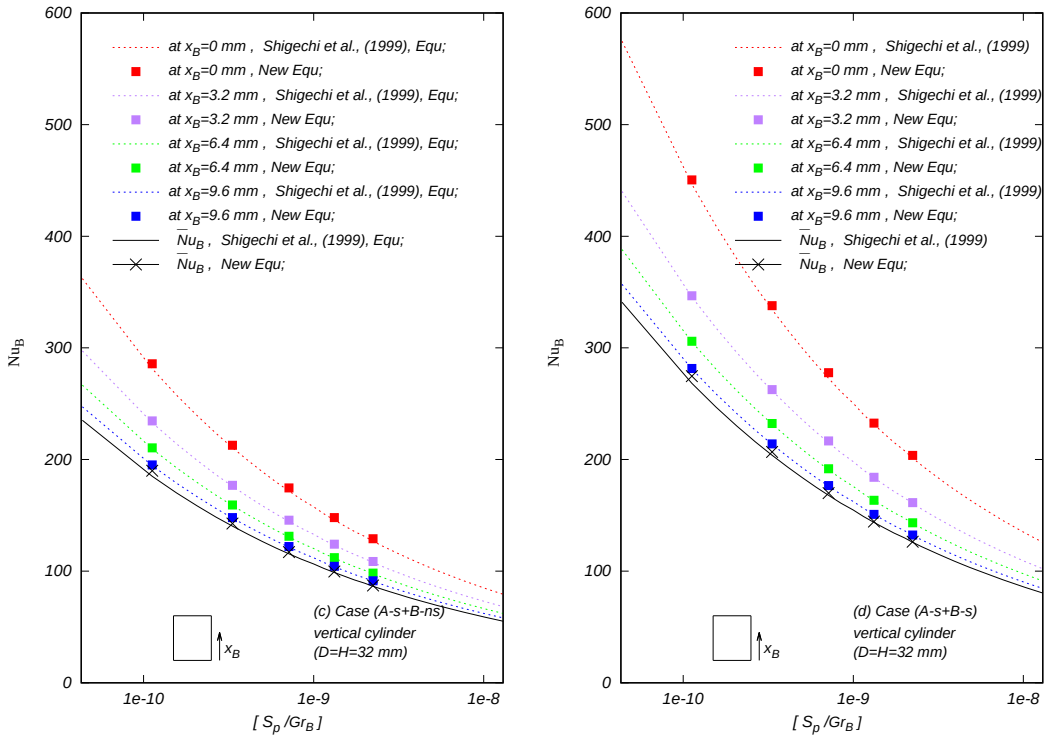

Fig. 2.8: Nusselt number on the vertical surface and degree of superheat

gives a minimum value and the corresponding wall superheat is referred to as $\Delta T_{\min}$. The value of lower limit of film boiling depends upon shapes and material of the heating object. From the experiment with the vertical silver cylinder of flat top and bottom surface, the lower limit of film boiling can be estimated round about 136 K for different aspect ratio in saturated film boiling (Yamada *et al.*(2004)). It is noted that $\Delta T_{\min}$ does not exactly corresponding to the wall temperature at the lower limit of film boiling where the vapor film covering the cylinder start to collapse.

2.2.6 Comparison of the predicted total heat transfer rate of the cylinder with the experimental results

The previous modification on film boiling heat transfer from the bottom surface, we can predict the local heat transfer coefficient near the edge of the bottom surface and vertical lateral surface with the finite value and also average heat transfer coefficient on each surface of the cylinder. It was noted that, the predicted average heat transfer coefficient on bottom surface is slightly smaller than predicted by the Shigechi *et al.* and the predicted average heat transfer coefficient for the vertical lateral surface with smooth vapor-liquid interface is nearly the same as predicted by Shigechi *et al.*(1999) method. Furthermore, the correlation equation for heat transfer coefficients to predict overall heat

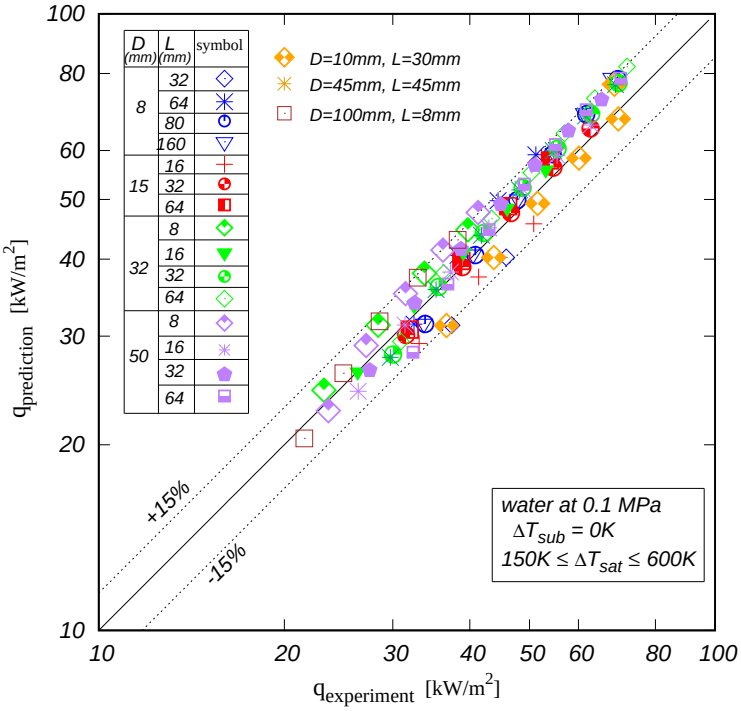

Fig. 2.9: Comparison of measured and predicted average heat flux on saturated film boiling

transfer rate from a cylinder have been proposed by Momoki *et al.* (2007) and these correlation equations for heat transfer are good agreement with the existing experimental data by quenching method. In this regard, the previous results on average heat flux predicted from average heat transfer coefficients on each surfaces are compared with the experimental results on saturated film boiling as shown in Fig. 2.9.

Here we found that modification method is not effected in prediction the heat transfer averaged over the entire cylinder in saturated film boiling by comparing the average heat flux predicted from the average heat transfer coefficient on each surface of the cylinder with the experimental results on quenching of the silver cylinders which diameter range varies from 8 to 100mm and length range from 8 to 160mm in saturated water. Figure 2.9 shows comparison of predicted total heat transfer rate of the cylinder with the experimental results on the film boiling region at degree of superheating, $\Delta\ T_{\rm sat}$ = 600 to 150K in saturated water and the predicted values by the previous modification agrees within $\pm$15% to the existing experimental values.

2.2.7 Local heat transfer coefficient on each surface of the vertical cylinder

In order to discuss the effect of local heat transfer coefficient on film collapse, in this study, we consider two velocity profile of non-slip and slip condition at the vapor-liquid

interface for the bottom surface and vertical lateral surface with smooth vapor-liquid interface. This physically possible combination of two velocity profile are referred as Case (Ans+Bns), Case (Ans+Bs), Case (As+Bns) and Case (As+Bs). So we predict for these four cases and discuss here for the applicable cases because one of the objectives are discussion about the highest heat transfer point and the film collapse. The predicted local heat transfer coefficients on all surfaces of the vertical cylinder are described in Fig. 2.10, for the combination of Cases (Ans+Bns) and (Ans+Bs) and the average heat transfer coefficients for Case (Ans+Bns) are only described for the comparison. Local heat transfer rate through all surfaces of the vertical cylinder are predicted for the degree of superheat at ΔT_{sat}= 200, 300, 400 and 500K. Hence, the value of local heat transfer coefficient at degree of superheat 300K is described in Fig. 2.10, because all the results show the similar trend. It will be noted that the trend of local heat transfer coeficient upon vertical lateral surface with smooth vapor-liquid interface (h_{B1}) is two fold depend upon the slip condition (Bs) and non-slip condition (Bns) at the vertical surface.

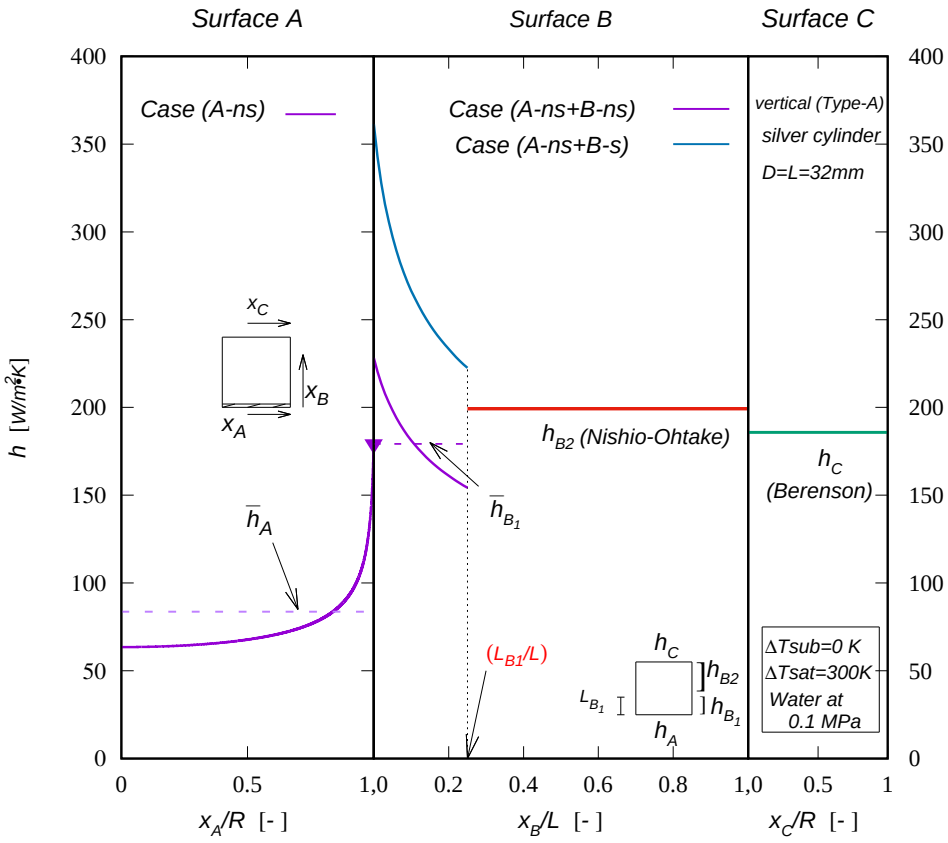

Fig. 2.10: Local heat transfer coefficient on each surface of the vertical cylinder

We discuss that the distribution of the predicted local heat transfer coefficients on all surface of the cylinder based on the present method. In the author's previous study, the estimated heat transfer rate based on the average heat transfer coefficients for the Case

(A-ns+B-ns) agreeds the experimental results, and the non-slip condition at the bottom surface (A) may be reasonable because the velocity of the vapor beneath the downward-facing horizontal surface is not so large and also there is no significant configuration at the bottom surface to be considered as slip condition. Therefore, the estimated result for the non-slip vapor-liquid interface condition for the downward-facing surface (A-ns) is described in Fig. 2.10. For the vertical surface with smooth vapor-liquid interface (B_1), the estimated results for both slip and non-slip condition at the vapor liquid interface are discussed because the velocity of the vapor might become so large at some region near the bottom due to the supplied vapor from the bottom surface passed a corner or ventage point and slip condition might be occured. Furthermore the combination of non-slip condition (A-ns) at the bottom surface and slip condition at the vertical surface (B-s), that is Case (A-ns+B-s) gives higher heat transfer rate than that of Case (A-ns+Bns). The reason that h_{B1} for Case (Ans+Bs) is the highest possible in actual application, is liked that as consider for the cylinder configuration, the velocity at the corner of the bottom surface and vertical surface might be high enough to be considered as non-slip condition at the vapor-liquid interface as the film thickness at that edge is invisible small. But for the bottom surface, we have already studied that the effect of the vapor mass flow generated under the horizontal bottom surface is to decrease the heat transfer rate. However, in actual application, overestimation of the heat transfer rate should be avoided and it can be conducted that even in non-slip condition at the vertical surface, local heat transfer coefficient at the corner of the vertical surface is highest compare to other surfaces. In prediction of the lowest temperature point on the cylinder surface with the average heat transfer coefficients, it seems to be the upper corner of the cylinder due to the much higher heat transfer coefficient at the upward-facing horizontal surface ($\overline{h}_C$) and at the upper region of the vertical ($\overline{h}_{B2}$), than that at the downward-facing horizontal surface ($\overline{h}_A$). As the results on predicted local heat transfer coefficient on vertical cylinder, the highest heat transfer coefficient are found at the end of bottom surface (at $\tilde{x}_A$=1) and at the lower corner of the vertical surface (at $\tilde{x}_B$=0) of the cylinder as in Fig. 2.10, and it suggests that the lowest temperature point may become the lower corner of the cylinder. That the highest heat transfer coefficient at the lower corner of the cylinder agreeds the author's previous experimental results on the film collapse start (Momoki et al. 2017)

2.3 Subcooled Film Boiling

The degree of liquid subcooling enhance the heat transfer performance of the cylinder and the heat transfer coefficient for the subcooled film boiling is treated based upon predicted results on local and average heat transfer coefficient by modified method in saturated film boiling. The physical model for the subcooled film boiling is shown in

Fig. 2.1 (b) with the thinner vapor film caused by the degree of subcooling liquid and its enhance the heat transfer performance. This enhancement factor, $\overline{h}/\overline{h}_{\rm sat}$, for the downward facing horizontal surface, vertical lateral surface with smooth and wavy vapor-liquid interface, and the upward-facing horizontal surface are examined separately by Yamada *et al.*(2007) and which are applied in Momoki *et al.*(2007) prediction method of heat transfer enhancement in liquid subcooling and as well as in this study. The length on the vertical surface with smooth vapor-liquid interface also extends in subcooled film boiling and the investigation on this expansion ratio, $L_{\rm B1}/L_{\rm B1,sat}$ has been empirically determined by Momoki *et al.*(2007).

The average and local heat transfer coefficients for each surfaces of the cylinder and the length of smooth vapor-liquid interface region, $L_{\rm B1}$ changed with the degree of subcooling are predicted in the following section for subcooled film boiling.

2.3.1 Downward facing horizontal surface

Correlation of heat transfer enhancement factor for the downward facing horizontal surface (A), $\overline{h}_A/\overline{h}_{\rm A,sat}$, is already proposed by Yamada *et al.* (1998) and this correlations were previously applied in prediction cooling rate of the vertical finite-length cylinder by Momoki *et al.* (2007) and also in this prediction.

$$\frac{\overline{h}_{\rm A}}{\overline{h}_{\rm A,sat}} = 0.699 + 0.411\phi_{\rm A} - 0.145{\phi_{\rm A}}^2 + 0.035{\phi_{\rm A}}^3 \tag{2.26}$$

where the numerical value of $\phi_{\rm A}$=$\left\{ \left(\frac{J_A}{J_{\rm A0}}\right)^3 \left(\frac{1+\beta J_{\rm A0}}{1+\beta J_A}\right) \right\}^{1/5}$ can be obtained by computing the dimensionless parameters J_A and

β as $J_A \equiv \left(F_{\rm A1}+\sqrt{F_{\rm A2}}\right)^{1/3} + \left(F_{\rm A1}-\sqrt{F_{\rm A2}}\right)^{1/3} + \frac{1}{3\beta}\left(\frac{Sc}{Sp}\right)$ and $\beta \equiv \left(\frac{R^2}{2SpPr_{\rm L}}\right)^{1/3}$. In subcooled film boiling, dimensionless degree of liquid subcooling can be defined as $Sc \equiv cp_{\rm L}$ $\Delta T_{\rm sub}/(Pr_L\ \ell)$ and the value of $J_{\rm A0}$ is obtained by applying Sc=0 in $F_{\rm A1}$ and $F_{\rm A2}$. By the relationship of degree of superheating and liquid subcooling $F_{\rm A1}$ and $F_{\rm A2}$ can be calculated as $F_{\rm A1} \equiv \frac{1}{2}+\frac{2}{3}\left(\frac{Sc}{Sp}\right)+\left\{\frac{1}{3\beta}\left(\frac{Sc}{Sp}\right)\right\}^3$ and $F_{\rm A2} \equiv \frac{1}{4}-\frac{64}{27}\beta^3+\frac{2}{3}\left(\frac{Sc}{Sp}\right)-\frac{4}{27}\left(\frac{Sc}{Sp}\right)^2+\left\{\frac{1}{3\beta}\left(\frac{Sc}{Sp}\right)\right\}^3$. And the ratio of density and viscosity is represented as $R \equiv \left(\frac{\rho_{\rm V}\mu_{\rm V}}{\rho_{\rm L}\mu_{\rm L}}\right)^2$.

The local and average heat transfer coefficient in the saturated condition, $h_{\rm A,sat}$ and $\overline{h}_{\rm A,sat}$, are already estimated by Eq.(2.19) and (2.20) by the modified prediction method and local heat transfer enhancement in subcooled film boiling can be computed by applying the same enhancement as in average heat transfer rate as, $h_{\rm A,sub} = h_{\rm A,sat}\left(\frac{\overline{h}_{\rm A,sub}}{\overline{h}_{\rm A,sat}}\right)$.

2.3.2 Vertical lateral surface

Degree of liquid subcooling affects the heat transfer from the vapor-liquid interface to the liquid in subcooled film boiling. As the $\Delta T_{\rm sub}$ increased, the energy transfer into the liquid phase is increased and decreased in vapor film thickness and higher heat transfer rate through the vapor, simultaneously the smooth vapor-liquid interface on the vertical lateral surface extends upward. For the height of the vertical lateral surface with smooth vapor-liquid interface in subcooled film boiling, Momoki *et al.* (2007) proposed the following empirical correlation,

$$\frac{L_{\rm B1}}{L_{\rm B1,sat}} = 1 + 56.3Sc \tag{2.27}$$

which is based upon the relationship of the height of the smooth vapor-liquid interface in saturated film boiling, $L_{\rm B1}$ and the dimensionless degree of liquid subcooling, Sc.

Vertical surface with smooth vapor-liquid interface

For the subcooled film boiling heat transfer from the vertical lateral surface, the authors (Yamada et al.(2004)) previously evaluated the Nishikawa *et al.*(1975) correlation and reported that the proposed correlation for the average heat transfer coefficient around the vertical cylinder agreed to the experimental value within -15% to +45%. In order to improve the prediction accuracy, Momoki *et al.*(2007) proposed the new correlation of the enhancement factor for the vertical lateral surface with smooth vapor-liquid interface, $\overline{h}_{\rm B1}/\overline{h}_{\rm B1,sat}$ and which can correlated within $\pm$ 15% with experimental data. These correlation are applied in present work and expressed as by the following equation,

$$\frac{\overline{h}_{\rm B1}}{\overline{h}_{\rm B1,sat}} = 1 + C_{\rm B1}\left(\frac{Sc}{Sp}\right) \tag{2.28}$$

where $C_{\rm B1}$ is determined from the experimental data for quenching method with the subcooled water as a coolant at atmospheric pressure and this empirical equation can be expressed as $\rm C_{B1} = 10.45 + 11.74L/(\ \pi\lambda_0)$.

The local heat transfer enhancement in vertical surface with smooth vapor-liquid interface also can be obtained by the relation, $h_{\rm B1,sub} = h_{\rm B1,sat}\left(\frac{\overline{h}_{\rm B1,sub}}{\overline{h}_{\rm B1,sat}}\right)$.

Vertical surface with wavy vapor-liquid interface

In this study, heat transfer enhancement factor for the vertical lateral surface with wavy vapor-liquid interface, $\frac{\overline{h}_{\rm B2}}{\overline{h}_{\rm B2,sat}}$, can be calculated by the following Nishio and Ohtake correlation (1992) which is also applied in Momoki *et al.* (2007) prediction method.

$$\frac{\overline{h}_{\rm B2}}{\overline{h}_{\rm B2,sat}} = 1 + 0.0905\left(\frac{c_{\rm pV}}{c_{\rm pL}}\right)\left(\frac{Pr_{\rm L}}{Pr_{\rm V}}\right)\left(\frac{{Pr_{\rm L}}^2}{R^2}\right)^{0.23}\left(\frac{Gr_{\rm B_{2L}}Sp^*}{Gr_{\rm B2,sat}}\right)^{1/4}\left(\frac{\lambda}{L_{\rm B2}}\right)\left(\frac{Sc}{Sp}\right) \tag{2.29}$$

where $Gr_{\mathrm{B2L}} \equiv (g\lambda^3/{\nu_L}^2)\left[(\rho_{\mathrm{LB}}/\rho_{\mathrm{L}}) - 1\right]$, $\overline{h}_{\mathrm{B2,sat}}$ and $Gr_{\mathrm{B2,sat}}$ can be predicted by the method described in section 2.2.3 with the physical properties of saturated liquid. It will be noted that the heat transfer coefficient of the vertical surface with wavy vapor-liquid interface is considered neither to be average nor local and the ratio $\frac{\overline{h}_{\mathrm{B2}}}{\overline{h}_{\mathrm{B2,sat}}}$ can be transform to $\frac{h_{\mathrm{B2}}}{h_{\mathrm{B2,sat}}}$ in this study.

2.3.3 Upward facing horizontal surface

For the subcooled film boiling, the heat transfer enhancement factor for the upward facing horizontal surface, $\overline{h}_C/\overline{h}_{\mathrm{C,sat}}$, is estimated by the following Hamill and Baumeister (1967) correlation which is also applied in Momoki *et al.*(2007) prediction method.

$$\frac{\overline{h}_{\mathrm{C}}}{\overline{h}_{\mathrm{C,sat}}} = 1 + 0.0395\left(\frac{C_{\mathrm{pV}}}{C_{\mathrm{pL}}}\right)\left(\frac{k_{\mathrm{L}}}{k_{\mathrm{V}}}\right)\left(\frac{Sp}{Gr_{\mathrm{C,sat}}}\right)^{1/4}\left(\frac{{\lambda_0}^3 \ell g \alpha_L {Pr_{\mathrm{L}}}^2 Sc}{cp_{\mathrm{L}}{\nu_{\mathrm{L}}}^2}\right)^{1/3}\left(\frac{Pr_{\mathrm{L}}}{Pr_{\mathrm{V}}}\right)\left(\frac{Sc}{Sp}\right) \tag{2.30}$$

where, α is a volumetric thermal expansion coefficient. The heat transfer coefficient under in the saturated condition, $h_{\mathrm{C,sat}}$ is obtained by the Eq.(2.25) with the physical properties of saturated liquid. As considered in saturated film boiling, the heat transfer rate of the upward facing horizontal surface independent upon the location and is can be said as only $h_{\mathrm{C,sat}}$.

2.3.4 Lower limit of subcooled film boiling

The degree of wall superheating at the lower limit of film boiling around a vertical silver cylinder to subcooled water at atmospheric pressure can be predicted by the correlation proposed by Momoki *et al.*(2007) as $\Delta T_{\mathrm{min}} = \left\{133.9^8 + (104 + 8.38\Delta T_{\mathrm{sub}})^8\right\}^{1/8}$. As in saturated film boiling, ΔT_{min} is independent of the aspect ratio in subcooled condition but the value is larger with increased in ΔT_{sub}.

2.3.5 Comparison of the predicted total heat transfer rate of the cylinder with the experimental results

For the subcooled film boiling, predicted average heat transfer coefficient from each surfaces of a vertical cylinder on saturated film boiling condition are applied with individual correlation to predict enhancement of average heat transfer rate due to liquid subcooling. As the case of the saturatd film boiling heat transfer, the predicted subcooled film boiling

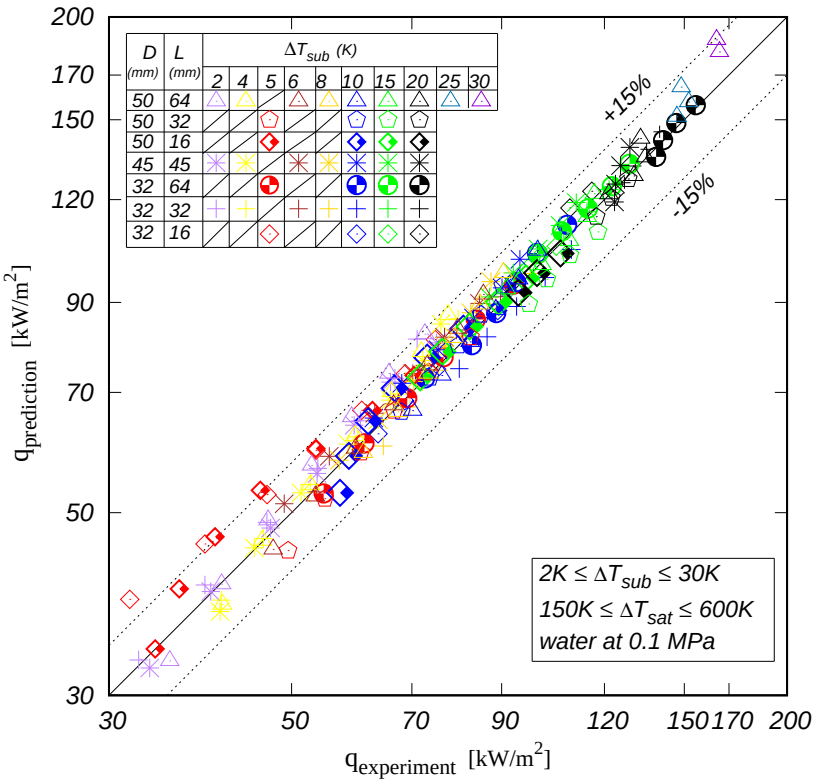

Fig. 2.11: Comparison of measured and predicted average heat flux on subcooled film boiling

heat transfer coefficients on each regimes are applied to predict heat transfer rate through the entire cylinder and this predicted heat transfer rate is compared to the experimental data and its agreed within ±15%. In this comparison, the experimental data on quenching of the silver cylinder, which diameter ranges from 32 to 50mm and length ranges from 16 to 64mm are applied. The degree of liquid subcooling, $\Delta\ T_{\mathrm{sub}}$ ranges from 2 to 30K and experiment are carried out during the film boiling region of degree of superheating $\Delta\ T_{\mathrm{sat}}$, 600 to 150K. Figure 2.11 shows the comparison of subcooed film boiling heat flux over the cylinder by taking into account the average heat transfer coefficients on each surfaces by the modified method and measured average heat flux from the experimental data.

2.3.6 Discussion on predicted local and average heat transfer performance for saturated and subcooled film boiling

Predicted average heat transfer rate from each surfaces of the cylinder can correlated well with entire average heat transfer rate of the cylinder and can predict the cooling rate of the cylinder in saturated and subcooled film boiling. In examination the average heat transfer rate, vertical surface with wavy vapor-liquid interface, (B_2) gives the highest values and the average heat transfer rate of the upper surface, h_C is larger than those of the

bottom surface, $\overline{h}_{\mathrm{A}}$ and vertical lateral surface with smooth vapor-liquid interface, $\overline{h}_{\mathrm{B1}}$. The bottom surface with stable film boiling, (A) always shows the lowest heat transfer rate and the average heat transfer rate of vertical lateral surface with smooth vapor-liquid interface, $\overline{h}_{\mathrm{B1}}$ is about two times larger than those of bottom surface, $\overline{h}_{\mathrm{A}}$ but still smaller than those of surfaces with wavy vapor-liquid interface, h_{B2} and h_{C}. The trand is same for all the different diameter and height of the cylinder. Figure 2.12 and 2.13 show the average heat transfer coefficient on each surface of the cylinder predicted by modified position of boundary condition. In estimation the temperature field inside the cylinder, the boundary conditions at the cylinder surface are applied by the value of average heat transfer coefficients on each surfaces. It suggests that the lowest temperature points are corresponding to the highest heat transfer rate at the upper corner of the cylinder and inconsistence with the experimental observation on film collapse start from the lower corner of the vertical cylinder in saturated and subcooled film boiling.

In prediction local heat transfer coefficient for the subcooled film boiling, here we simply proposed h_{sub} is equivalent to $h_{\mathrm{sat}}\left(\frac{\overline{h}_{\mathrm{sub}}}{\overline{h}_{\mathrm{sat}}}\right)$ as the enhance of average heat transfer rate due to liquid subcooling. Here we compare the heat transfer enhancement for the local and average heat transfer coefficient for the different height of the cylinder on saturated and subcooled film boiling. Enhancement on the local and average heat transfer coefficient due to liquid subcooling is slightly effected on downward facing horizontal surface(A) and strongly effected on the regimes on vertical surface where vapor-liquid interface is smooth(B_1), not significant in the regime of vertical surface with wavy vapor-liquid interface(B_2) and upward facing horizontal surface(C). From the experimental observation, as the degree of liquid subcooling increased the vertical length of the smooth vapor-liquid interface increased and these increment on smooth vapor-liquid interface mostly effected to nhance the heat transfer rate at the region of smooth vapor-liquid interface, (B_1) in liquid subcooling. From the prediction results on two cylinders of same diameter, D=32mm and different vertical length with H=32mm and H=64mm, it seems to be the enhancement of heat transfer rate due to liquid subcooling on vertical lateral surface with smooth vapor-liquid interface depends upon the height of the cylinder as the same degree of liquid subcooling shows different increasing rate of heat transfer enhancement. It was due to the empirical equation used in prediction of heat transfer enhancement in vertical surface with smooth vapor-liquid interface include the terms for the effects of cylinder configuration, especially the vertical length of the cylinder. The local heat transfer rate increased about 43% for the 32mm height cylinder and about 81% for the 64mm height cylinder due to the same degree of liquid subcooling(ΔT_{sub}=2K) at the lower end of the cylinder. However, local heat transfer rate at the end of smooth vapor-liquid interface is not increased as much as at the lower corner of the vertical surface on both saturated and subcooled film boiling. The highest values of local heat transfer rate at the lower corner of

the cylinder corresponding to the thinnest vapor film thickness with high velocity vapor passing through it. The results on local heat transfer performance at the lower corner of the cylinder suggests that lowest surface temperature at that corner where the film collapse would like to start.

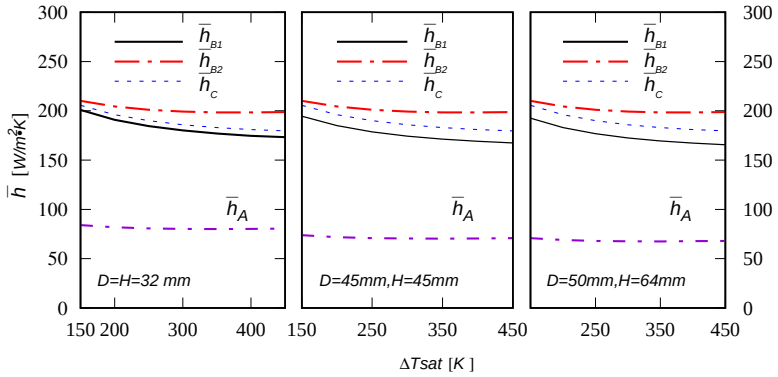

Fig. 2.12: Predicted average heat transfer coefficients on each surface of the vertical cylinders on saturated film boiling

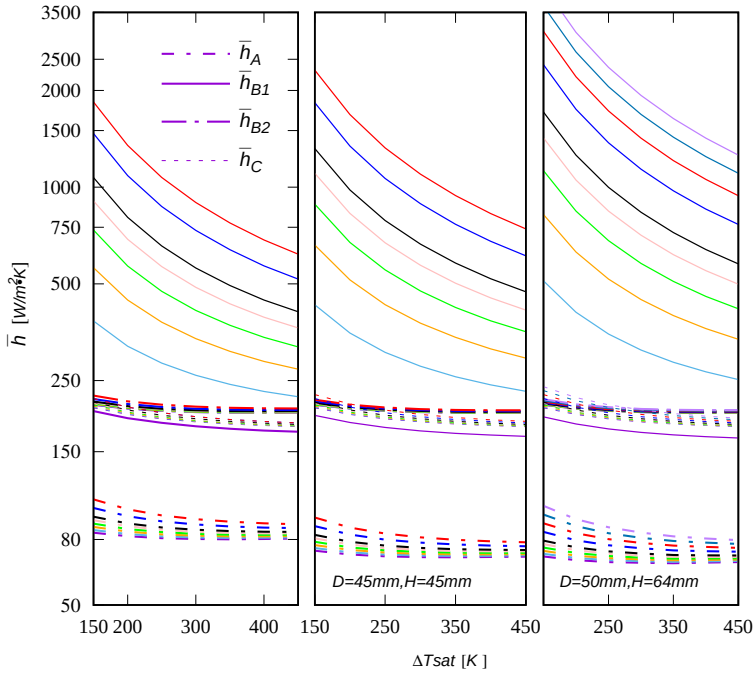

Fig. 2.13: Predicted average heat transfer coefficients on each surface of the vertical cylinders for ΔT_{sub}=0 to 20K

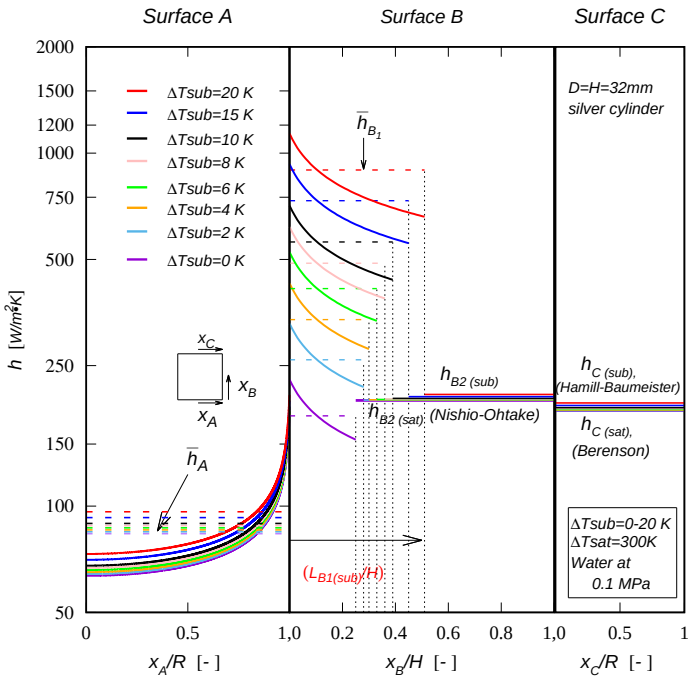

(a) D=32mm, H=32mm

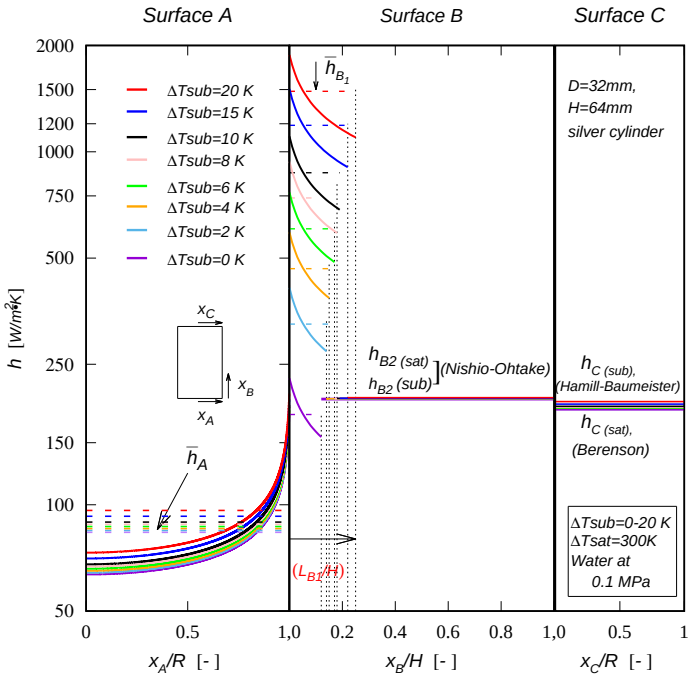

(b) D=32mm, H=64mm

Fig. 2.14: Predicted local and average heat transfer coefficient on saturated and subcooled film boiling

Chapter 3

Discussion on Experimental Result on Lower Limit of Film Boiling

Quenching expriment on the transient film boiling heat transfer with a vertical finite-length cylinder to quiescent saturate and subcooled water at atmosphric pressure have been carried out consistently to investigate the film boilng phenomena around the surfaces of the vertical cylinder. The experiment is performed by keeping the bulk temperature of the water constant and the temperature variation at the center of the heated cylinder is recorded by a data acquainting/control unit or oscilloscope with a simpling time of 0.05 second near the lower limit of film boiling. The experimental apparatus used in film boiling experiment have been already described in details in Fig. 3.1. In this study, the collapse phenomena of vapor film in the transient film boiling around the finite-length vertical cylinder of silver is examined by doing quenching experiment in saturated and subcooled water at atmospheric pressure. Experimental observation on film boiling phenomena, we have already confirmed that the film collapse starts from the lower corner of the vertical finite-length cylinder. However, the prediction of the surface temperature by using the average heat transfer coefficients for each surfaces, the downward facing bottom, vertical and upward facing top surfaces, gives that the lowest temperature point on the cylinder surface might be at the upper corner but that the estimated maximum temperature difference on the cylinder surface is below only 3K for silver cylinder with 32×32 diameter and length. Although, the local heat transfer coefficient at the lower corner of the cylinder is high enough to start the film collapse, so we consider more experimental investigation on the film collapse are needed. Therefore, in this chapter, we performed again the film boiling experiments with the vertical finite-length cylinder of silver to the saturated and subcooled water by using the higher speed video camera of 10000 frames per second with the help of trigger mode and discussed the behavior of the vapor film near the lower limit of the film boiling by frame by frame investigation of the recorded movies.

3.1 Experimental Apparatus and Procedure

3.1.1 Apparatus

The experimental apparatus is made up of (1) a boiling bath, (2) a lifting/submerging device, (3) an electronic furnace for the heating of the test cylinder, (4) an observation device and (5) data acquisition unit. A schematic view of these experimental apparatus are described in detail in Fig. 3.1.

A glass box with 300×300×600mm is placed inside the boiling bath and two submerged heaters of 2 kW power are placed between the boiling bath and the glass box, four windows are attached on the side and bottom walls of the boiling bath for observation of boiling phenomena by eye and video camera. In order to heat constantly the bulk liquid up to the prescribed temperature and to prevent bubbles generated around the two submerged heaters from disturbing the bulk liquid. The liquid is water cleaned through an ion-exchange resin. In the previous experimental study on film boiling heat transfer by quenching method, 18 kinds of silver cylinder with flat top and bottom surfaces are tested in saturated and subcooled water. For the saturated film boiling experiments, the diameter and length of test cylinders range from 8 to 100mm and from 8 to 160mm, respectively. For the subcooled film boiling experiments, the diameter and length are

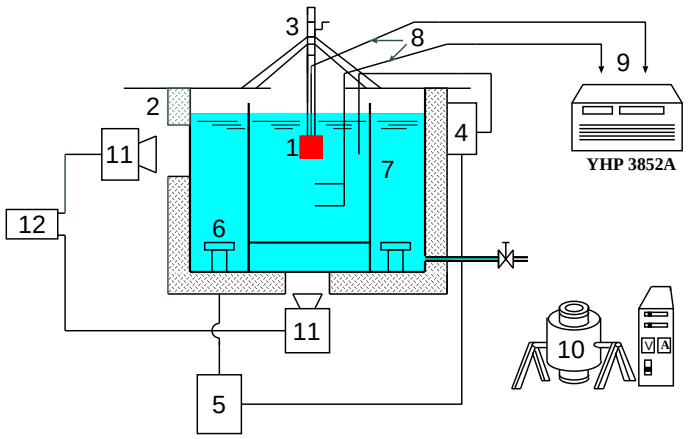

1. Test cylinder 2. Boiling bath 3. Lifting device
4. Temperature controller 5. Power controller 6. Immersion heater
7. Glass box 8.K-type thermocouple 9. Data acquisition
10. Electric furnace 11. Video Camera 12. Video recorder

Fig. 3.1: Experimental apparatus

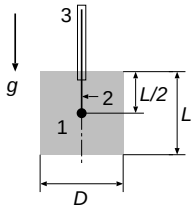

1. Silver cylinder
2. K-type sheath thermocouple (ϕ1mm)
3. Supporting stainless tube (ϕ3mmxϕ2mm)

D [mm]	*L* [mm]			
8	32	64	80	160
10	30			
15	16	32	64	
32	8	16	32	64
45	45			
50	8	16	32	64
100	8			

Fig. 3.2: Dimension and location of the thermocouple on the test cylinder

32×16, 32×32, 32×64, 45×45, 50×16, 50×32 and 50×64mm, respectively, and the degree of liquid subcooling, ΔT_{sub} range from 2 to 30 K. One sheathed K-type thermocouple with outside diameter of 1mm is placed on the cylinder axis through a stainless steel support tube to measure the transient temperature of the test cylinder. For the cylinder with 45mm in diameter and length, another sheathed K-type thermocouple is placed at the position 2mm inside the side wall of a cylinder with a depth of 22.5mm to examin a temperature change in the cylinder due to liquid subcooling effect. The dimension of the test cylinders and location of thermocouple are illustrated in Fig. 3.2. This previous experimental data are used in comparing the average heat flux of the tested cylinder and predicted heat flux by using predicted average and local heat transfer coefficient on each surface of the cylinder.

3.1.2 Procedures

Prior to heating, the surface of the test cylinder was mirror-finished by a diamond compound and made clean by alcohol to keep the surface condition constant. After heating up the cylinder to the designated degree(that is about 600°C for silver and stainless steel cylinder, about 500°C for aluminium cylinder) by an electric furnace, the test cylinder is submerged with a depth of 100mm into the saturated or subcooled water at atmospheric pressure by a lifting device and cooled down to the bulk liquid temperature of the water. The temperature history during quenching is recorded by a data acquainting/control unit with a simpling time of 0.25 secondor or by an oscilloscope with a simpling time of 0.05 second near the lower limit of film boiling. Duration of transfering time from the electric furnace to the boiing batch is kept to be minimum and its not recorded in the recorded data. The film boiling phenomena around the cylinder were observed by visual and also still photograph and high-speed video camera. Just start the film to be collapse, the end trigger mode is on because it take only some milisecond and can interpret with the recorded frame by frame.

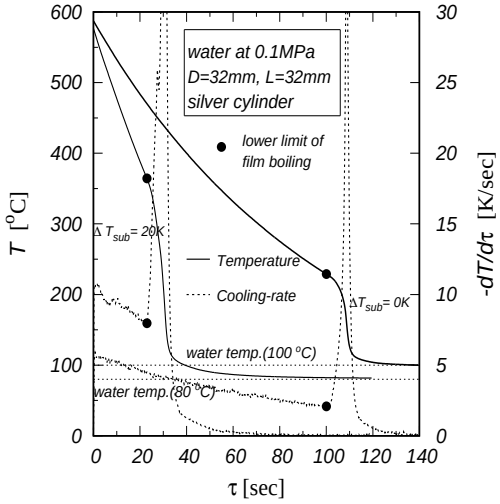

(a) Cooling curve and cooling rate

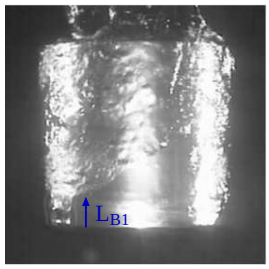

(b) saturated film boiling at τ=100.04 [sec], $\Delta T_{\rm sat}$=128 [K], ($\Delta T_{\rm min}$ ≅127 [K]) $L_{\rm B1}$=7.87mm film collapse ↓ lower corner

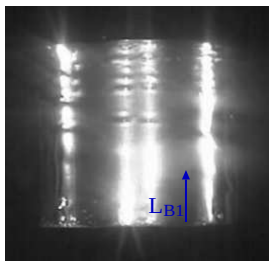

(c) subcooled film boiling at τ=22.41 [sec], $\Delta T_{\rm sat}$=272 [K], ($\Delta T_{\rm min}$ ≅264 [K]) $L_{\rm B1}$=16.26mm film collapse ↓ lower corner

Fig. 3.3: Experimental results on cooling curve, cooling rate and film boiling phenomena on saturated and subcooled liquid

3.1.3 Experimental results

The inside part of the test cylinder is assumed to be cooled uniformly and its temperature field is calculated as a lumped parameter system as the cylinder is made of silver with high thermal conductivity. Thus, the heat flux averaged on the total surface, q, is given as

$$q = Q/A = -\rho c \frac{V}{A}\frac{dT}{d\tau} \tag{3.1}$$

where A, c, T, V, ρ, τ and $dT/d\tau$ are total heating surface, specific heat, temperature, volume, density, time and cooling rate respestively. The lumped parameter system adopted in the present study, i.e., the validity to calculate the heat flux using Equation 3.1, is confirmed through numerical calculation of two-dimensional unsteady heat conduction in the test cylinder and small Biot number which was estimated as less than 0.06.

The experimental results on cooling curve , cooling rate and behavior of the vapor film around the silver cylinder of 32mm×32mm diameter and length are shown in Figs. 3.3(a), (b) and (c), respectively, for saturated and subcooling film boiling. Figure 3.3.(a) is the cooling curve and cooling rate for the saturated film boiling $\Delta T_{\rm sub}$ =0 and subcooling film boiling $\Delta T_{\rm sub}$ =20K. The vertical axis is the measured temperature at the center of the cylinder and horizontal axis is the time. A symbol of • on each cooling curve and cooling

rate shows the lower limit of film boiling. As degree of subcooling increased 0 to 20K , the slope of the curve in the film boiling region becomes greater and the point at the lower limit becomes higher and also the cooling rate is faster. It also can be observed that the film boiling phenomena in the film boiling region and near the lower limit of film boiling from the quenching experiment. Figure 3.3(b) is the photo taken during saturated film boiling, the bottom surface of the test cylinder is covered with a stable vapor film having a smooth vapor-liquid interface. The vapor generated under the bottom surface flows along the surface and turns upward at the bottom edge and goes up along the lateral surface. The vapor-liquid interface at the vertical surface is smooth at the region near the bottom edge and wavy near the top edge. These two regions on the vertical surface can be divided by the length L_{B1}. It was always seen that there is a wavy vapor-liquid interface at the upward-facing horizontal surface of the cylinder. As the case of subcooled film boiling, the vapor film thickness leads to decrease as increased in ΔT_{sub} and the length of the smooth vapor-liquid interface, L_{B1} also increased simultaneously as shown in Fig. 3.3(c). From the visual and photographic observation and also experimental results on solid-liquid contact on heating surface, it was already confirmed that film collapse start from the lower corner of the vertical surface in both saturated and subcooled film boiling.

In addition, we have already pointed out the location of the film collapse start; it was the lower edge of the vertical surface. So far, near the minimum-heat-flux-point, the solid-liquid contacts occur intermittently and the wet and dry area appears alternately. The rapid cooling starts when the thermal condition of the cylinder surface reaches the point where the heat flux from the cylinder surface is not large enough to evaporate the liquid on the surface. Therefore, the frequency and duration length of the solid-liquid contacts upon the cylinder surface may be the dominant factors of the surface temperature fluctutation and the mechanism of the collapse of the vapor film. In this study, the direct solid-liquid contacts near the lower limit of film boiling were observed by viewing using still photograph and the high-speed video camera. The frame rate of the high-speed video camera was set up 10000 frames per second at which the resolution of the recorded image is 1280 (horizontal)×96(vertical), and the trigger mode at the time of film collapse was used. In this setting of the video camera, it cannot catch the whole view of the test cylinder. Therefore we did the same experiments to observe the wider area that covers the lower corner of the cylinder (Imaging area [1] as described in the Fig. 3.4) and the transition region of the flow condition of the vapor film on the vertical surface (Imaging area [2] in the Fig. 3.4). As three kinds of data (bulk temperature of water, center temperature of the tested cylinder and the quenching time) are sampled and the detail verification of the film collapse phenomena around the cylinder is obtained by processing the frame-by-frame observation of the recorded movie images.

Here in this section, we need to explain the specification of the high speed video

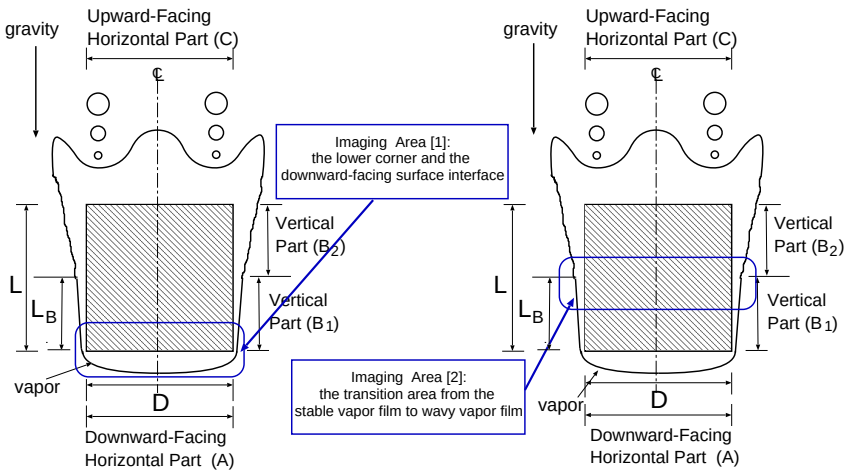

Fig. 3.4: Film boiling model and recording areas

camera (MEMRECAM fx-K3) and the usage of trigger mode. Its avaiable memory is 4GB at 1000 picture per second within 2.4 second (picture size is horizontal-1280, vertical-1024) and within 9.8 second (picture size is horizontal-640, vertical-512), at 10000 picture per second within 2.8 second (picture size is horizontal-1280, vertical-96) and within 5.2 second (picture size is horizontal-640, vertical-96) for the three mode of trigger, start, center and end. In this saturation, for the recording of 10000 frames per second, we can recorded vertical length of the picture only 96mm and recording area is divided into two parts as shown in Figure 3.4.

Figure 3.5 and 3.6 shows the detail of cooling rate near the lower limit of the film boiling at degree of subcooling, $\Delta T_{\mathrm{sub}} = 0$K and 5K for the silver cylinder of 32×32 diameter and length with the red dotted line at lower limit and at the time of film collapse in second.

3.1.4 Solid-liquid contacts and the start of film collapse at saturated film boiling

The solid-liquid contacts affect the surface temperature; it relates the cooling process and collapse of the film. In the present study we investigate the aspect of the solid-liquid contacts from measured temperature data and recorded images of the recorded video-images for both at the lower corner of the cylinder (Imaging area [1] in Fig. 3.4) and the transition area from the stable vapor film to wavy vapor film (Imaging area [2]).

For the saturate film boiling, at the lower corner of the cylinder where the very thin stable vapor film exists, the frequency of the direct contact between the cylinder wall and liquid is increasing slightly before the lower limit of film boiling and reaches to the peak number of the solid-liquid contact, as shown in the Fig.3.7. Then this frequency starts

decreasing because the area of continuous liquid film starts increasing after the initiating of the film collapse. The behaviors of the vapor film at the L2 region of the cylinder (see Fig.3.8) for saturated film boiling, are different from those at the lower region of the vertical cylinder shown in the Fig.3.7. In this region as shown in Fig.3.8, at the film collapse point that is determined by the analysis of the recorded video images and denoted by '1', the cooling rate already started increasing and the fluctuation of the solid-liquid contacts rapidly decrease. The frequency of the contacts between the liquid and the lower surface of the cylinder wall is increasing after minimum-heat-flux-point in the results for this region. This suggests that the vapor collapse occurs at first at the lower corner at the minimum-heat-flux-point, and this collapse propagates upward. After this collapse reaches to this imaging area, the frequencies of the solid-liquid contact decrease drastically.

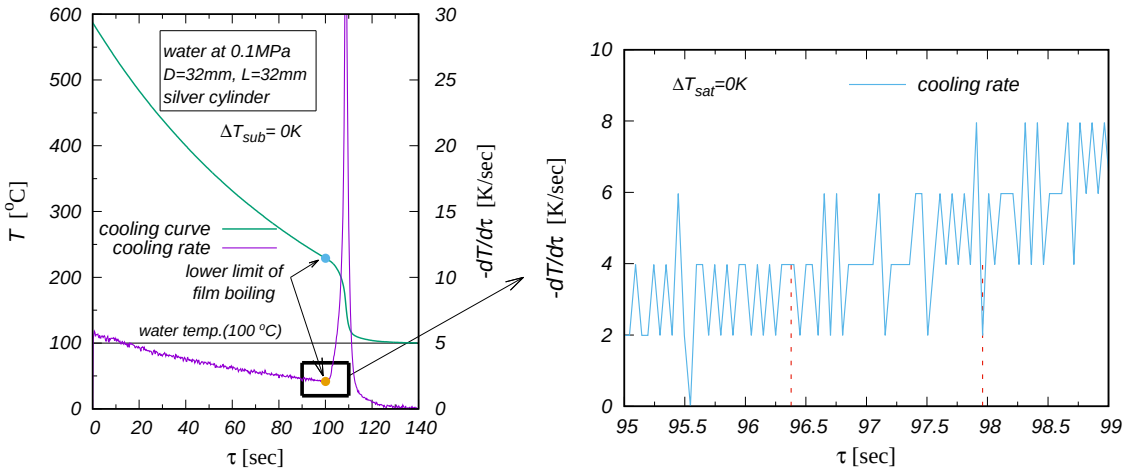

Fig. 3.5: Cooling curve and cooling rate near the lower limit of saturated film boiling

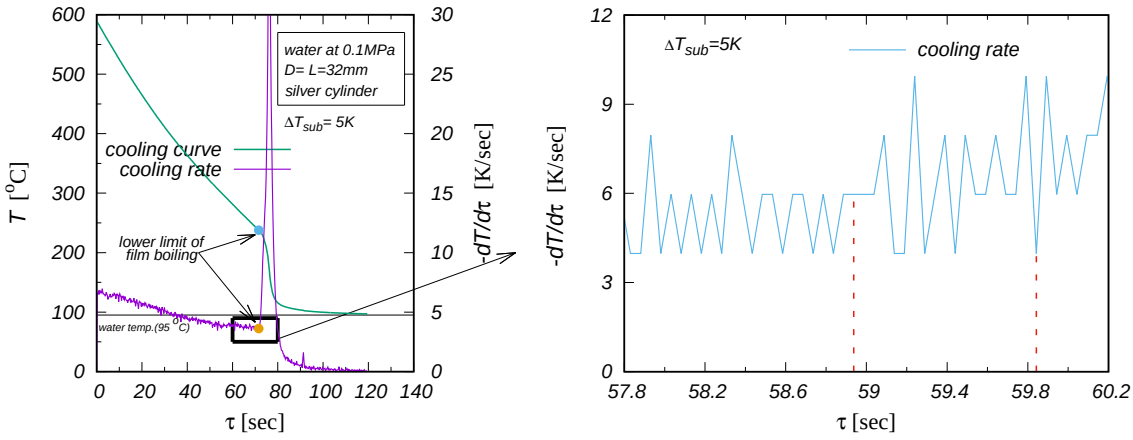

Fig. 3.6: Cooling curve and cooling rate near the lower limit of subcooled film boiling

(a) Photo image at the point 1(96.3787 sec)

(b) Photo image at the point 2(97.9600 sec)

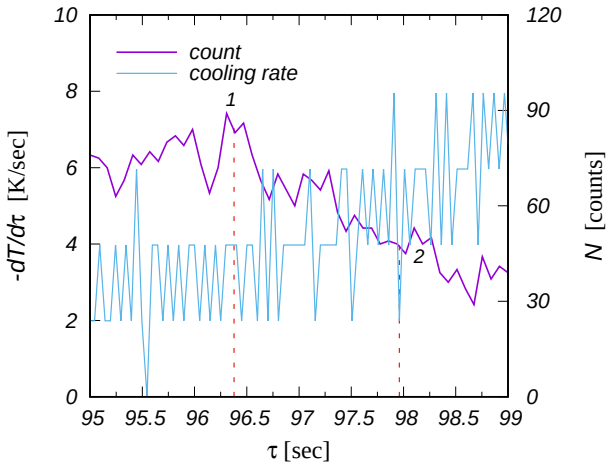

Fig. 3.7: Solid-liquid contacts at the lower part of the vertical surface (L1) for ΔT_{sub}=0K

(a) Photo image at the point 1 (67.2900 sec)

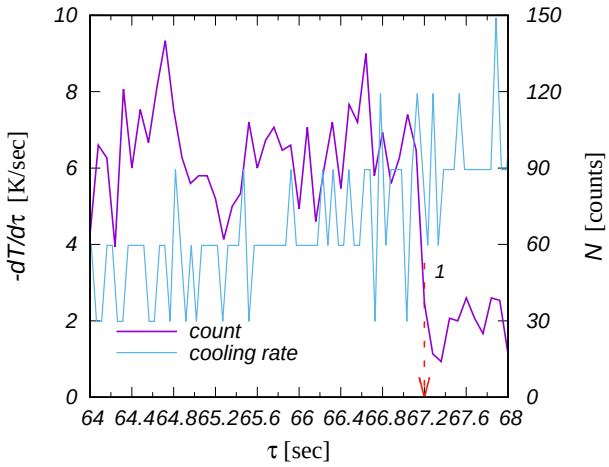

Fig. 3.8: Solid-liquid contacts at the region L2 for ΔT_{sub}=0K

3.1.5 Solid-liquid contacts and the start of film collapse at subcooled film boiling

In subcooled film boiling, the heat transfer from the vapor liquid interface to the liquid increases with increasing ΔT_{sub} and the energy going to the vapor phase decreases and as a result vapor film thickness is more thinner than saturated condition. As the vapor film is thin, neglectable amount of solid-liquid contacts were likely to occur and the number of solid-liquid contacts start to increase from the lower limit of film boiling as cooling rate also increasing at the transition to the turbulent interface, L2. The temperature at the cylinder wall lower with the increasing the average time per count as the next the surface

temperature difference corresponding to the film collapse must be negative value as the change in surface temperature due to the contacts between the cylinder surface and the liquid increase sufficient or sharply increasing. As the cylinder wall is already covered with the liquid in some area and there is less number of solid-liquid contacts at that time and the wall temperature is not high enough to evaporate the vapor.

For the comparison, Fig. 3.9 to 3.12 shows the number of counting solid-liquid contacts

(a) Photo image at the point 1(58.9371 sec)

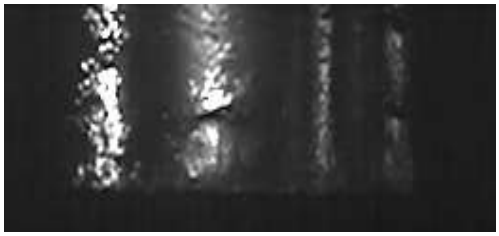

(b) Photo image at the point 2(59.8420 sec)

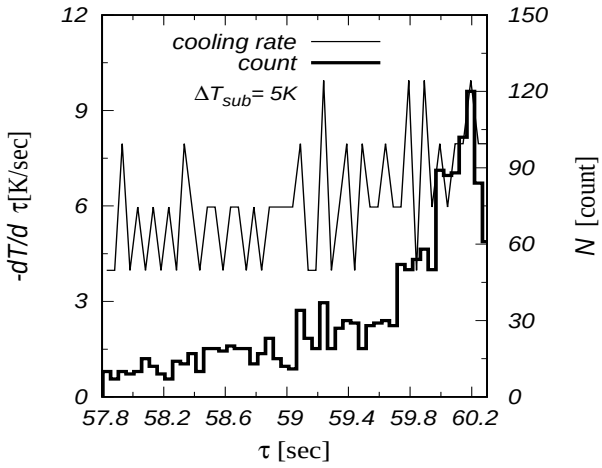

Fig. 3.9: Solid-liquid contacts at the lower part of the vertical surface (L1) for ΔT_{sub}=5K

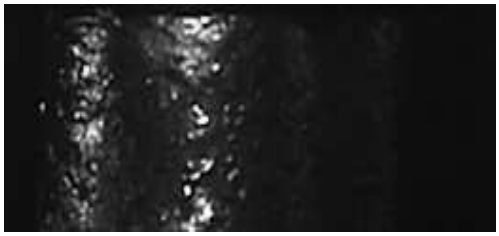

(a) Photo image at the point 1 (68.7360 sec)

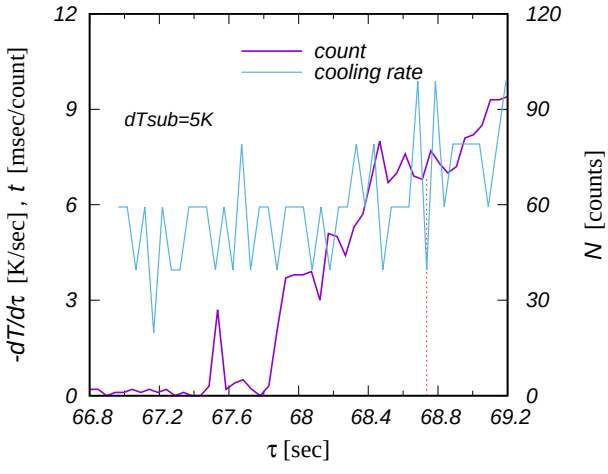

Fig. 3.10: Solid-liquid contacts at the region L2 for ΔT_{sub}=5K

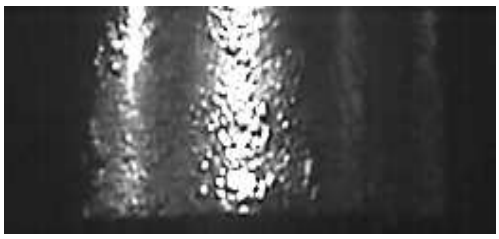

(a) Photo image at the point 1(52.1126 sec)

(b) Photo image at the point 2(52.2610 sec)

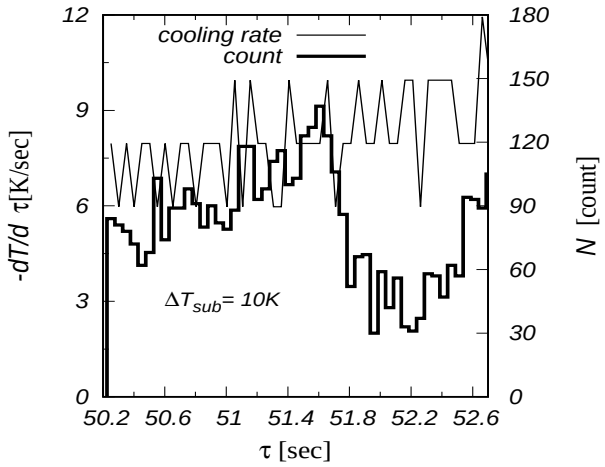

Fig. 3.11: Solid-liquid contacts at the lower part of the vertical surface (L1) for ΔT_{sub}=10K

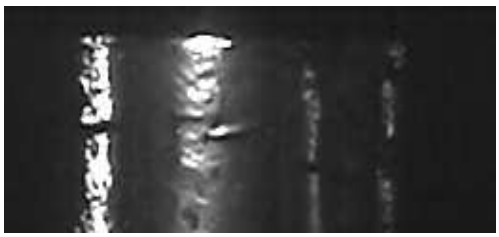

(a) Photo image at the point 1 (51.7350 sec)

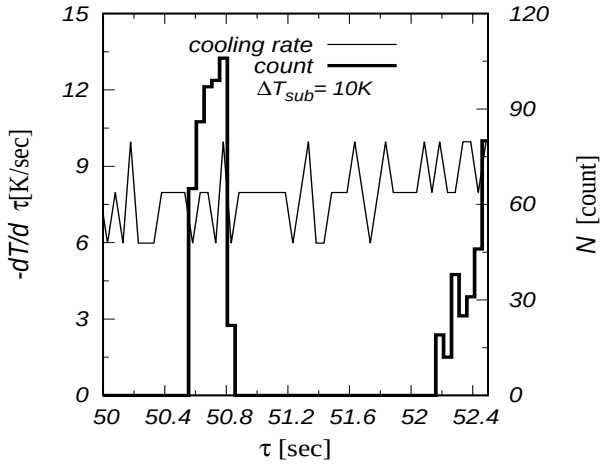

Fig. 3.12: Solid-liquid contacts at the region L2 for ΔT_{sub}=10K

at the imaging area I and II with the photo image (with the time) at lower limit of film boiling. Moreover, the time that the vapor film began to collapse is observed on the basis of the image form the high-speed video camera.

3.1.6 Discussion on experimental result on lower limit of film boiling corresponding to the vapor film collapse and predicted local heat transfer coefficients

The vapor film collapse of the film boiling phenomena is formed the lower end of the cylinder, where the vapor film becomes the thinnest. In saturated boiling, the number of contacts decreased with the lower limit of film boiling as the boundary, the time from ripple generation to disappearance per solid-liquid contact increases but the solid-liquid contact increases as the result. As the degree of subcooling increased as the cooling rate rises and the vapor film became thin and stable in any of image area I or II. Also as the degree of subcooling is higher, the time from generation of ripple due to solid-liquid contact per one time to disappearance becomes shorter. When the degree of subcooling is increased, the vapor film becomes thin and stable. Particularly, at subcooling degree of ΔT_{sub}=10K as the film becomes too thin, solid-liquid occurance due to a slight distrubance of the vapor-liquid interface. Also, since the vapor film is too thin, the distance betweeen the heat transfer surface and the liquid is closed and solid-liquid contact cannot be increased.

Since, solid-liquid contact is thought to be affected the temperature change, it related to the cooling process and collapse point of film boiling. The region where the vapor

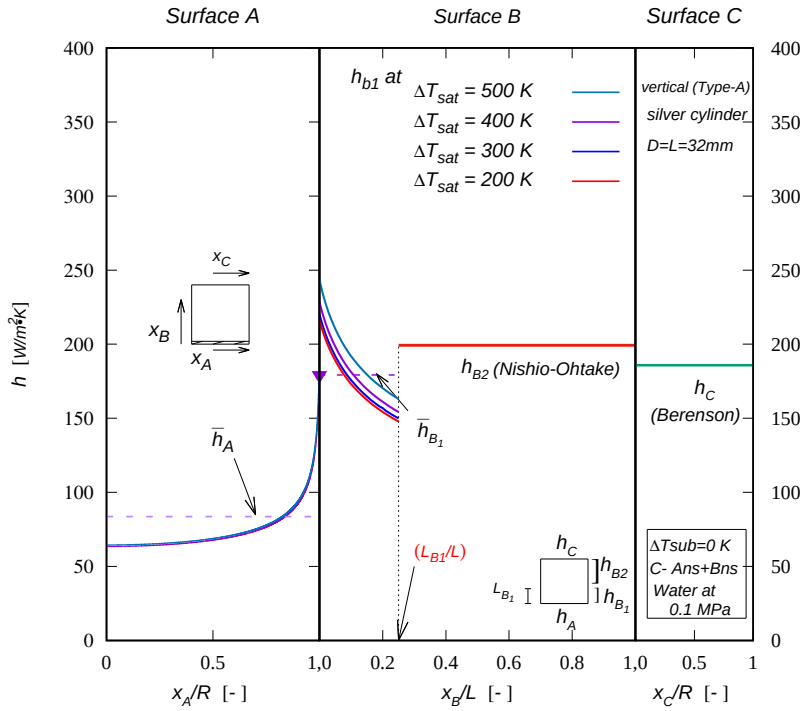

Fig. 3.13: Predicted local heat transfer coefficients at the corner of the bottom surface and vertical lateral surface of the vertical cylinder

film collapse associated with the lower limit of film boiling occurs is at the lower end of the vertical cylinder where the vapor film thickness is the thinnest on the heat transfer surface. The state of solid-liquid contact at the lower limit of film boiling and the time at whih the film collapse start are shown in Fig. 3.12.

Figure 3.13 show the local heat transfer performance at the lower corner of the vertical cylinder, which is at first (1.0) point on x-axis of the figure where local heat transfer rate at the lower end of the vertical surface is higher than the average heat transfer rate at that surface, on the other hand the heat transfer rate at the upper end of the vertical cylinder also give higher value than other surfaces. Moreover, the local heat transfer rate at the end of the bottom surface is as high as average heat transfer rate at the upward facing horizontal surface. The heat transfer performance upon these two corner can be clear when prediction the surface temperature distribution is predicted by applying these predicted heat transfer rate as a boundry condition.

Chapter 4

Analysis on Temperature Distribution on the Surface of the Vertical Finite-Length Cylinder

4.1 Two-Dimensional Unsteady Heat Conduction Equation

So far, we have already defined that the minimum heat flux point as a lower limit of the film boiling region because our primary object was the heat transfer performance in the film boiling region and it also able to be determined by the measured temperature at the center of the cylinder. To investigate the difference between the temperature at the center of the cylinder and at the surface of the cylinder at the time near the lower limit of film boiling, we need to know the temperature measured at the center of cylinder and the surface temperature at the surface at film collapse, so numerical prediction of temperature

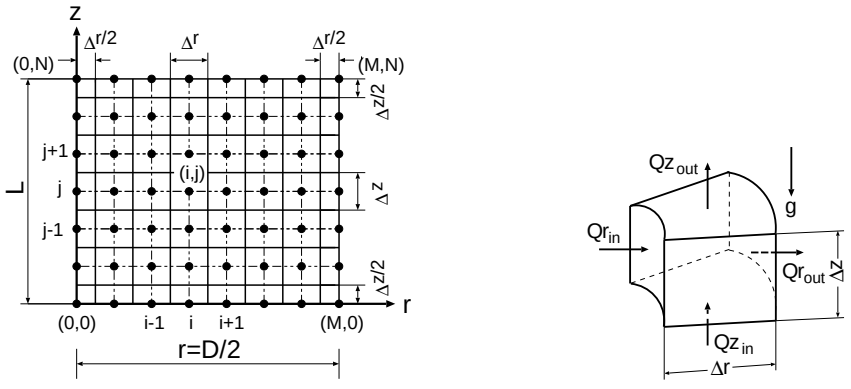

Fig. 4.1: Two-dimensional finite-difference grid

distribution of the vertical finite-length cylinder was already done by the previous author with the average heat transfer coefficient as the boundary of the cylinder. The temperature field inside the vertical finite-length cylinder is treated as the two dimensional unsteady heat conduction problem of the cylinder with the diameter, D and the length, L. In this study the radius, r=$\frac{D}{2}$ is divided into M parts, and L is divided into N parts respectively. The value of M and N are given in the following sections. The radial grid along the radius of the cylinder is designated as Δr and the vertical grid along the vertical surface of the cylinder is designated as Δz.

Fig. 4.1 shows how the number of grid point on radius of the cylinder, i=0, 1, 2, 3, ..., M, and on the vertical surface, j=0, 1, 2, 3, ..., N.

$$\left\{Q^p_{r_{in(i,j)}} - Q^p_{r_{out(i,j)}}\right\} + \left\{Q^p_{z_{in(i,j)}} - Q^p_{z_{out(i,j)}}\right\} = \rho c V\left(\frac{T^{p+1}_{(i,j)} - T^p_{(i,j)}}{\Delta\tau}\right) \tag{4.1}$$

in this equation, superscript p represents for the time increasement $p\Delta\tau$, subscript in heat flux into the element area, out heat flux out of the element area. Each term on the left side of the area is in contact with the bulk liquid (saturated or subcooled liquid) on the whole area or parts of the area, so it can be considered case by case in computation of the the surface temperature.

Figure 4.2 shows the type of the area which are at the 9 regions of interest. Here we explain how to calculate and the symbol used in calculation of the temperature distribution on type 1 $\sim$ type 9. For the temperature distribution around the vertical cylinder, the boundary condition at the surfaces are firstly given by the estimated average heat transfer coefficient and then estimated local heat transfer coefficient at the bottom surface and vertical lateral surface with smooth vapor-liquid interface. The estimated value of average

Type	Grid area
type 1	(0, 0)
type 2	($1 \leq i \leq M$-1, 0)
type 3	(M, 0)
type 4	(0, $1 \leq j \leq N$-1)
type 5	($1 \leq i \leq M$-1, $1 \leq j \leq N$-1)
type 6	(M, $1 \leq j \leq N$-1)
type 7	(0, N)
type 8	($1 \leq i \leq M$-1, N)
type 9	(M, N)

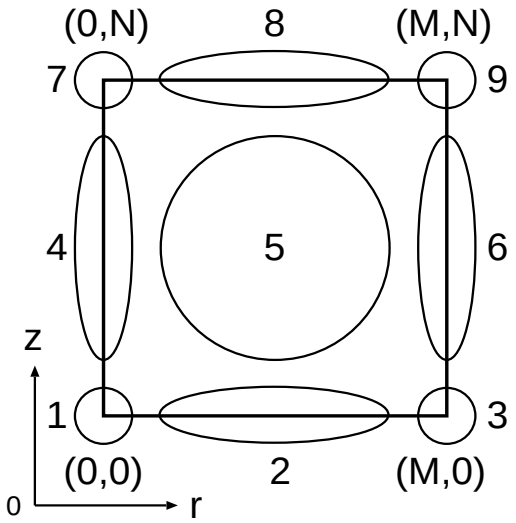

Fig. 4.2: Grid area to be calculated

heat transfer coefficients with the degree of superheat are listed in Table 5.3 in Appendix and local heat transfer coefficients at the bottom surface and lower vertical surfaces are listed in Table 5.5, 5.6 in Appendix with their position and degree of superheat. The thermal properties of the steam at saturation condition are aslo given in Appendix, which were used in calculation of heat transfer coefficient at the degree of superheat. It is also noted that in calculation the thermeal properties of the saturated steam, the properties are interpolate at the temperature at the vaopr film is calculated as the average to the measured temperature at the cylinder center and saturation temperature of water.

a	: thermal conductivity($\equiv k/\rho \cdot c$)	Δr	: Radial width of the element ($=0.5D/M$)
$A_{r_{\rm in}}$	: Element inside side wall of element	$A_{r_{\rm out}}$	: Element outside the side wall
A_z	: Top and bottom surface element area	Δz	: Vertical width of the element ($=L/N$)
$\overline{h}_{\rm A}$	: Average heat transfer coefficient at the bottom surface of the cylinder	V	: Elemental volume
$\overline{h}_{\rm B1}$	: Average heat transfer coefficient at the lower vertical surface		
$\overline{h}_{\rm B2}$	: Average heat transfer coefficient at the upper vertical surface		
$\overline{h}_{\rm C}$	: Average heat transfer coefficient at the top surface of the cylinder		
$h_{\rm A}$	: Local heat transfer coefficient at the bottom surface of the cylinder		
$h_{\rm B1}$	: Local heat transfer coefficient at the lower vertical surface		
$h_{\rm B2}$	: Local heat transfer coefficient at the upper vertical surface		

(1) type 1 : $i = 0,\ j = 0$

$$\Big(\frac{T^p_{(1,0)} - T^p_{(0,0)}}{\Delta r}\Big)A_{r_{\rm out}} + \Big(\frac{T^p_{(0,1)} - T^p_{(0,0)}}{\Delta z}\Big)A_z + \Big(\frac{1}{k}\Big)h_{\rm A}(T_{\rm sat} - T^p_{(0,0)})A_z = \Big(\frac{1}{a}\Big)\Big(\frac{T^{p+1}_{(0,0)} - T^p_{(0,0)}}{\Delta\tau}\Big)V \tag{4.2}$$

where, $A_{r_{\rm out}} = 2\pi\Big(0.5\Delta r\Big)\Big(0.5\Delta z\Big)$,
$A_z = \pi\Big(0.5\Delta r\Big)^2$ and elemental volume is
$V = A_z\Big(0.5\Delta z\Big)$ and
$\Big(A_{r_{\rm in}} = 0.0\Big)$

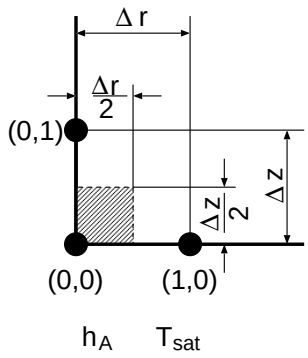

Fig. 4.3: Element including the boundary condition of the heat conduction at the center(r=0) side inner wall and boundary condition of convective heat transfer coefficient at the bottom surface (Type 1)

(2) type 2 : $1 \leq i \leq M-1,\ j=0$

$$\Big(\frac{T^p_{(i-1,0)}-T^p_{(i,0)}}{\Delta r}\Big)A_{r_{\rm in}}+\Big(\frac{T^p_{(i+1,0)}-T^p_{(i,0)}}{\Delta r}\Big)A_{r_{\rm out}}+\Big(\frac{T^p_{(i,1)}-T^p_{(i,0)}}{\Delta z}\Big)A_z+\Big(\frac{1}{k}\Big)h_{\rm A}(T_{\rm sat}-T^p_{(i,0)})A_z = \Big(\frac{1}{a}\Big)\Big(\frac{T^{p+1}_{(i,0)}-T^p_{(i,0)}}{\Delta\tau}\Big)V \tag{4.3}$$

where, $A_{r_{\rm in}}=2\pi\Big(i-0.5\Big)\Delta r\Big(0.5\Delta z\Big)$, $A_{r_{\rm out}}=2\pi\Big(i+0.5\Big)\Delta r\Big(0.5\Delta z\Big)$,
$A_z=\Big(2\pi i\Delta r\Big)\Delta r$ and $V=A_z\Big(0.5\Delta z\Big)$.

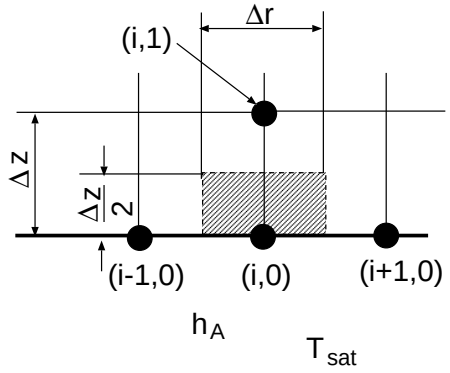

Fig. 4.4: Element including the boundary condition of the convective heat transfer coefficient at the bottom surface (Type 2)

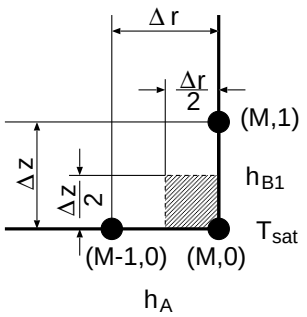

Fig. 4.5: Element including the boundary condition of the convective heat transfer at the bottom and lower vertical surfaces (Type 3)

(3) type 3 : $i = M,\ j = 0$

$$\Big(\frac{T^p_{(M-1,0)} - T^p_{(M,0)}}{\Delta r}\Big)A_{r_{\rm in}} + \Big(\frac{1}{k}\Big)h_{\rm B1}\Big(T_{\rm sat} - T^p_{(M,0)}\Big)A_{r_{\rm out}} + \Big(\frac{T^p_{(M,1)} - T^p_{(M,0)}}{\Delta z}\Big)A_z + \Big(\frac{1}{k}\Big)h_{\rm A}\Big(T_{\rm sat} - T^p_{(M,0)}\Big)A_z = \Big(\frac{1}{a}\Big)\Big(\frac{T^{p+1}_{(M,0)} - T^p_{(M,0)}}{\Delta\tau}\Big)V \qquad (4.4)$$

where, $A_{r_{\rm in}} = 2\pi\Big(M - 0.5\Big)\Delta r\Big(0.5\Delta z\Big)$, $A_{r_{\rm out}} = 2\pi\Big(M\Delta r\Big)\Big(0.5\Delta z\Big)$,
$A_z = \pi\Big(M - 0.25\Big)\Big(\Delta r\Big)^2$ and $V = A_z\Big(0.5\Delta z\Big)$.

(4) type 4 : $i = 0,\ 1 \le j \le N - 1$

$$\Big(\frac{T^p_{(1,j)} - T^p_{(0,j)}}{\Delta r}\Big)A_{r_{\rm out}} + \Big(\frac{T^p_{(0,j-1)} - T^p_{(0,j)}}{\Delta z}\Big)A_z + \Big(\frac{T^p_{(0,j+1)} - T^p_{(0,j)}}{\Delta z}\Big)A_z = \Big(\frac{1}{a}\Big)\Big(\frac{T^{p+1}_{(0,j)} - T^p_{(0,j)}}{\Delta\tau}\Big)V \qquad (4.5)$$

where,
$A_{r_{\rm out}} = 2\pi\Big(0.5\Delta r\Big)\Delta z$, $A_z = \pi\Big(0.5\Delta r\Big)^2$,
$V = A_z\Delta z$ and $\Big(A_{r_{\rm in}} = 0.0\Big)$.

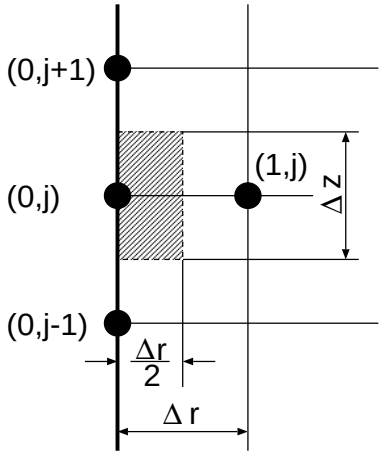

Fig. 4.6: Element including the boundary condition of insulation of the inner wall of the cylinder center (r=0) (Type 4)

(5) type 5 : $1 \leq i \leq M-1,\ 1 \leq j \leq N-1$

$$\begin{aligned} &\Big(\frac{T^p_{(i-1,j)} - T^p_{(i,j)}}{\Delta r}\Big)A_{r_{\text{in}}} + \Big(\frac{T^p_{(i+1,j)} - T^p_{(i,j)}}{\Delta r}\Big)A_{r_{\text{out}}} \\ &+\Big(\frac{T^p_{(i,j-1)} - T^p_{(i,j)}}{\Delta z}\Big)A_z + \Big(\frac{T^p_{(i,j+1)} - T^p_{(i,j)}}{\Delta z}\Big)A_z = \Big(\frac{1}{a}\Big)\Big(\frac{T^{p+1}_{(i,j)} - T^p_{(i,j)}}{\Delta \tau}\Big)V \end{aligned} \tag{4.6}$$

where,

$$A_{r_{\text{in}}} = 2\pi\Big(i-0.5\Big)\Delta r\Delta z\ A_{r_{\text{out}}} = 2\pi\Big(i+0.5\Big)\Delta r\Delta z\ A_z = 2\pi i\Big(\Delta r\Big)^2 \text{ and } V = A_z\Delta z$$

(6) type 6 : $i = M,\ 1 \leq j \leq N-1$

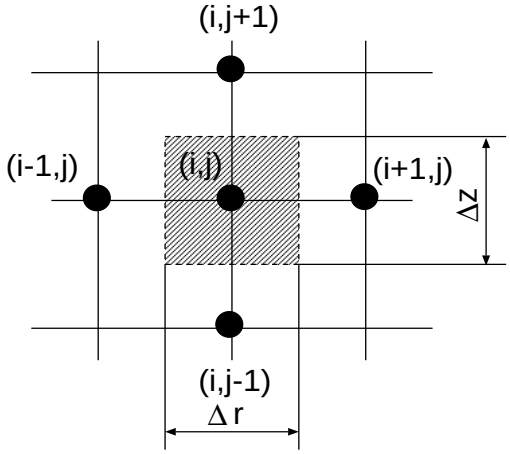

Fig. 4.7: Elements composed of heat conduction boundary only (Type 5)

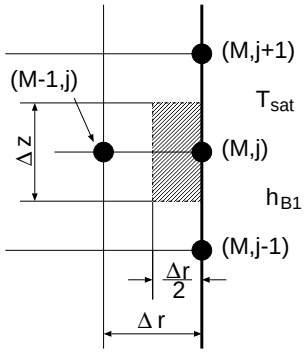

Fig. 4.8: Elements including boundary condition of convective heat transfer coefficients on the vertical wall (Type 6)

$$\Big(\frac{T^p_{(M-1,j)}-T^p_{(M,j)}}{\Delta r}\Big)A_{r_{\rm in}}+\Big(\frac{1}{k}\Big)h_{\rm B}\Big(T_{\rm sat}-T^p_{(M,j)}\Big)A_{r_{\rm out}}+\Big(\frac{T^p_{(M,j-1)}-T^p_{(M,j)}}{\Delta z}\Big)A_z +\Big(\frac{T^p_{(M,j+1)}-T^p_{(M,j)}}{\Delta z}\Big)A_z=\Big(\frac{1}{a}\Big)\Big(\frac{T^{p+1}_{(M,j)}-T^p_{(M,j)}}{\Delta\tau}\Big)V \tag{4.7}$$

where, $A_{r_{\rm in}}=2\pi\Big(M-0.5\Big)\Delta r\Delta z$, $A_{r_{\rm out}}=2\pi\Big(M\Delta r\Big)\Delta z$, $A_z=\pi\Big(M-0.25\Big)\Big(\Delta r\Big)^2$ and $V=A_z\Delta z$.

(7) type 7 : $i=0,\ j=N$

$$\Big(\frac{T^p_{(1,N)}-T^p_{(0,N)}}{\Delta r}\Big)A_{r_{\rm out}}+\Big(\frac{T^p_{(0,N-1)}-T^p_{(0,N)}}{\Delta z}\Big)A_z+\Big(\frac{1}{k}\Big)\overline{h}_{\rm C}\Big(T_{\rm sat}-T^p_{(0,N)}\Big)A_z=\Big(\frac{1}{a}\Big)\Big(\frac{T^{p+1}_{(0,N)}-T^p_{(0,N)}}{\Delta\tau}\Big)V \tag{4.8}$$

where, $A_{r_{\rm out}}=2\pi\Big(0.5\Delta r\Big)\Big(0.5\Delta z\Big)$, $A_z=\pi\Big(0.5\Delta r\Big)^2$, $V=A_z\Big(0.5\Delta z\Big)$ and $\Big(A_{r_{\rm in}}=0.0\Big)$.

(8) type 8 : $1\le i\le M-1,\ j=N$

$$\Big(\frac{T^p_{(i-1,N)}-T^p_{(i,N)}}{\Delta r}\Big)A_{r_{\rm in}}+\Big(\frac{T^p_{(i+1,N)}-T^p_{(i,N)}}{\Delta r}\Big)A_{r_{\rm out}}+\Big(\frac{T^p_{(i,N-1)}-T^p_{(i,N)}}{\Delta z}\Big)A_z+\Big(\frac{1}{k}\Big)\overline{h}_{\rm C}\Big(T_{\rm sat}-T^p_{(i,N)}\Big)A_z =\Big(\frac{1}{a}\Big)\Big(\frac{T^{p+1}_{(i,N)}-T^p_{(i,N)}}{\Delta\tau}\Big)V \tag{4.9}$$

where, $A_{r_{\rm in}}=2\pi\Big(i-0.5\Big)\Delta r\Big(0.5\Delta z\Big)$, $A_{r_{\rm out}}=2\pi\Big(i+0.5\Big)\Delta r\Big(0.5\Delta z\Big)$, $A_z=2\pi i\Big(\Delta r\Big)^2$ and $V=A_z\Big(0.5\Delta z\Big)$.

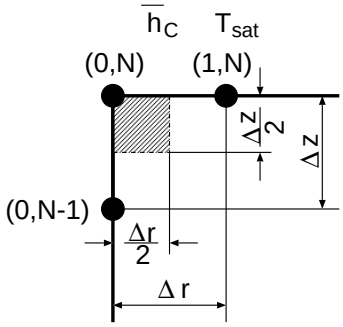

Fig. 4.9: Element including boundary condition of heat insulation at the inner wall and top wall convective heat transfer (Type 7)

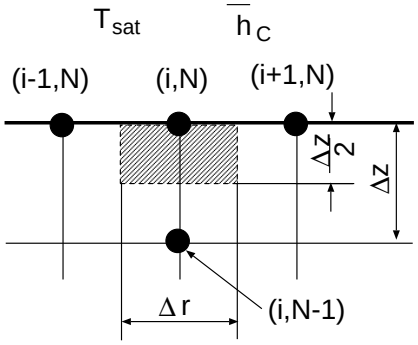

Fig. 4.10: Element including boundary condition of convective heat transfer coefficient on the top surface (Type 8)

(9) type 9 : $i = M,\ j = N$

$$\Big(\frac{T^p_{(M-1,N)} - T^p_{(M,N)}}{\Delta r}\Big)A_{r_{\rm in}} + \Big(\frac{1}{k}\Big)\overline{h}_{\rm B}\Big(T_{\rm sat} - T^p_{(M,N)}\Big)A_{r_{\rm out}} + \Big(\frac{T^p_{(M,N-1)} - T^p_{(M,N)}}{\Delta z}\Big)A_z + \Big(\frac{1}{k}\Big)\overline{h}_{\rm C}(T_{\rm sat} - T^p_{(M,N)}\Big)A_z = \Big(\frac{1}{a}\Big)\Big(\frac{T^{p+1}_{(M,N)} - T^p_{(M,N)}}{\Delta\tau}\Big)V \tag{4.10}$$

where, $A_{r_{\rm in}} = 2\pi\Big(M - 0.5\Big)\Delta r\Big(0.5\Delta z\Big)$, $A_{r_{\rm out}} = 2\pi\Big(M\Delta r\Big)\Big(0.5\Delta z\Big)$, $A_z = \pi\Big(M - 0.25\Big)\Big(\Delta r\Big)^2$ and $V = A_z\Big(0.5\Delta z\Big)$.

Although the temperature inside the finite-length cylinder is calculated from the element area of type 1 to type 9 as described in aboved figure, to consider the area in and out, the volume of the elemental area, the different formula for the element are described in each figure. For the first case average heat transfer coefficient on the vertical surface of

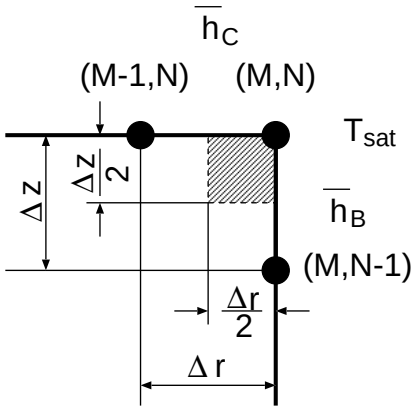

Fig. 4.11: Element including boundary condition of convective heat transfer coefficient on the top and side surfaces (Type 9)

the cylinder for the type 3, type 6 and type 9, $\overline{h}_{\mathrm{B}}$ along the vertical length of the cylinder, L changes into $L_{\mathrm{B_1}}$ and vertical length with smooth vapor-liquid interface and ($L \leq L_{\mathrm{B_1}}$) ($L > L_{\mathrm{B_1}}$) vertical length with wavy vapor liquid interface, this two interface are divided by the length $L \leq L_{\mathrm{B_1}}$, $L > L_{\mathrm{B_1}}$. For the upper surface, $\overline{h}_{\mathrm{C}}$ is applied as a boundary condition. For the bottom surface, local h_A and average heat transfer coefficient $\overline{h}_A$ are applied as the boundary condition. Prediction with local heat transfer coefficient at the lower end of the vertical surface, local heat transfer coefficient is applied as a boundary condition. For the subcooled film boiling, the length of the smooth vapor-liquid interface, (L_{B1}) changed with the degree of subcooling, its effect is not considered and the value of L_{B1} at saturation condition is considered in calculation of the temperature distribution of the cylinder. Calculation of the grid temperature $T^{p+1}_{(i,j)}$ inside the cylinder is calculated by the following equation,

$$T^{p+1}_{(i,j)} = \frac{\Delta Q^{p}_{(i,j)} \Delta\tau}{\rho_{\mathrm{m}} c_{\mathrm{m}} V_{(i,j)}} + T^{p}_{(i,j)} \tag{4.11}$$

The initial temperature at the center of the cylinder ($T^{p+1}_{(i,j)}$) was set as the temperature measured at the cylinder center, $(0, \frac{N}{2})$ and decreased with time step. The calculation is aborted when the value of the temperature at the center, (i.e at $0, \frac{N}{2}$) approached to 150°C or lower. As Equ 4.12 contained the density, specific heat and thermal conductivity of the material, these properties are changed with the temperature are described in Appendix. Table 4. (A) in appendix shows the interpolation equation to calculate the properties of the cylinder material (silver, aluminium, carbon steel and stainless steel), which is used in temperature distribution inside the cylinder. According to the thermal properties of the cylinder material, an interpolation equation was prepared by the least square method in order to take temperature dependency into account. Data at the time of interpolation formula is based on heat transfer engineering materials (3rd Edition, 4th Edition).

4.2 Stability of Numerical Calculation

The following equation shows the conditional expression for measuring the stability of the two-dimensional numerical calculation excluding the boundary condition. To satisfy the stability of numerical calculation, setting the equation in such with the grid number and $\Delta\tau$ upon thermal diffusity of the material.

$$\Delta\tau \leq \frac{1}{a}\Big(\frac{0.5(\Delta r)^2(\Delta z)^2}{(\Delta r)^2+(\Delta z)^2}\Big) \tag{4.12}$$

where $a[=k_{\mathrm{m}}/(c_{\mathrm{m}}\cdot\rho_{\mathrm{m}})]$ thermal conductivity, Δr grid element width in the radial direction of the cylinder, Δz it is the finite element width in the longitudinal direction of the cylinder $\Delta\tau$ is influenced by the size of the cylinder, the cylinder material and the number of divisions therefore, silver having the highest temperature conductivity among the common materials. (a=1.6549×10^{-4} m^2/sec)Against, diameter D=32mm, length L=32mm and diameter D=45mm, length L=45mm with two kinds of cylinders, radial division number of cylinder M and the number of divisions in the vertical direction N As a parameter, the limit value of the stable evaluation of calculation was obtained. The results are shown in Table 4.1.

Table 4.1 Limit value of $\Delta\tau$ and divided grid for silver

Cylinder [mm]	Grid no.	grid [mm]	silver [sec]
D=32	M=N=8	Δr=2.0, Δz=4.0	9.668×10^{-3}
L=32	M=N=10	Δr=1.6, Δz=3.2	6.188×10^{-3}
	M=N=20	Δr=0.8, Δz=1.6	1.547×10^{-3}
	M=N=40	Δr=0.4, Δz=0.8	3.867×10^{-4}
D=45	M=N=8	Δr=2.8125, Δz=5.625	0.0191
L=45	M=N=10	Δr=2.25, Δz=4.5	0.0122
	M=N=20	Δr=1.125, Δz=2.25	0.0031
	M=N=40	Δr=0.5625, Δz=1.125	0.000765

From Table 4.1, when the value of $\Delta\tau$ is more than or equal to 0.001, the stability of the numerical calculation can be obtained. But in this calculation, we use $\Delta\tau$=0.0001 for both case.

4.3 Flow Chart for the Numerical Calculation of the Temperature Distribution of the Vertical Finite-Length Cylinder

Figure 4.10 shows flow chart for the numerical calculation of the temperature distribution of the vertical finite length cylinder. To predict surface temperature with the local heat transfer coefficient, there is the input file as the name caseA-ns-newbar.dat which is the dimensionless vapor film thickness at the bottom surface of the cylinder which also calculated for the diameter and length 32mm. In declearing the variable, for the calculation of the temperature with local heat transfer coefficient the valiable type is changed for local heat transfer coefficient at the bottom surface and lower vertical lateral surface. Moreover, for the subcooling film boiling case, there is necessary to input the degree of subcooling. Numerical calculation of the temperature inside the cylinder is originally predicted by the average heat transfer coefficients at the bottom surface, vertical lateral surface and upward facing horizontal surface. In this study, the local heat transfer coefficient at the corner of the bottom surface and vertical lateral is applied as the boundary condition of the bottom surface and lower vertical surface and predict the temperature distribution of the cylinder.

4.4 Results and Discussion on Calculation of Temperature Field inside the Cylinder with Average and Local Heat Transfer Coefficient

Temperature distribution at the surface of the cylinder is numerically calculate by using local heat transfer coefficient at the bottom surface and vertical lateral surface with smooth vapor-liquid interface. Here, we divided the radius of the cylinder into 40 grids and on each grid at the bottom surface (that is the bottom boundary), each value of the local heat transfer coefficient already predicted are substituted. And also at the vertical lateral surface with smooth vapor liquid interface, first we consider the length of the smooth interface from the bottom the vertical surface (which is always change due to the degree of liquid subcooling) and the value of local heat transfer coefficient at the vertical grid point change according to the degree of subcooling. Here also each grid point at

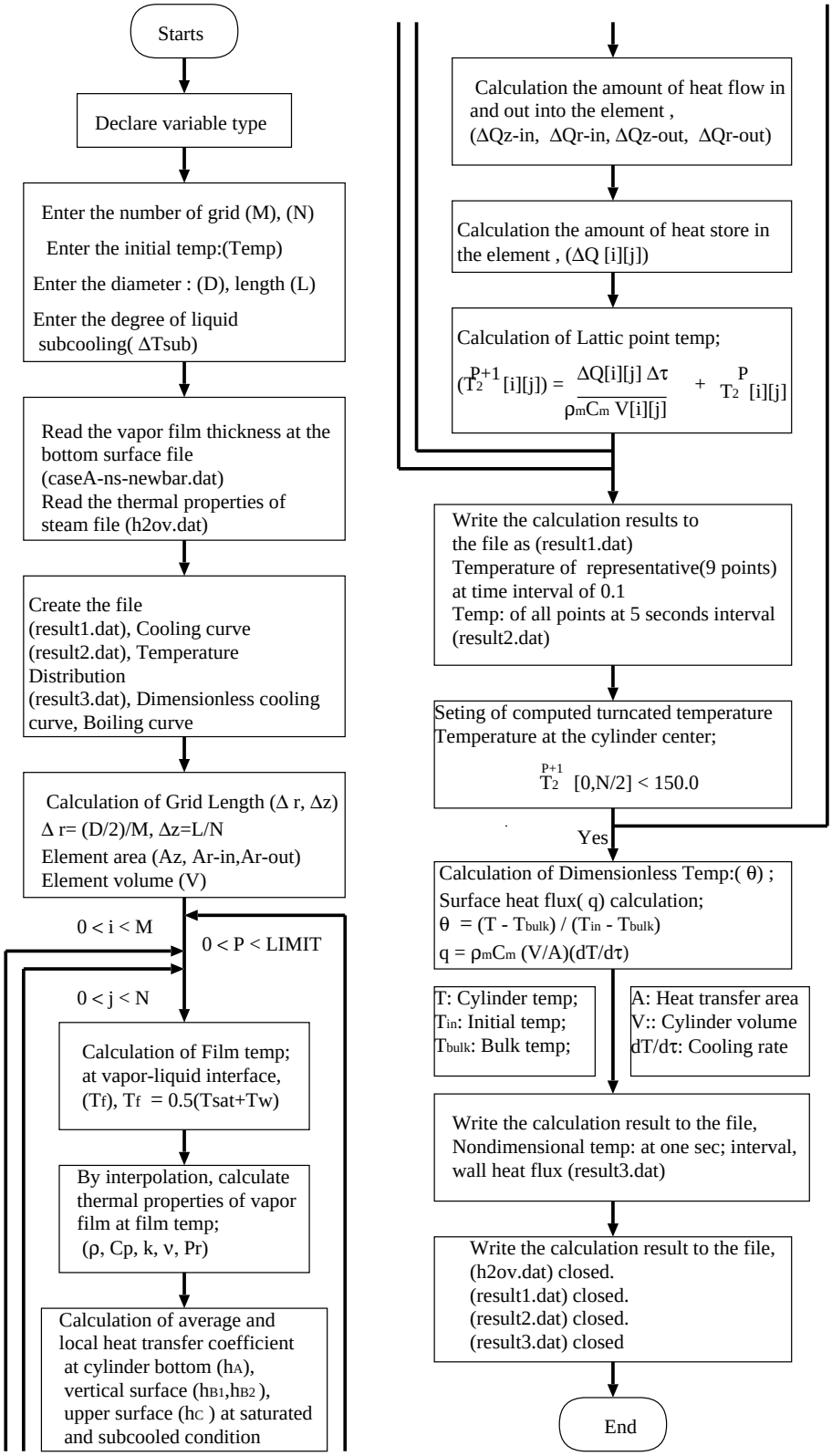

Fig. 4.12: Flow chart for the temperature distribution of the cylinder in saturated and subcooled film boiling

the lower vertical surface (that is at the vertical boundry of the grid point) we substituted the value already predicted. The vertical length over the vapor liquid interface and upper horizontal surfaces are the boundery condition as alrady predicted by the average heat transfer coefficient as we considered as these two boundary conditions are not varies with the position. Finally we found that the temperature distribution with the local heat transfer coefficient at the bottom surface and lower vertical surface gives , the lowest temperature point at the lower corner of the cylinder and its concide with the experimental results of film collapse start at the lower corner. Figure 4.12 compare the center, upper corner, lower corner temperature by applying average and local heat transfer coefficient. The temperature contour of the vertical finite length cylinder of silver are also compared by the boundary conditon with average and local heat transfer coefficient. In saturated film boiling, the temperature different between the minimum heat flux point temperature (lower limit of film boiling) and the collapse point temperature is not dominant but in subcooled film boiling, as the degree of liquid subcooling increased, the temperature difference between the film collapse point and minimum heat flux point temperature also increased. This phenomena is also the same between the temperature at the lower and upper corner of the vertical finite-length cylinder. Moreover, the temperature difference at the center of the cylinder from the lower or upper corner of the vertical cylinder are campared at the time of lower limit of film boiling (i.e the center temperature is lower limit temperature). For the saturated film boiling, the difference between lower and upper corner temperature is just 0.2 and for the subcooling film boiling, ΔT_{sub}=5K, the difference between lower and upper corner temperature is 2.88 and for the subcooling film boiling, ΔT_{sub}=10K, the difference between lower and upper corner temperature is 5.426 and is increased in increasing degree of liquid subcooling.

Figure 4.11 shows the comparison of predicted temperature at the center, upper corner and lower corner of the vertical silver cylinder for the degree of subcooling, ΔT_{sub}=0K, 5K, 10K, 15K, 20K and 30K. There are twelve figure in Fig. 4.11 to show the resuls on the predicted temperature distribution at the cylinder center (at 0,N/2), at the lower corner of the cylinder (at M,0) and at the upper corner of the cylinder (at M,N) for the silver cylinder of diameter and length 32mm respectively. The left hand side figures are predicted temperature by applying average heat transfer coefficient as a boundary condition in all boundaries of the cylinder and it was found that the upper corner temperature is lower than the lower corner temperature. The right hand side figures are predicted temperature by applying the local heat transfer coefficients at the bottom surface and vertical lateral surface with smooth vapor-liquid interface as the boundary condition and for the vertical lateral surface with wavy vapor-liquid interface and upward facing horizontal surface, the boundary condition were not changed, its results were like that, the lower corner temperature is to be the lowest temperature. The number of grids on radial direction, vertical direction and time step are the same for all figures. The temperature variation with the time were described as at the center temperature(represented by blue line), upper corner temperature (represented by red dotted line) and lower corner temperature (represented by green dotted line) in all figures. First row of figure is the temperature variation at above mention three location for the ΔT_{sub}=0K, which is saturate conditon Fig. 4.11 (a) and (b). The second row is for the temperature variation at ΔT_{sub}=5K Fig. 4.11 (c) and (d) and the third row is the temperature variation at ΔT_{sub}=10K Fig. 4.11 (e) and (f). In saturated condition, as we applied high thermal conductivity material in prediction surface temperature distribution, the temperaure difference between three difference location are not so much and the difference between the lower and upper corner temperature is about 0.2 in prediction with local heat transfer coefficient and 1.02 in prediction with average heat transfer coefficient. The temperature are compared with the same input temperature at the center and the time at the compare temperature are the same. For the subcooled film boiling, the temperature difference between the upper corner and lower corner temperature are increased in increasing degree of liquid subcooling that is (ΔT_{sub} increasing). For the high degree of liquid subcooling, such as ΔT_{sub} =30K, the difference between the upper corner temperature and lower corner temperature is smaller in prediction with local heat transfer coefficient at bottom surface and lower vertical surface as shown in Fig. 4.11 (k) and (l). In numerical calculation of the temperature distribution of the vertical cylinder, the radius and height of the cylinder is divided into 40 grid point and the temperature on each grid points are predicted firstly on one second interval on 9 interesting point and secondly on time inteval of 5 second over the entire cylinder. The predicted temperature contour during the cooling process are described in Figure 4.12 to 4.17 with their time for degree of subcooling ΔT_{sub} = 0K, 5K, 10K,

15K, 20K and 30K. In Fig. 4.12, the temperature contours at first 75 second and 100 second interval were described as different boundary condition at bottom surface and lower vertical surface. As the sturated film boilin, the decreasing rate of temperature is lower in comparing with the subcooled film boiling and temperature decreasing rate also low. Here we described the predicted temperature decreasing rate at time 75sec, 100sec. In saturated film boiling, the temperature distribution with average heat transfer coefficient in all boundary condition of the cylinder, the result shows lowest temperature point is at the upper corner of the vertical cylinder. As the average heat transfer rate at the upper boundary of the cylinder is greater than the lower boundary and also the heat transfer rate at the upper region of the vertical surface also higher heater transfer rate than lower region of the vertical surface. So we change the boundary condition at the bottom surface and lower vertical surface with local heat transfer coefficient and then predict the temperature distribution. In this result, the lowest temperaure point is till at the upper corner of the vertical surface but the temperature difference between the lower corner temperature and upper corner temperature is less than by rediction with average heat transfer coefficient. Although the local heat transfer coefficient at the lower end of the vertical surface is higher than other surfaces, the local heat transfer rate at the end of the bottom surface is still lower than others surfaces and also the local heat transfer rate at the lower vertical surface also highest rate at only at the lower end of the vertical surface and it decrease with height and its smaller than average heat transfer rate as its approach to the interface of smooth to wavy vapor-liquid interface. However the highest heat transfer rate near the lower limit of film boiling influence upon the film collapse and its start from the lower corner of the vertical lateral surface in saturated film boiling. For the saturated film boiling the lower limit of film boiling is at the time of round about 95 sec and we can see the temperature contour near the lower limit of film boiling as in Fig. 4.12 (a), (b) and (c), (d). Furthermore, we have already predicted the temperature distribution of the vertical finite-cylinder of silver, with the boundary condition at the lower vertical surface of the cylinder which is divided by the grid number and the first two grid is given by the boundary condition with local heat transfer coefficient and the other grid are given by the average heat transfer rate and the boundary condition on bottom surface is the local heat transfer rate, it was found that the lowest temperature point is at the lower corner of the vertical cylinder and its agrees with the observation phenomena on film collapse start from the lower corner of the vertical surface.

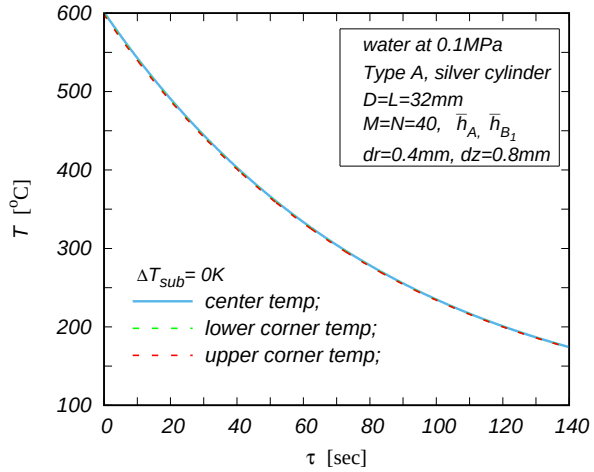

(a) $\Delta T_{sub} = 0$[K]

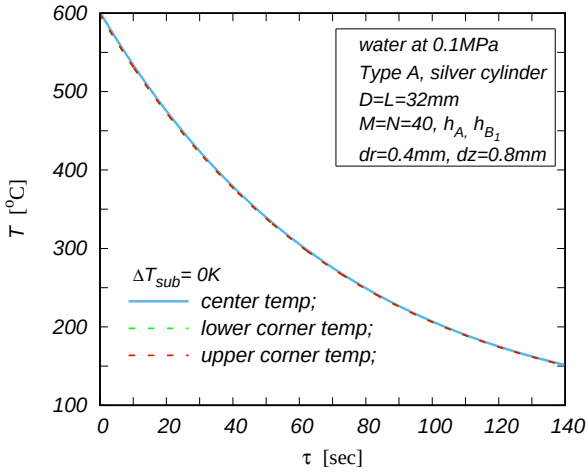

(b) $\Delta T_{sub} = 0$[K]

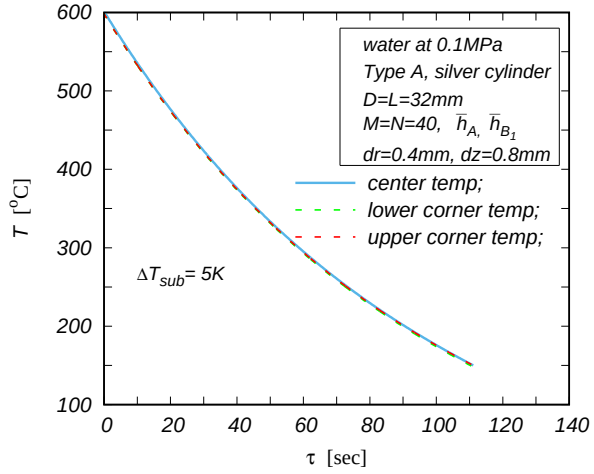

(c) $\Delta T_{sub} = 5$[K]

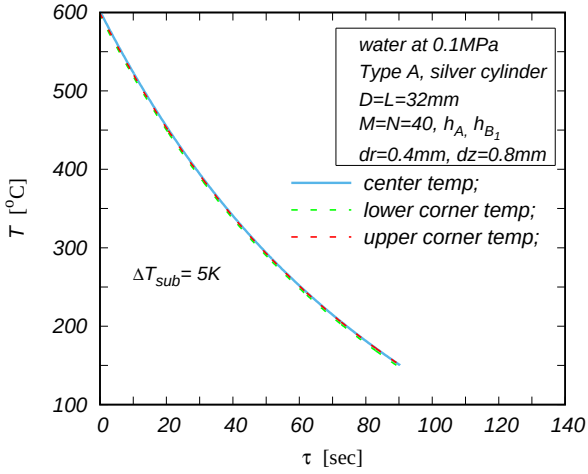

(d) $\Delta T_{sub} = 5$[K]

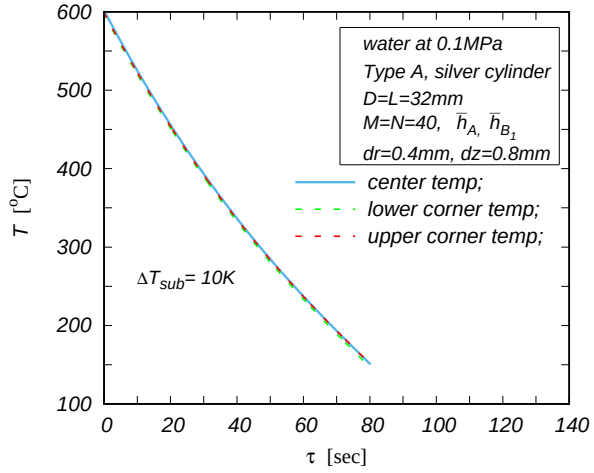

(e) $\Delta T_{sub} = 10$[K]

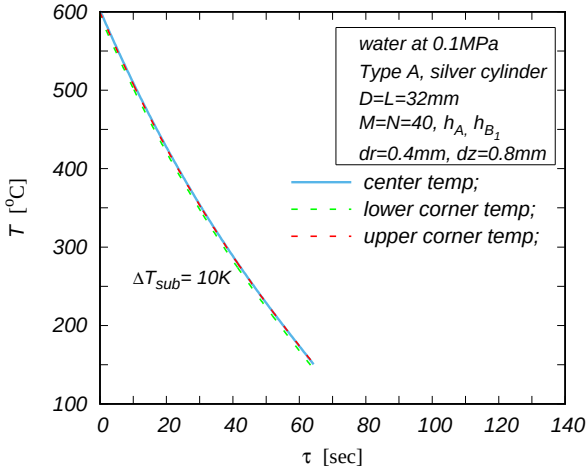

(f) $\Delta T_{sub} = 10$[K]

Fig. 4.13: (a)∼(f) Predicted temperature at the center, upper edge and lower edge of the silver cylinder by using the average heat transfer coefficient in all surfaces and local heat transfer coefficient at bottom and lower vertical surface

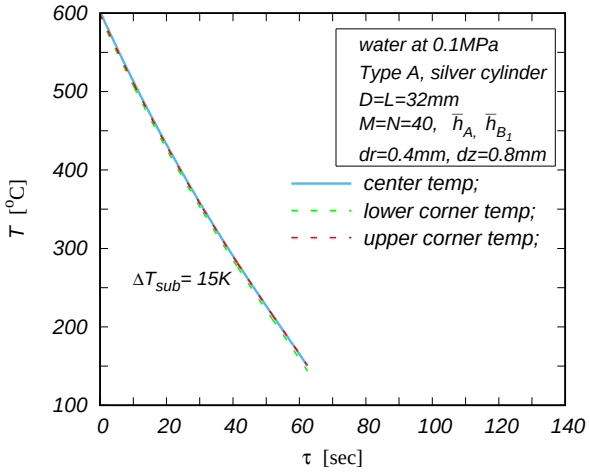

(g) $\Delta T_{sub} = 15$[K]

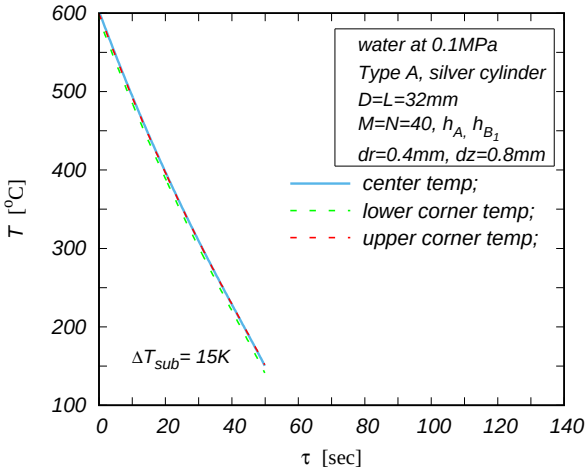

(h) $\Delta T_{sub} = 15$[K]

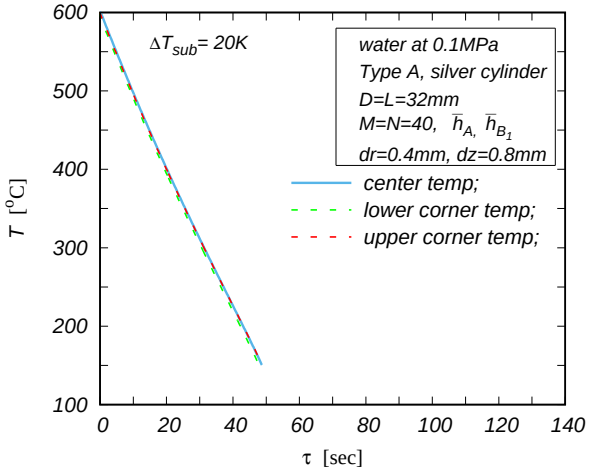

(i) $\Delta T_{sub} = 20$[K]

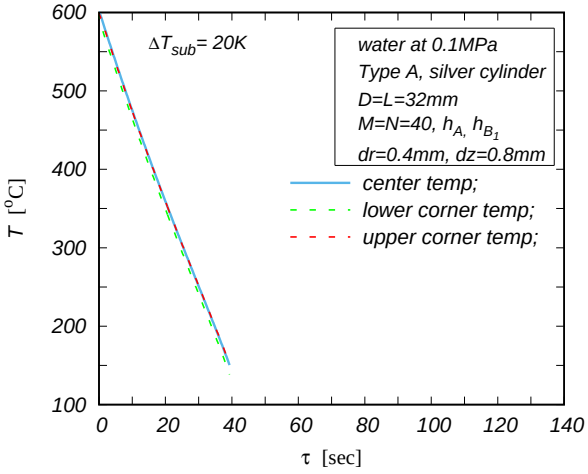

(j) $\Delta T_{sub} = 20$[K]

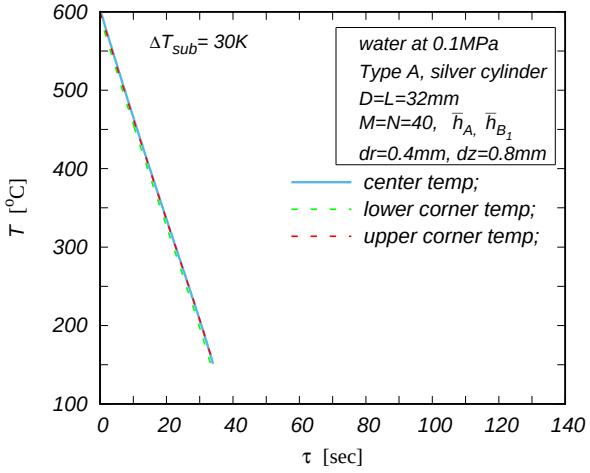

(k) $\Delta T_{sub} = 30$[K]

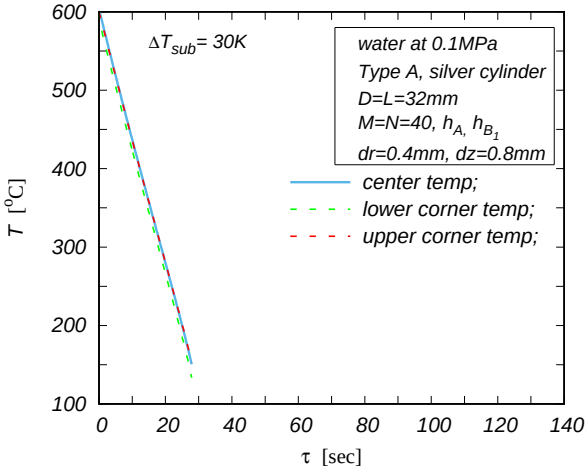

(l) $\Delta T_{sub} = 30$[K]

Fig. 4.13: (g)∼(l) Predicted temperature at the center, upper edge and lower edge of the silver cylinder by using the average heat transfer coefficient in all surfaces and local heat transfer coefficient at bottom and lower vertical surface

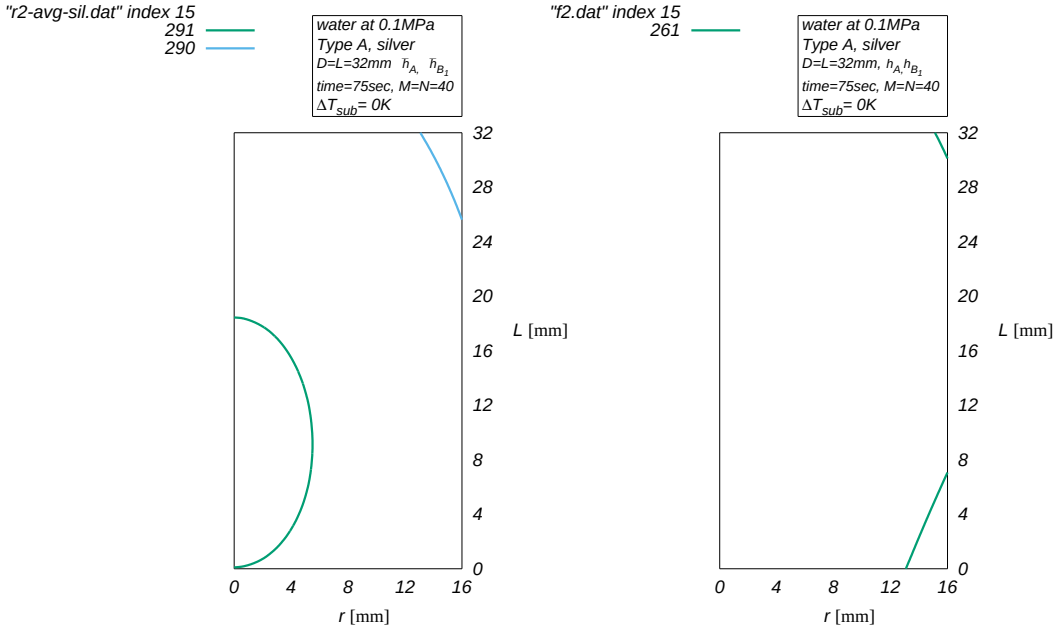

(a) $\tau = 75$[s],$(\overline{h}_A, \overline{h}_{B1})$ (b) $\tau = 75$[s],$(\ h_A, h_{B1})$

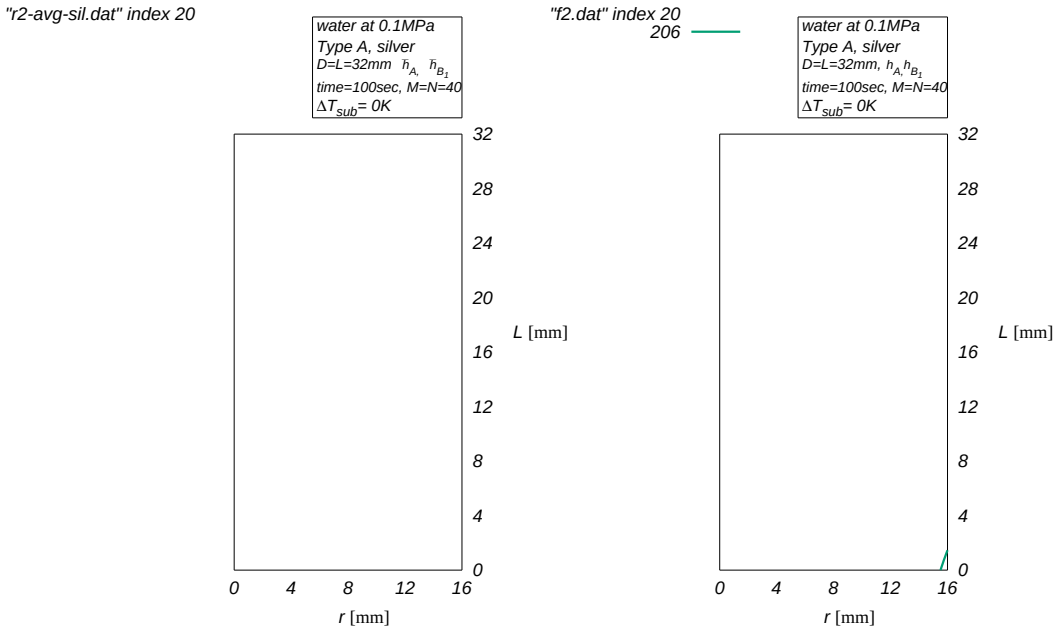

(c) $\tau = 100$[s],$(\overline{h}_A, \overline{h}_{B1})$ (d) $\tau = 100$[s],$(\ h_A, h_{B1})$

Fig. 4.14: (a)∼(d) Predicted temperature distribution of the silver cylinder by average and local heat transfer coefficient at bottom and vertical surface $\Delta T_{sub} = 0K$ (τ=75 and 100 sec)

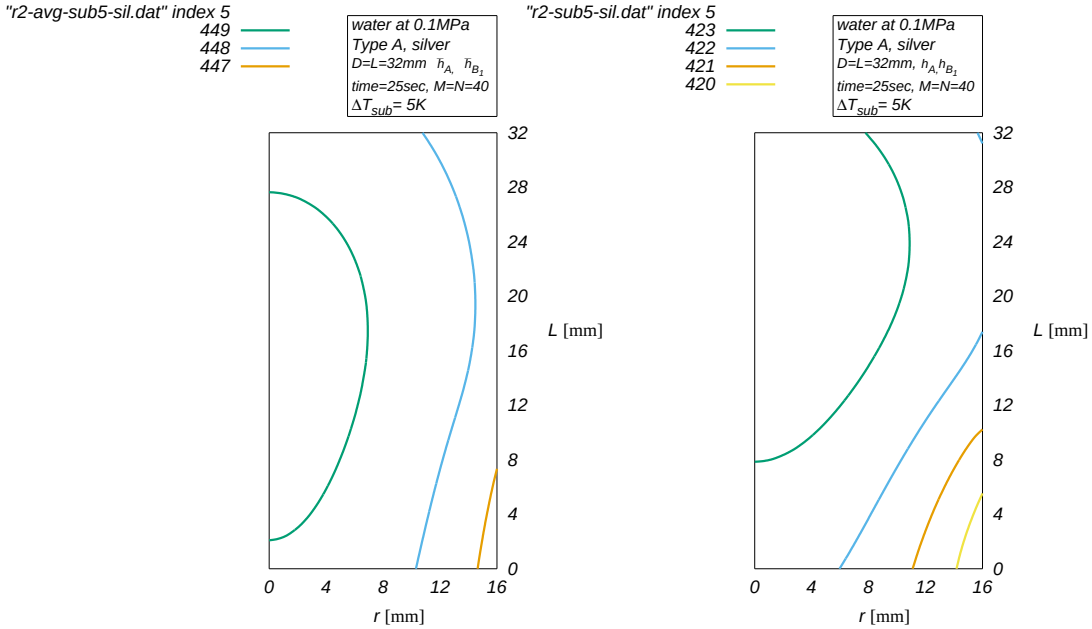

(a) $\tau = 25$[s],($\overline{h}_A$,$\overline{h}_{B1}$) (b) $\tau = 25$[s],(h_A,h_{B1})

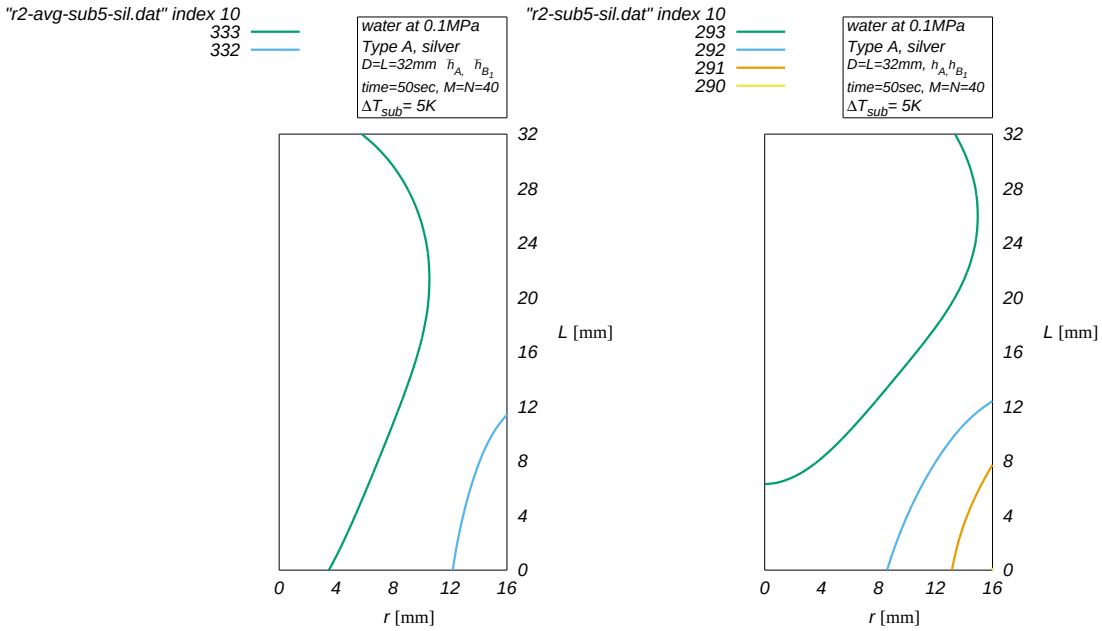

(c) $\tau = 50$[s],($\overline{h}_A$,$\overline{h}_{B1}$) (d) $\tau = 50$[s],(h_A,h_{B1})

Fig. 4.15: (a)∼(d) Predicted temperature distribution of the silver cylinder with average and local heat transfer coefficient at bottom and vertical surface for the $\Delta T_{sub} = 5K$ (τ=25 and 50 sec)

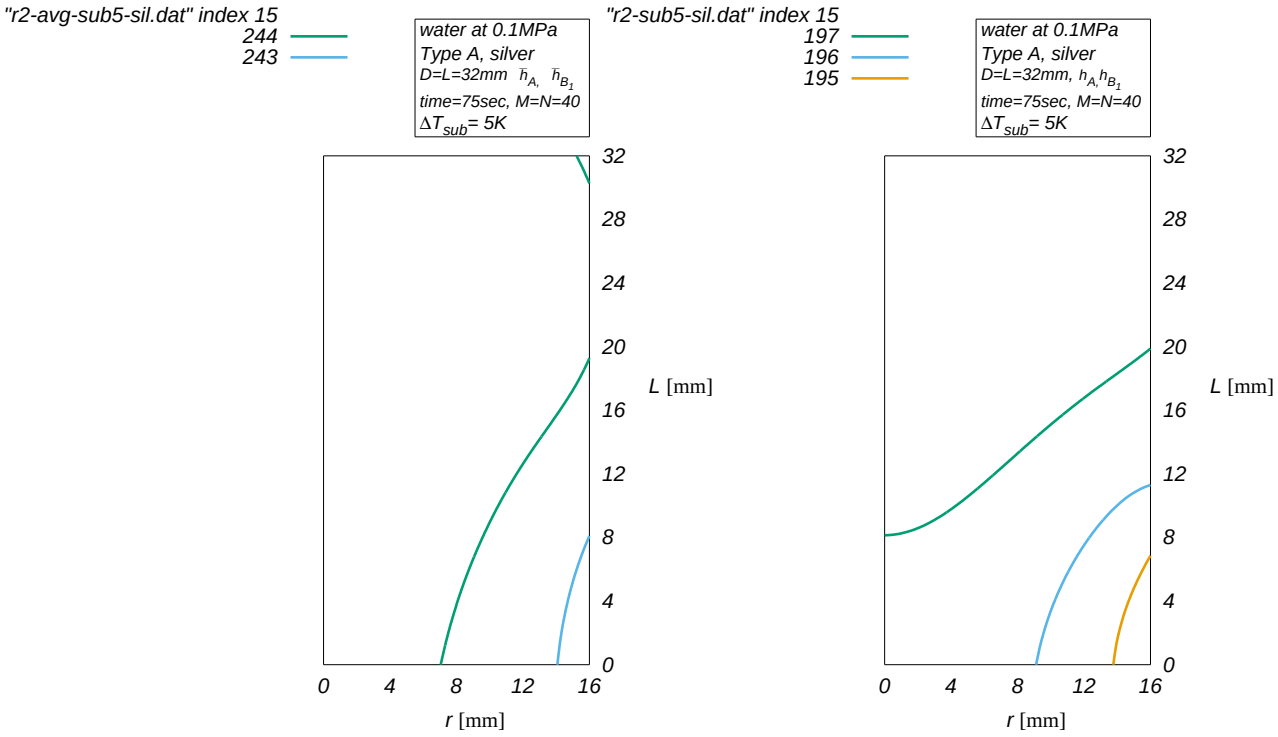

(e) $\tau = 75$[s],($\overline{h}_A$,$\overline{h}_{B1}$)

(f) $\tau = 75$[s],(h_A,h_{B1})

Fig. 4.15: (e)∼(f) Predicted temperature distribution of the silver cylinder with average and local heat transfer coefficient at bottom and vertical surface at $\Delta T_{sub} = 5K$ (τ=75 sec)

For the subcooled degree of ΔT_{sub}=5K, the temperature contour at the time in cooling process are described as after 25sec, 50sec and 75sec. In subcooled degree of ΔT_{sub}=5K, the lower limit of film boiling is about 65 sec and the temperature distribution near the lower limit are shown in Fig. 4.13. The difference in temperature distribution with the average and local heat transfer coefficient are compared as in Fig. 4.13 for the cooling process at 25 sec,(a), (b) for the cooling process at 50 sec, (c), (d) and for the cooling process at 75 sec,(e),(f). For the subcooling film boiling with the degree of subcooling, ΔT_{sub}=5 [K], the lowest temperature point is at the lower corner of the vertical finite-length cylinder in both prediction with average and local heat transfer coefficient but differ in temperature difference between lower corner temperature and upper corner temperature. Temperature prediction with local heat transfer rate give lower temperature difference between these two points in subcooled film boiling.

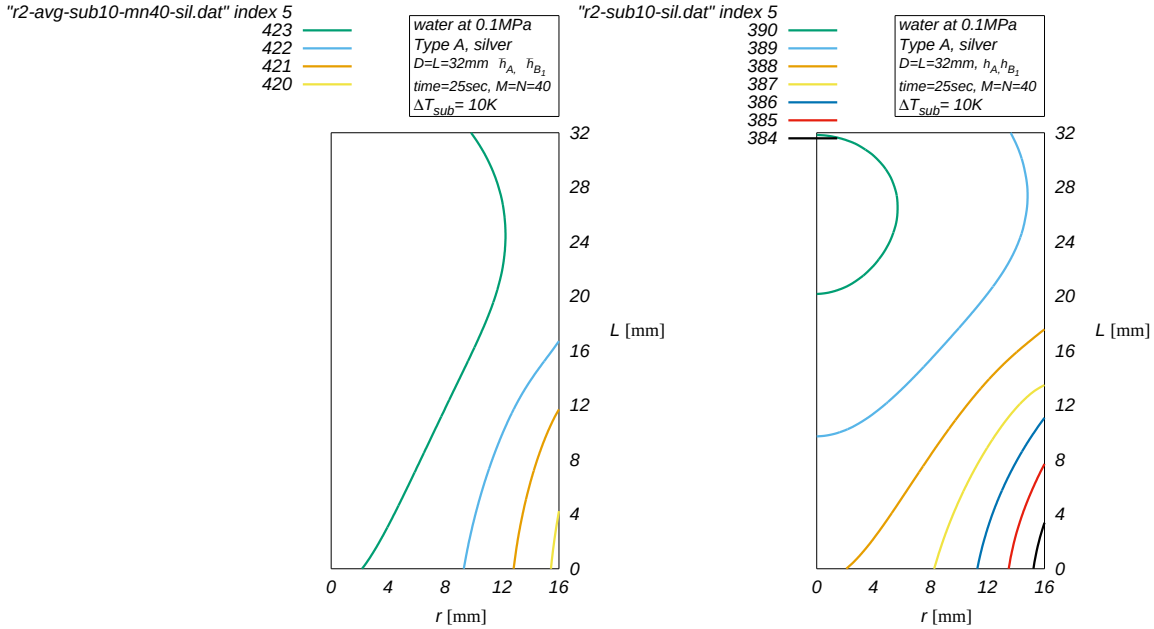

(a) $\tau = 25$[s],($\overline{h}_A$,$\overline{h}_{B1}$) (b) $\tau = 25$[s],(h_A,h_{B1})

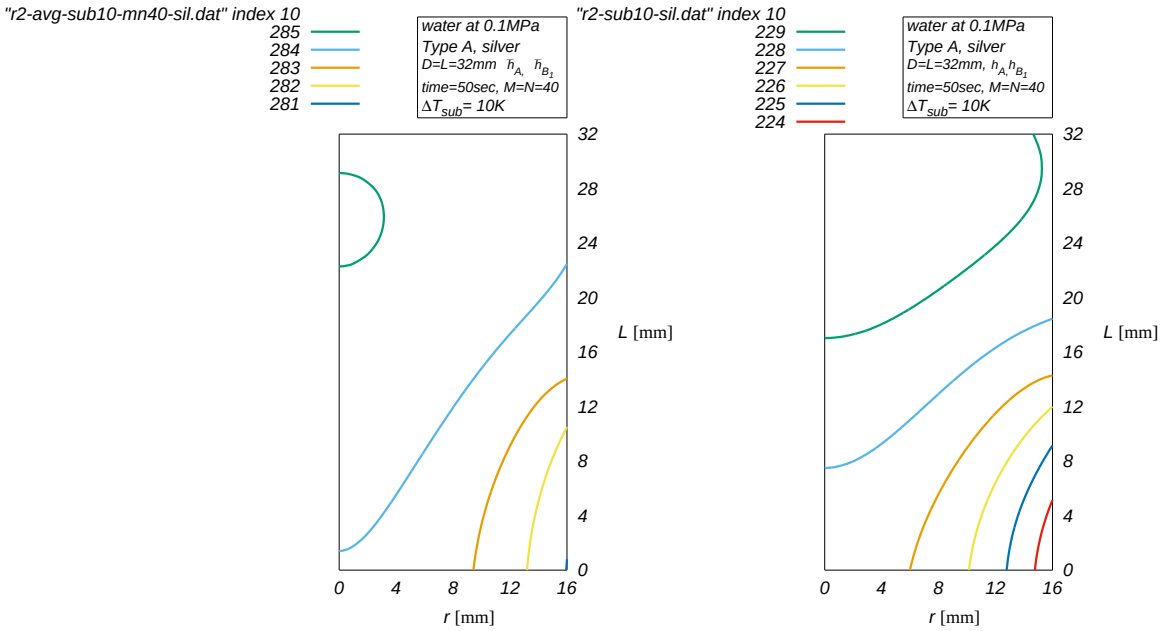

(c) $\tau = 50$[s],($\overline{h}_A$,$\overline{h}_{B1}$) (d) $\tau = 50$[s],(h_A,h_{B1})

Fig. 4.16: (a)∼(d) Predicted temperature distribution of the silver cylinder with average and local heat transfer coefficient at bottom and vertical surface for the $\Delta T_{sub} = 10K$ (τ=25 and 50 sec)

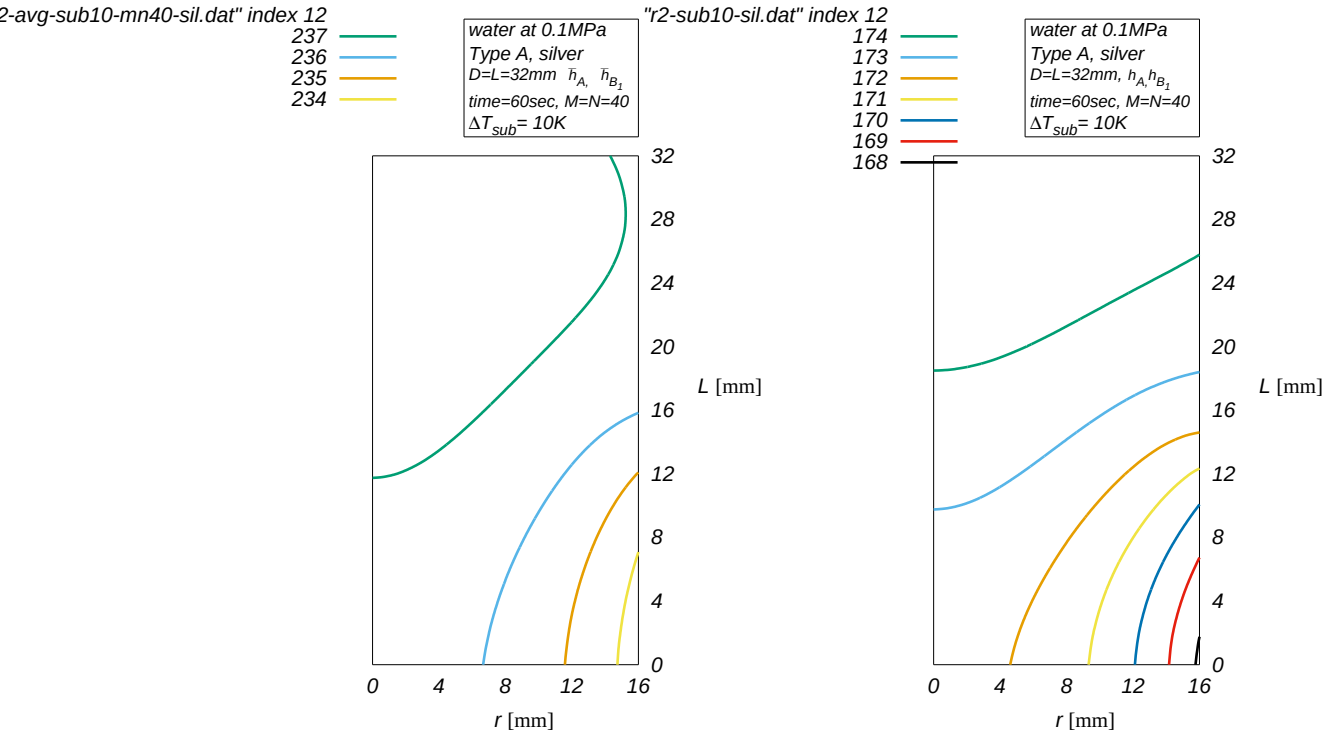

(e) $\tau = 60$[s],($\overline{h}_A$,$\overline{h}_{B1}$)

(f) $\tau = 60$[s],(h_A,h_{B1})

Fig. 4.16: (e)∼(f) Predicted temperature distribution of the silver cylinder with average and local heat transfer coefficient at bottom and vertical surface at $\Delta T_{sub} = 10$ K (τ=60 sec)

For the subcooled degree of ΔT_{sub}=10K, the temperature contour at the time in cooling process are described as after 25sec, 50sec and 60sec. In subcooled degree of ΔT_{sub}=10K, the lower limit of film boiling is about 40 sec and the temperature distribution near the lower limit are shown in Fig. 4.14. The difference in temperature distribution with the average and local heat transfer coefficient are compared as in Fig. 4.14 for the cooling process at 25 sec,(a), (b) for the cooling process at 50 sec, (c), (d) and for the cooling process at 60 sec,(e),(f). For the subcooling film boiling with the degree of subcooling, ΔT_{sub}=10 [K], the lowest temperature point is at the lower corner of the vertical finite-length cylinder in both prediction with average and local heat transfer coefficient but differ in temperature difference between lower corner temperature and upper corner temperature. Temperature prediction with local heat transfer rate give lower temperature difference between these two points in subcooled film boiling.

For the subcooled degree of ΔT_{sub}=15K, the temperature contour at the time in cooling process are described as after 25sec and 45sec. In subcooled degree of ΔT_{sub}=15K, the

lower limit of film boiling is about 30 sec and the temperature distribution near the lower limit are shown in Fig.4.15.

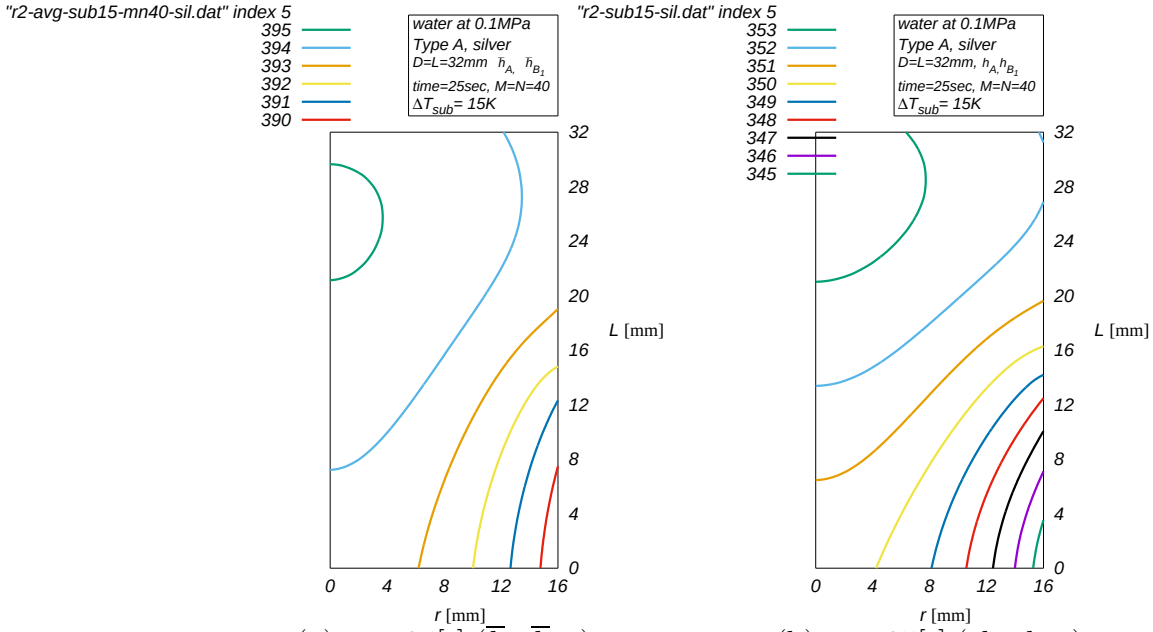

(a) $\tau = 25$[s],($\overline{h}_A$,$\overline{h}_{B1}$) (b) $\tau = 25$[s],(h_A,h_{B1})

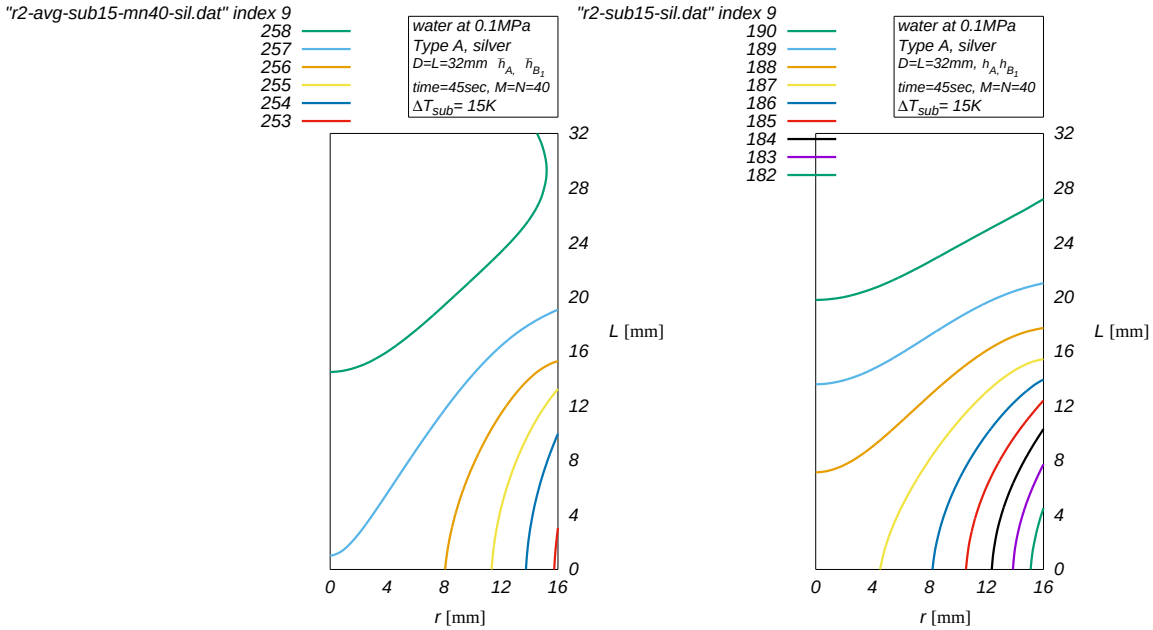

(c) $\tau = 45$[s],($\overline{h}_A$,$\overline{h}_{B1}$) (d) $\tau = 45$[s],(h_A,h_{B1})

Fig. 4.17: (a)∼(d) Predicted temperature distribution of the silver cylinder with average and local heat transfer coefficient at bottom and vertical surface for the $\Delta T_{sub} = 15K$ (τ=25 and 45 sec)

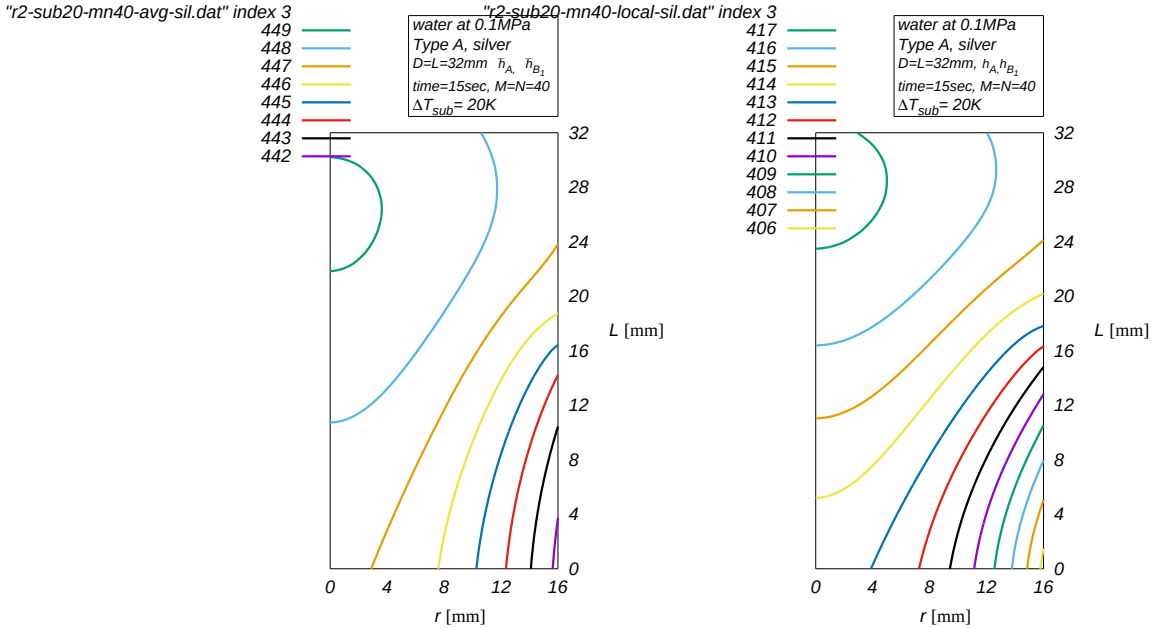

(a) $\tau = 15$[s],($\overline{h}_A$,$\overline{h}_{B1}$) (b) $\tau = 15$[s],(h_A,h_{B1})

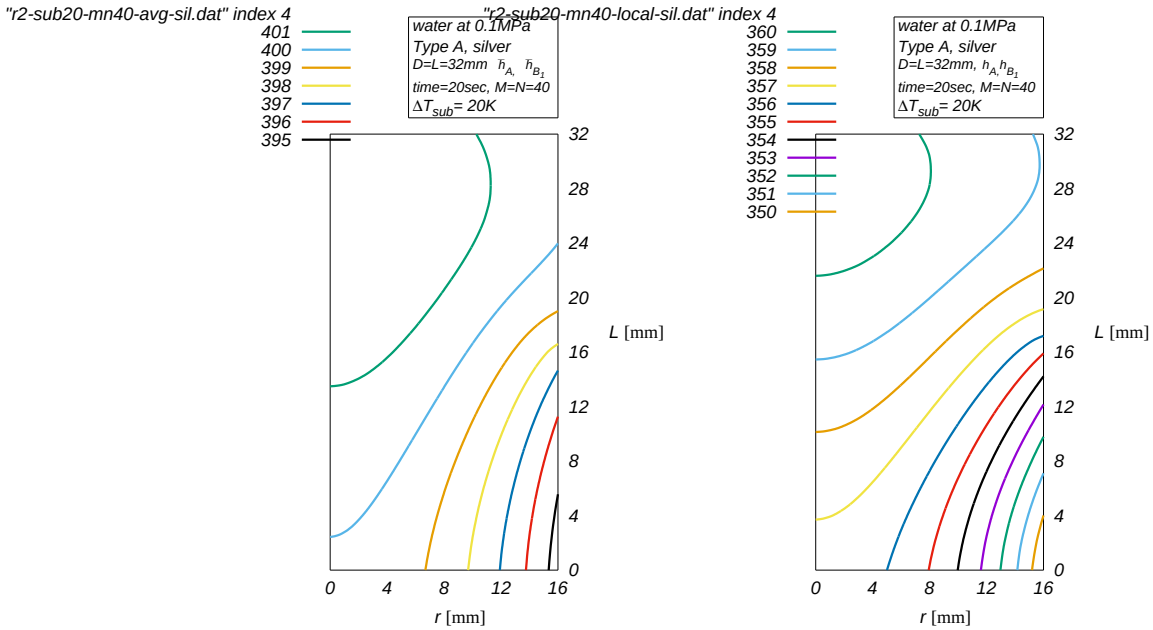

(c) $\tau = 20$[s],($\overline{h}_A$,$\overline{h}_{B1}$) (d) $\tau = 20$[s],(h_A,h_{B1})

Fig. 4.18: (a)∼(d) Predicted temperature distribution of the silver cylinder with average and local heat transfer coefficient at bottom and vertical surface for the $\Delta T_{sub} = 20K$ (τ=15 and 20 sec)

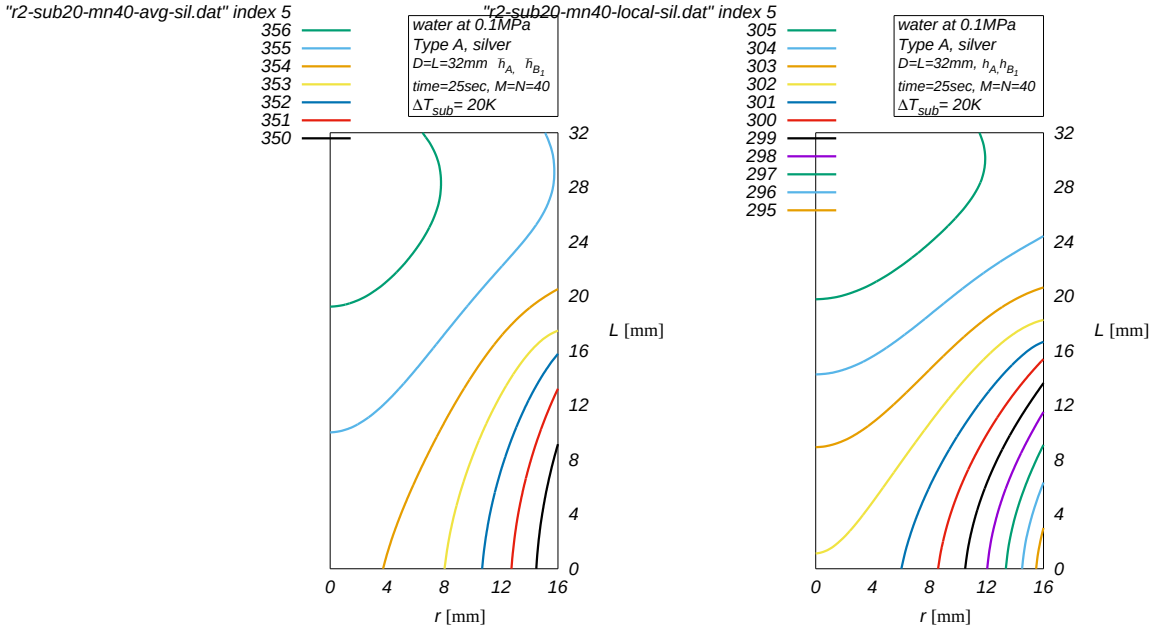

(e) $\tau = 25$[s],($\overline{h}_A$,$\overline{h}_{B1}$)

(f) $\tau = 25$[s],(h_A,h_{B1})

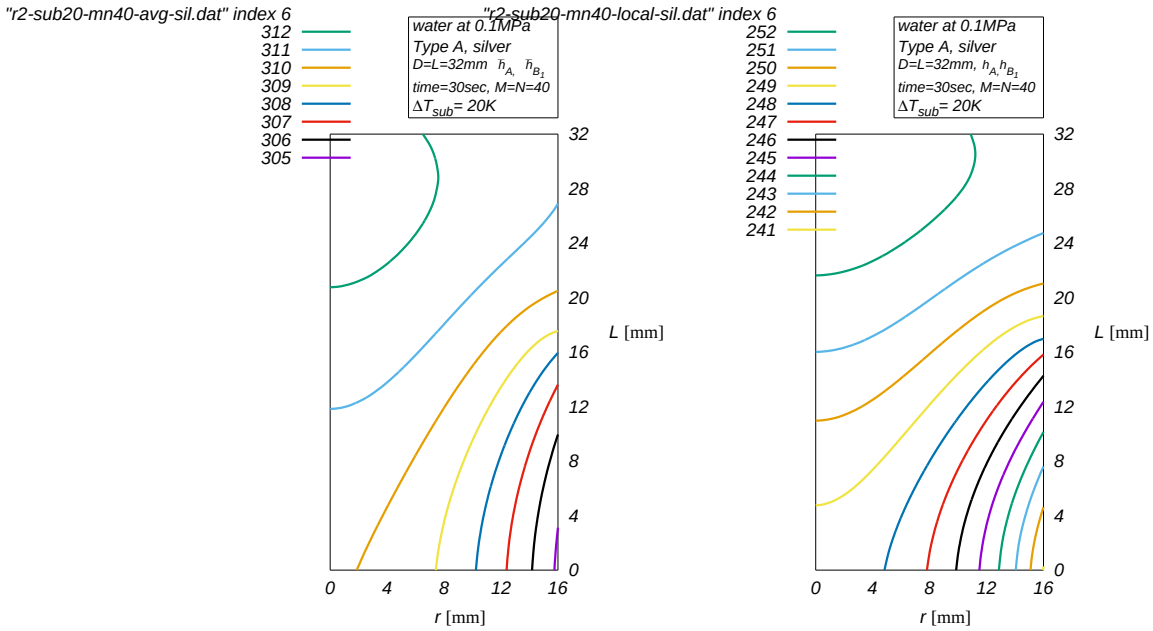

(g) $\tau = 30$[s],($\overline{h}_A$,$\overline{h}_{B1}$)

(h) $\tau = 30$[s],(h_A,h_{B1})

Fig. 4.18: (e)∼(h) Predicted temperature distribution of the silver cylinder with average and local heat transfer coefficient at bottom and vertical surface for the $\Delta T_{sub} = 20K$ (τ=25 and 30 sec)

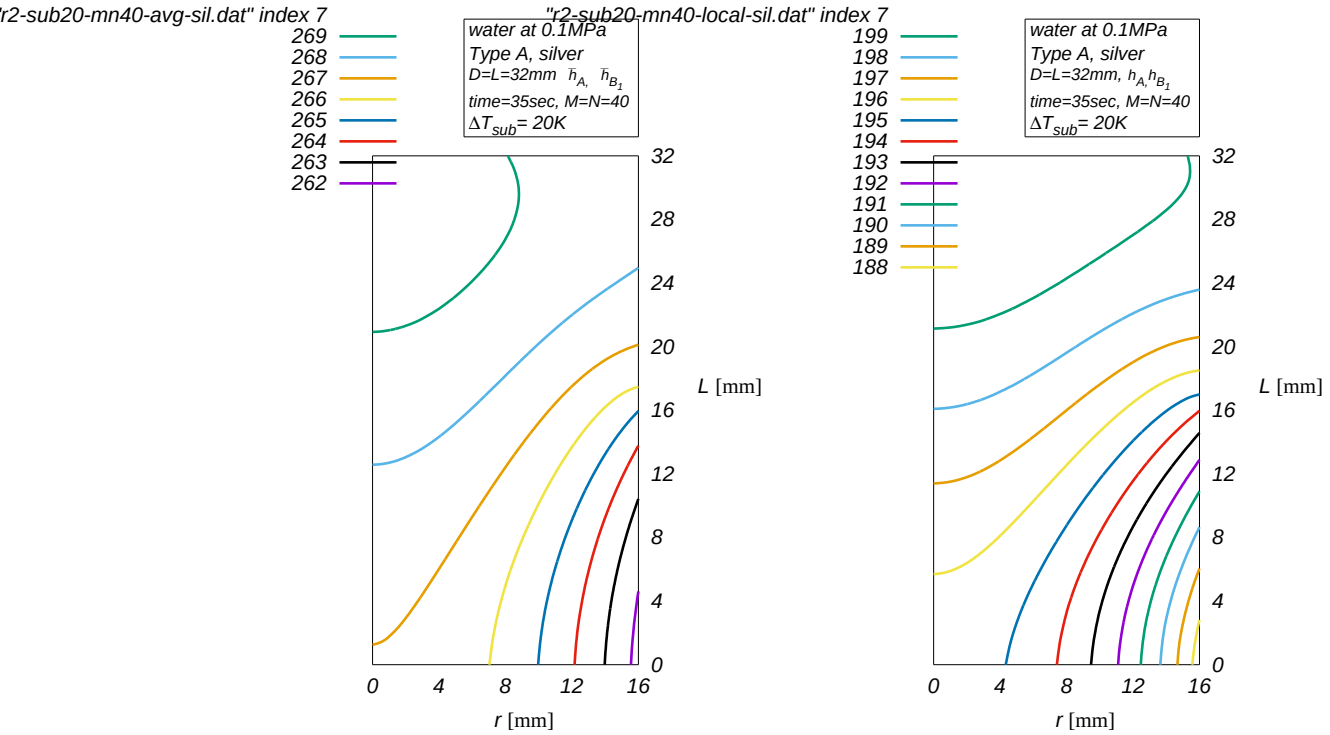

(i) $\tau = 35$[s],($\overline{h}_A$,$\overline{h}_{B1}$)

(j) $\tau = 35$[s],(h_A,h_{B1})

Fig. 4.18: (i)∼(j) Predicted temperature distribution of the silver cylinder with average and local heat transfer coefficient at bottom and vertical surface at $\Delta T_{sub} = 20K$ (τ=35 sec)

For the subcooled degree of ΔT_{sub}=20K, the temperature contour at the time in cooling process are described as after 15sec, 20sec, 25sec, 30sec and 35sec. In subcooled degree of ΔT_{sub}=20K, the lower limit of film boiling is about 20 sec and the temperature distribution near the lower limit are shown in Fig. 4.16. The difference in temperature distribution with the average and local heat transfer coefficient are compared as in Fig. 4.16 for the cooling process at 15 sec,(a), (b) for the cooling process at 20 sec, (c), (d) and for the cooling process at 25sec,(e),(f). For the subcooling film boiling with the degree of subcooling, ΔT_{sub}=20 [K], the lowest temperature point is at the lower corner of the vertical finite-length cylinder in both prediction with average and local heat transfer coefficient but differ in temperature difference between lower corner temperature and upper corner temperature. Temperature prediction with local heat transfer rate give lower temperature difference between these two points in subcooled film boiling.

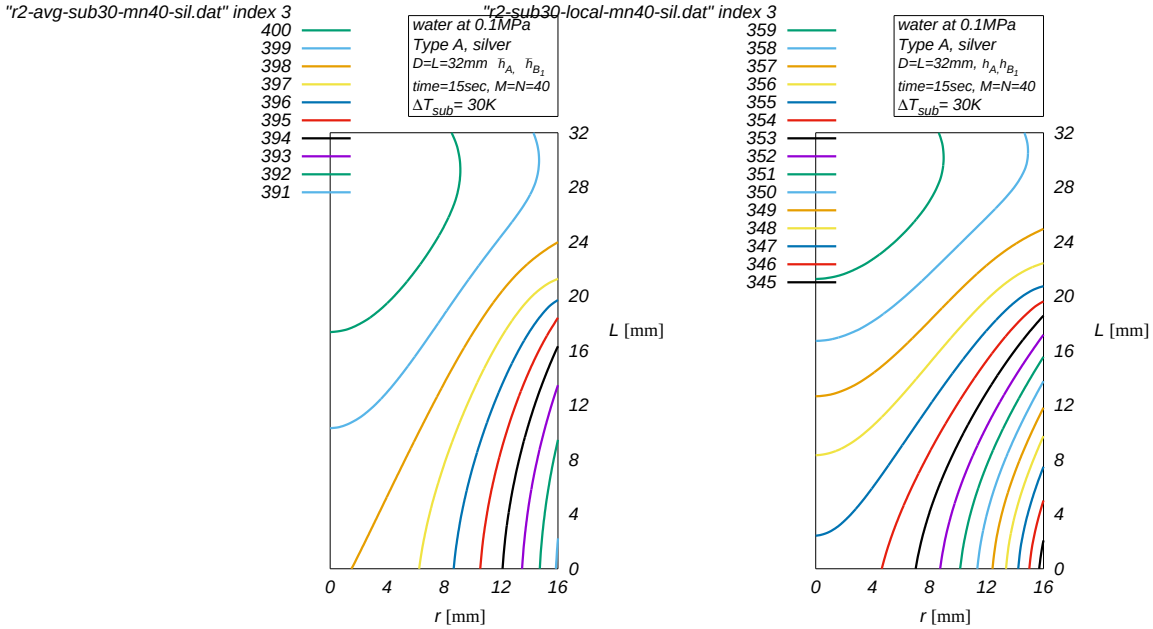

(a) $\tau = 15$[s],($\overline{h}_A$,$\overline{h}_{B1}$) (b) $\tau = 15$[s],(h_A,h_{B1})

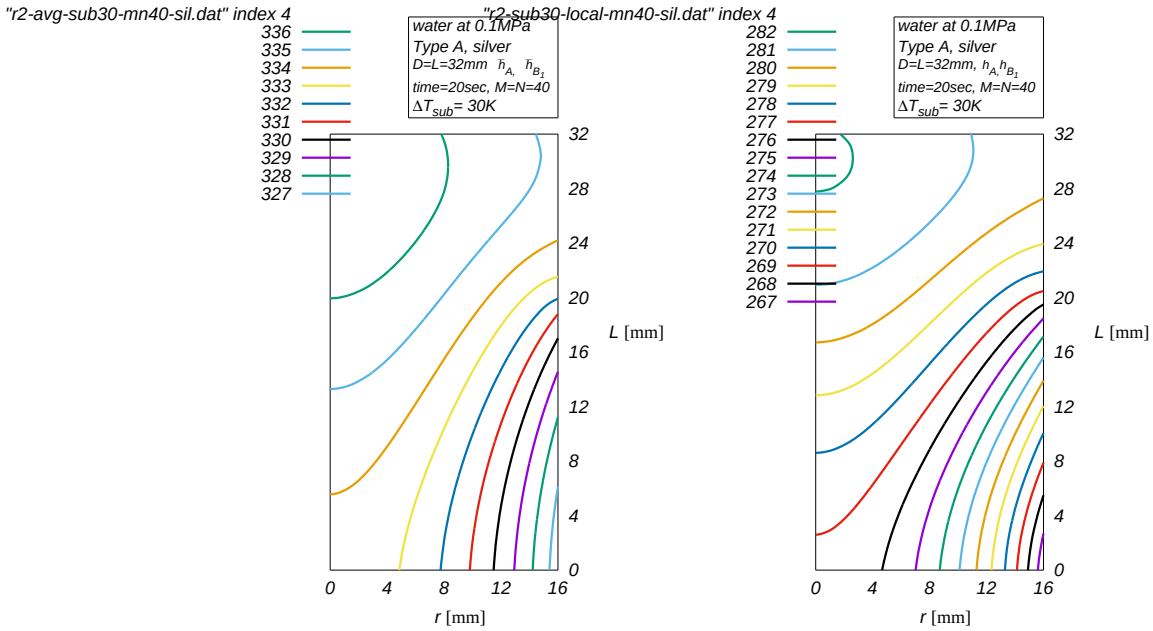

(c) $\tau = 20$[s],($\overline{h}_A$,$\overline{h}_{B1}$) (d) $\tau = 20$[s],(h_A,h_{B1})

Fig. 4.19: (a)∼(d) Predicted temperature distribution of the silver cylinder with average and local heat transfer coefficient at bottom and vertical surface for the $\Delta T_{sub} = 30K$ (τ=15 and 20 sec)

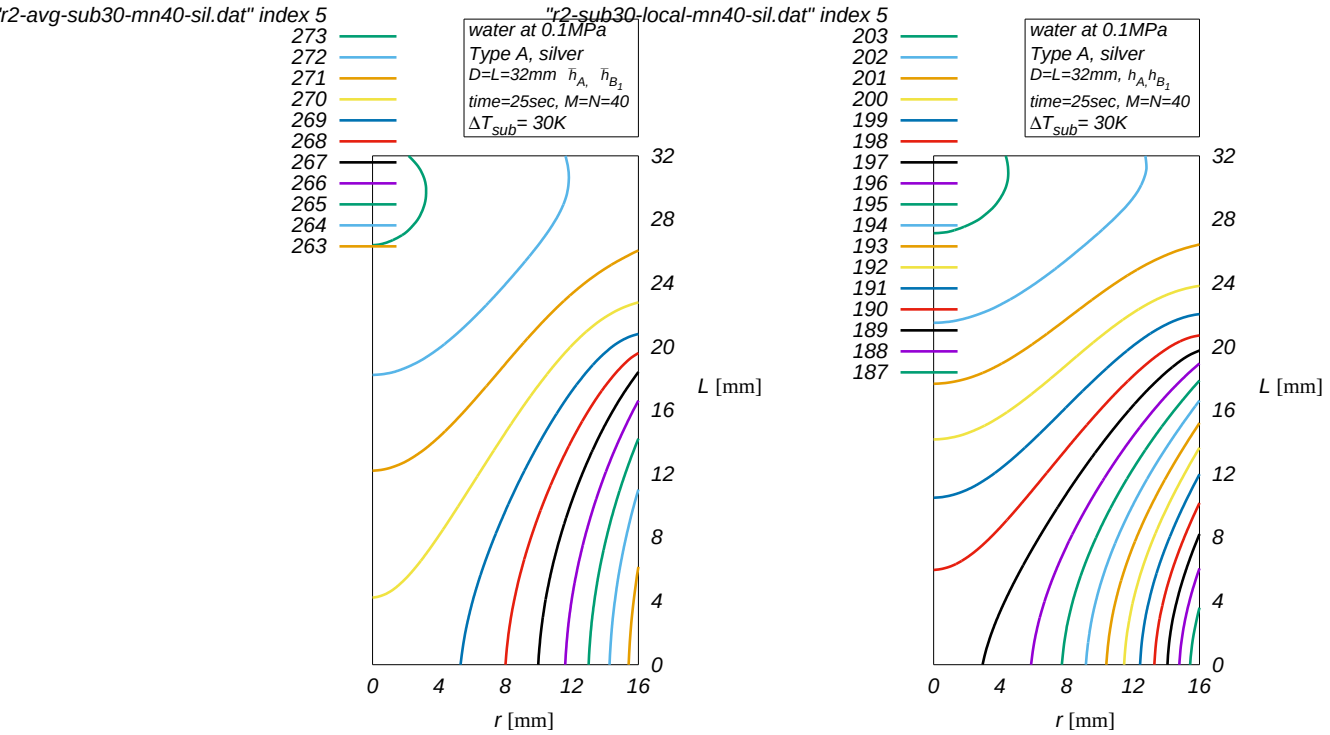

(e) $\tau = 25$[s],($\overline{h}_A$,$\overline{h}_{B1}$)

(f) $\tau = 25$[s],(h_A,h_{B1})

Fig. 4.19: (e)∼(f) Predicted temperature distribution of the silver cylinder with average and local heat transfer coefficient at bottom and vertical surface at $\Delta T_{sub} = 30K$ (τ=25 sec)

For the subcooled degree of ΔT_{sub}=30K, the temperature contour at the time in cooling process are described as after 15sec, 20sec and 25sec. In subcooled degree of ΔT_{sub}=30K, the lower limit of film boiling is about 10 sec and the temperature distribution near the lower limit are shown in Fig. 4.17. The difference in temperature distribution with the average and local heat transfer coefficient are compared as in Fig. 4.17 for the cooling process at 15 sec,(a), (b) for the cooling process at 20 sec, (c), (d) and for the cooling process at 25sec,(e),(f). For the subcooling film boiling with the degree of subcooling, ΔT_{sub}=30 [K], the lowest temperature point is at the lower corner of the vertical finite-length cylinder in both prediction with average and local heat transfer coefficient but differ in temperature difference between lower corner temperature and upper corner temperature. Temperature prediction with local heat transfer rate give lower temperature difference between these two points in subcooled film boiling.

Chapter 5

Conclusion

5.1 Conclusion and Recommendation

This thesis concern about the prediction of local heat transfer rate through the bottom surface and vertical lateral surface of the vertical finite-length cylinder at saturated and subcooled film boiling condition of water at atmospheric pressure and discuss the highest local heat transfer point with the film collapse. The heat transfer coefficient at the lower corner of the bottom surface and vertical lateral surface of the vertical cylinder are predicted at saturated condition by modification of the Shigechi et al. (1999) analysis. The present modification shows the result of average heat transfer rate through each surface of the vertical cylinder coincide with the predicted one's by Shigechi et al. Moreover, it was found that the local heat transfer coefficients at the end of downward facing bottom surface gives finite value to discuss the local heat transfer performance at the lower corner of the cylinder and the resultants local heat transfer rate the lower end of the vertical surface gives maximum value over the entire area of the cylinder surface and in good agreement with the experimental result of the vapor film collapse start at the corner of the vertical cylinder.

It can be concluded like that,

(1) Previous experimental study on film boiling heat transfer by quenching method, it was already confirmed that lower limit of film boiling and experimental average heat transfer rate through the vertical finite-length cylinder agreed ±15% with the predicted total heat transfer rate of the cylinder by taking into account the average heat transfer rate through bottom, vertical lateral and upper surfaces of the cylinder. These experimental results and correlations are also in this present study.

(2) The previous author already predicted the average heat transfer rate on each surface of the vertical cylinder and temperature distribution of the vertical finite-length cylinder is already treated as the two dimensional unsteady heat conduction problem and

the boundary condition at the cylinder surfaces are given by the average heat transfer coefficients on their respective surfaces. As the the average heat transfer coefficient of the downward facing horizontal surface, $\overline{h}_A$, is less than half of other three heat transfer coefficients, $\overline{h}_{B1}$, $\overline{h}_{B2}$ and $\overline{h}_C$, and the value of vertical lateral surface with smooth vapor-liquid interface, $\overline{h}_{B1}$, is smaller than both, $\overline{h}_{B2}$ and $\overline{h}_C$. It suggested that the lowest temperature point was at the upper corner of the vertical cylinder and contrary to experimental observation on vapor film collapse start from the lower corner of the vertical silver cylinder.

(3) In this study, local heat transfer performance at the lower corner of the vertical cylinder is area of interest and on the other hand, the confirmation of the vapor film collapse start from the lower corner of the vertical finite-length cylinder of silver is experimentally done by investigation the cooling rate near the lower limit, solid-liquid contacts on the cylinder wall etc.

(4) To predict local heat transfer coefficient at the corner of the horizontal bottom surface and vertical lateral surface with smooth vapor-liquid interface, the boundary condition for the physical model for the horizontal bottom surface is modified. Modification results on the position of the boundary condition at the horizontal bottom surface can give the vapor film thickness at the end of the bottom surface to be a finite value to predict local heat transfer coefficient at the end.

(5) Firestly, modification results are compared by prediction the vapor film thickness and average and local Nusselt number on the horizontal bottom surface with the previous method and modified method.

(6) For the subcooling case, in order to predict and and investigate the local heat transfer coefficients on the horizontal and vertical lateral srface, for each surfaces we applied the average enhancement factor by the liquid subcooling to the estimated local values by the method by the methods for saturated film boiling.

(7) Comparison of the experimental results on average heat flux over the entire surface of the cylinder with the average heat flux predicted by taking into account the predicted average heat transfer by the modified method shows $\pm$ 15% as the comparison of the previous author. Moreover, the local heat transfer coefficient at the lower end of the vertical cylinder can be predicted.

(8) The value of the local heat transfer coefficient at the lower corner of the bottom and vertical later surfaces give the highest value than any other surfaces of the cylinder and its consistent with the vapor film collapse start from the lower corner of the vertical finite-length cylinder of silver in saturated and subcooled film boiling heat transsfer.

(9) Finally, the temperautre distribution of the vertical silver cylinder with diameter and length of 32mm is treated as the two dimensional unsteady heat conduction problem and the boundary condition at the cylinder surfaces are given by the local heat transfer

coefficients on their respective grid. As the value of local heat transfer coefficient of the downward facing horizontal surface, h_A and those of vertical lateral surface with smooth vapor-liquid interface, h_{B1}, are the highest, its suggeste that the lowest temperature point was at the lower corner of the vertical cylinder and agreed to experimental observation on vapor film collapse start from the lower corner of the vertical silver cylinder.

5.2 Further Study

For the further study, the temperature distribution of the cylinder with low thermal conductivity material such as stainless steel should be predicted by the unsteady heat conduction numerical calculation. More experimental investigation about the film collapse with different approach should be treated. The more analysis on surface temperature distribution are required with the numerical simulation.

Acknowledgments

Firstly the author wishes to epress her deep appreciation to her supervisor Professor Satoru Momoki who give me the opportunity to do the research work on Thermal and Multi-phase Energy Laboratory at Nagasaki University. The author also would like to thank for his kindness, understanding, giving helpful guidance through discusions, suggestions and encouragement throughout the research. Special thanks are due to our laboratory members, Noguchi, Kubota, Kumura, Daiichi, Egawa, Nishimura and Noda for their help and supporting during the experiment. The authors appreciate the partial support of this effort by a co-operative Research Program of IOES, Institute of Ocean Energy, Saga University, Acceptance Number 17A07 and JICA EEHE project. Moreover, the candidate also sincerely thankful to her Board of Examiner, Professor Sakaguchi Daisaku and Associate Professor Tomohiko Yamaguchi for their helpful comments and valuable suggestions to improve the thesis. Furthermore, the author would like to express her deep gratitude to her teachers who taught her everthing from childhood till now. And also the most intensive debt of thanks goes to her parents and her husband for their mental support, encouragement and patient throughout the study. Finally, the author sincerely wishes to thank all persons who helped directly or indirectly towards the successful completion of the study, without them study in Nagasaki University will not be meaningful.

References

[1] Araki, K., Momoki, S., Shigechi, T., Yamada, T., Yamaguchi, T. and Toyoda, K., 2010, Cooling rate in the film boiling region for vertical metal cylinders of finite-length, Proceedings of the 21^st International Symposium on Transport Phenomena, 2010.

[2] Berenson, P.J., 1961, Film boiling heat transfer from a horizontal surface, Transactions of ASME, Journal of Heat Transfer, Vol.83, pp.351-358.

[3] Bromely, L.A., 1950, Heat transfer in stable film boiling, Chemical engineering Progress, Vol.46, No.5, pp.221-227.

[4] Dhir, V.K. and Purohit. G.P., 1978, Subcooled film boiling heat transfer from spheres, Nuclear Engineering and Design, Vol.47, Issue 1, pp.49-66.

[5] Hamill, T.D. and Baumeister, K.J., 1967, Effect of subcooling and radiation on film boiling heat transfer from a flat plate, National Aeronautics and Space Administration, TN D-3925, pp.1-39.

[6] Kumura, M., Momoki, S., Todaka, D., and Egawa, K., 2015, Observation of solid-liquid contact during subcooled film boiling cooling around vertical silver cylinder with different bottom shape, Proceedings of the 52^{nd} National Heat Transfer Symposium, 52^{nd}NHTS(2015-6) No. SP303. (in Japanese)

[7] Lienhard, J. H., and Wong, P.T.Y., 1963, The dominant unstable wavelength and minimum heat flux during film boiling on a horizontal cylinder, Journal of Heat Transfer, Transactions of the ASME, Paper No. 63 -HT-3.

[8] Momoki, S., Shigechi, T., Yamada, T., Kanemaru, K., 1995, Effect of liquid subcooling on the film boiling heat transfer from a finite-size horizontal plate facing downward, Proceedings of the 6^{th} ASME-JSME Thermal Engineering Conference, Volume 2, ASME 1995.

[9] Momoki, S., Yamada, T., Shigechi, T., Nakano, A. and Yamaguchi, T., 2003, Prediction of the cooling rate for a finite-size vertical cylinder in the film boiling region,

Proceedings of the 6^{th} ASME-JSME Thermal Engineering Joint Conference, AJTEC 2003, p.302.

[10] Momoki, S., Koutoku, K., Shigechi, T., Yamada, T., Yamaguchi, T., and Kanemaru, K., 2005, Experimental study on effect of the material thermophysical properties upon quench point in transient film boiling around a vertical cylinder, Journal of Thermal Science and Engineering, Vol.13 No.4, p-13-14.

[11] Momoki, S., Yamada, T., Shigechi, T., Kanemaru, K. and Yamaguchi, T., 2007, Film boiling around a vertical cylinder with top and bottom horizontal surfaces, Proceedings of the 2007 ASME-JSME Thermal Engineering Summer Heat Transfer Conference, HT2007-32733.

[12] Momoki, S., Yamada, T., Shigechi, T., Ohkouchi, S. and Toyoda, K., 2008, Solid-liquid contact characteristics during saturated pool film boiling cooling of vertical cylinders with various bottom surface configuration, Proceedings of the 2008 Mechanical Engineering Congress, 2008 Japan, MECJ-08, No. 08-1, p-3,4. (in Japanese)

[13] Momoki, S., Shigechi, T., Yamada, T., Yamaguchi, T. and Toyoda, K., 2011, Effect of the bottom and top configuration on pool film boiling around a vertical finite-length cylinder, Proceedings of the ASME/JSME 2011 8^th Thermal Engineering Joint Conference, AJTEC2011, AJTEC2011-44122.

[14] Momoki, S., Shigechi, T., Yamada, T., Yamaguchi, T. and Toyoda, K., 2011, Effect of the bottom configuration on film boiling heat transfer from a vertical finite-length cylinder, Proceedings of the 19^th International Conference on Nuclear Engineering, ICONE19-43320.

[15] Momoki, S., Shigechi, T., Yamada, T., Yamaguchi, T. and Toyoda, K., 2012, Effect of the bottom and top configurations of a vertical finite-length cylinder on the lower limit of film boiling, Proceedings of the 3^rd International Forum on Heat Transfer, paper No.127.

[16] Momoki, S., Pa Pa Myo, W. and Yamaguchi, T., 2017, Consideration of heat transfer performance and the collapse point of vapor film in the saturated transient film boiling around a finite-length vertical cylinder, Proceedings of the 54^{th} National Heat Transfer Symposium, 54^{th}NHTS(2017-5) No. F112.

[17] Nishikawa, K., Ito, T., Matsumoto, K. and Kuroki, T., 1975, A correlation of pool film boiling heat transfer from a horizontal cylinder of uniform surface temperature to subcooled liquids, Technology Reports of Kyushu University, Vol.48, No.6, pp.815-821. (in Japanese)

[18] Nishio, S., A fundamental study on liquid-solid contact process in Leidenfrost system, Report of the Institute of Industrial Science , The University of Tokyo, Vol.28, No.6, 1980. (in Japanese)

[19] Nishio, S., Prediction technique for minimum-heat-flux(MHF)-point condition of saturated pool boiling, International Journal of Heat and Mass Transfer, Vol.30, No.10,pp. 2045-2057, 1987.

[20] Nishio, S., Uemura, M., and Sakaguchi, K., Film boiling heat transfer and minimum-heat-flux(MHF)-point condition in subcooled pool boiling, JSME International Journal, Vol.30, No.266, 1987.

[21] Nishio, S., Chanderatilleke G.R., and Ozu, T., Natural-Convection film- boiling heat transfer (Saturated film boiling with long vapor film), JSME International Journal, Series II, Vol.34, No.2, 1991.

[22] Nishio, S. and Ohatake, H., 1992, Natural-Convection film boiling heat transfer (6^{th} Report: Heat transfer correlation of film boiling with wavy interface), Transactions of Japanese Society of Mechanical Engineers, Vol.58, No.554, B, pp.3161-3166. (in Japanese)

[23] Nukiyama, S., The maximum and minium values of heat Q transmitted from metal to boiling water under atmospreric pressure, International Journal of Heat and Mass transfer, Vol.9, pp.1419-1433.

[24] Pa Pa Myo, W., Momoki, S. and Yamaguchi, T., 2016, Study on the collapse point of vapor film in the transient film boiling around the finite-length vertical cylinders with various geometries, Proceedings of the 53^{rd} National Heat Transfer Symposium, 53^{rd} NHTS (2016-5), No. J211.

[25] Pa Pa Myo, W., Momoki, S. and Yamaguchi, T., 2016, Effect of local heat transfer coefficient on lower limit of saturated film boiling of finite length vertical cylinder, Proceedings of the 4^{th} International Forum on Heat Transfer, IFHT2016, IFHT2016-2044.

[26] Pa Pa Myo, W., Momoki, S. and Yamaguchi, T., 2017, Modification on prediction method of heat transfer coefficient from a vertical-finite-length cylinder in saturated film boiling to discuss local heat transfer performance near the lower corner, Journal of Thermal Science and Technology, Vol.13, No.1, 2018.

[27] Pa Pa Myo, W., Momoki, S. and Yamaguchi, T., 2017, Correlations of film boiling heat transfer around a vertical-finite-length cylinder with top and bottom horizontal surfaces, Already submitted to the Journal of Thermal Science and Technology.

[28] Shigechi, T., Kawae, N., Tokita, Y.and Yamada, T., 1989, Film boiling heat transfer from a horizontal circular plate facing downward, JSME International Journal, Vol.32, No.4, pp.646-651.

[29] Shigechi, T., Tokita,Y., Yamada, T., Momoki, S., and Kanemaru, K., An analysis on convective heat transfer of film boiling from a finite-size horizontal plate facing downward, International Journal of Fluid Mechanics Research, Vol.25, No.s 103, 1998. ISSN 1064-2285

[30] Shigechi, T., Y.and Yamada, T., Momoki, S., Kanemaru, K. and Yamaguchi, T., 1999, Effect of horizontal bottom surface on film boiling heat transfer from a vertical cylinder, Proceedings of the 5^{th} ASME/JSME Thermal Engineering Joint conference, CD-ROM.

[31] Yamada, T., Shigechi, T., Momoki, S., Kanemaru, K. and Yamaguchi, T., 1998, Effect of liquid subcooling on film boiling heat transfer from finite-size horizontal surfaces facing downward, Trans, Jpn. soc. Mech. Eng., Vol. 64, No. 628, B, pp.4159-4165 (in Japanese).

[32] Yamada, T., Shigechi, T., Momoki, S. and Kanemaru, 2000, Film boiling heat transfer around a vertical finite-length cylinder, Proceedings of the 4^{th} JSME/KSME Thermal Engineering Conference, pp.427-432.

[33] Yamada, T., Shigechi, T., Momoki, S. and Kanemaru, 2000, An analysis of film boiling around a vertical finite-length cylinder, Reports of the Faculty of Engineering, Nagasaki Uniersity, Vol.31, No.56.

[34] Yamada, T., Shigechi, T., Momoki, S., Kanemaru, K. and Yamaguchi, T., 2004, Film boiling heat transfer around a vertical finite-length cylinder, Trans, Jpn. soc. Mech. Eng., Vol. 70, No. 695, B, pp.1762-1768 (in Japanese).

Appendices

Table. 5.1: Vapor film thickness at the bottom and vertical surface of the cylinder (D=L=32mm) at $\Delta T_{sat} = 300K$ during film boiling

Case	ΔT_{sat}[K]	$\tilde{\delta}_{\mathrm{A},0}$ [-]	$\tilde{r}_E$ [-]	$\int_0^{1/2} \left(\tilde{r}/\tilde{\delta}_A\right) d\tilde{r}$	$\tilde{\delta}_{\mathrm{B},0}$	$\delta_{\mathrm{B},0}$ [mm]
Ans-Bns	500	1.2750	0.5071	0.1232	1.0460	0.2269
	400	1.2741	0.5062	0.1237	1.0369	0.1973
	300	1.2732	0.5052	0.1242	1.0132	0.1677
	200	1.2722	0.5043	0.1248	0.9996	0.1373
Ans-Bs	500	1.2724	0.5045	0.1247	0.6589	0.1433
	400	1.2718	0.5039	0.1251	0.6532	0.1247
	300	1.2712	0.5033	0.1255	0.6400	0.1060
	200	1.2706	0.5027	0.1259	0.6325	0.0867
As-Bns	500	0.9668	0.5078	0.1622	1.14725	0.2482
	400	0.9660	0.5068	0.1628	1.1373	0.2163
	300	0.9652	0.5057	0.1636	1.1080	0.1838
	200	0.9645	0.5047	0.1644	1.0983	0.1504
As-Bs	500	0.9646	0.5050	0.1642	0.7142	0.1571
	400	0.9642	0.5043	0.1647	0.7164	0.1367
	300	0.9636	0.5036	0.1653	0.6745	0.1162
	200	0.9631	0.5030	0.1659	0.6619	0.0949

Table. 5.2: Vapor film thickness at the bottom and vertical surface of the cylinder for the different diameter at $\Delta T_{\rm sat}$ =300K

Case	D[mm]]	$\tilde{\delta}_{\rm A,0}$ [-]	$\tilde{r}_E$ [-]	$\int_0^{1/2}\left(\tilde{r}/\tilde{\delta}_A\right)d\tilde{r}$	$\delta_{\rm B,0}$ [mm]
Ans-Bns	8	1.2835	0.5156	0.11958	0.1248
	10	1.2810	0.5131	0.1205	0.1311
	15	1.2780	0.5096	0.1220	0.1439
	32	1.2732	0.5052	0.1242	0.1677
	45	1.2718	0.5039	0.1251	0.1755
	50	1.2716	0.5037	0.1252	0.1840

Table. 5.3: Average heat transfer coefficients on each surface of the vertical cylinder

Case Ans-Bns (D=L=32mm)						
ΔT_{sat} [K]	Lower-Surface		Vertical-Surface			Upper-Surface
	$\overline{h}_{A,sat}$ (Yamada)	$\overline{h}_{A,sat}$ (Present)	$\overline{h}_{B1,sat}$ (Yamada)	$\overline{h}_{B1,sat}$ (Present)	$\overline{h}_{B2,sat}$ W/(m^2.K)	$\overline{h}_{C,sat}$ W/(m^2.K)
150	86.656	83.409	199.955	200.857	210.124	205.623
200	84.643	81.471	190.016	190.777	204.363	196.083
250	83.687	80.551	183.543	184.509	201.088	189.968
300	83.347	80.224	179.085	180.106	199.289	185.846
350	83.402	80.277	175.922	176.986	198.456	183.004
400	83.727	80.589	173.649	174.580	198.299	181.040
450	84.245	81.088	172.013	173.191	198.635	179.706
500	84.905	81.723	170.855	171.963	199.348	178.842

Table 4. (A) Physical properties of the test cylinders

Material	Interpolated Equ.(Applicable range: $0 < T < 600$ [°C])
silver(pure)	$\rho_{\mathrm{m}} = 10501.7 - 0.586T - 0.134\times10^{-3}T^2$ $c_{\mathrm{m}} = 232.865 + 0.0267T + 2.641\times10^{-5}T^2$ $k_{\mathrm{m}} = 408.52 - 0.0633T - 1.590\times10^{-5}T^2$
silver(ordinary)	$\rho_{\mathrm{m}} = 8904.3 - 0.218\mathrm{T} - 0.00033T^2$ $c_{\mathrm{m}} = 415.528 + 0.1559T - 4.232\times10^{-5}T^2$ $k_{\mathrm{m}} = 372.94 - 0.0408T - 1.777\times10^{-5}T^2$
Aluminium(ordinary)	$\rho_{\mathrm{m}} = 2702.4 - 0.11T - 0.00015T^2$ $c_{\mathrm{m}} = 891.863 + 0.4143T + 9.915\times10^{-5}T^2$ $k_{\mathrm{m}} = 203.29 + 0.0122T - 7.461\times10^{-5}T^2$
carbon steel(S35C)	$\rho_{\mathrm{m}} = 7858.1 - 0.3T$ $c_{\mathrm{m}} = 456.602 + 0.3139T$ $k_{\mathrm{m}} = 43.418 - 0.0147T - 2.867\times10^{-5}T^2$
carbon steel(S45C)	$\rho_{\mathrm{m}} = 7855.7 - 0.208T - 0.00017T^2$ $c_{\mathrm{m}} = 469.699 + 0.1088T + 0.0005T^2$ $k_{\mathrm{m}} = 51.919 - 0.0148T - 2.633\times10^{-5}T^2$
stainless steel(SUS304)	$\rho_{\mathrm{m}} = 7930.6 - 0.332T - 9.54774\times10^{-5}T^2$ $c_{\mathrm{m}} = 495.721 + 0.0941T + 0.0003T^2$ $k_{\mathrm{m}} = 15.813 + 0.0043T + 1.608\times10^{-5}T^2$

Table. 5.4: (B) The value of dimensionless vapor film thickness at the bottom surface of the cylinder (D=L=32mm) used to predict local heat transfer coefficient and local temperature distribution

$\tilde{r}_E$ [-]	$\tilde{\delta}_{A,0}$ [-]	ϕ	$\tilde{r}_E$ [-]	$\tilde{\delta}_{A,0}$ [-]	ϕ
0.0000	1.271200900	0.0000000	0.2625	1.181684338	-0.7773943
0.0125	1.271021590	-0.0287163	0.2750	1.171587751	-0.8388792
0.0250	1.270482639	-0.0575372	0.2875	1.160690184	-0.9056915
0.0375	1.269582445	-0.0865298	0.3000	1.148919395	-0.9787676
0.0500	1.268318313	-0.1157823	0.3125	1.136190092	-1.0592699
0.0625	1.266686425	-0.1453861	0.3250	1.122400661	-1.1486623
0.0750	1.264681801	-0.1754362	0.3375	1.107428771	-1.2488168
0.0875	1.262298241	-0.2060332	0.3500	1.091125350	-1.3621714
0.1000	1.259528248	-0.2372840	0.3625	1.073306144	-1.4919661
0.1125	1.256362938	-0.2693037	0.3750	1.053739562	-1.6426107
0.1250	1.252791933	-0.3022170	0.3875	1.032128654	-1.8202779
0.1375	1.248803222	-0.3361605	0.4000	1.008083391	-2.0339042
0.1500	1.244383001	-0.3712850	0.4125	0.981076098	-2.2969706
0.1625	1.239515480	-0.4077581	0.4250	0.950365849	-2.6308910
0.1750	1.234182650	-0.4457678	0.4375	0.914861057	-3.0720282
0.1875	1.228364000	-0.4855269	0.4500	0.872846101	-3.6879430
0.2000	1.222036185	-0.5272774	0.4625	0.821365059	-4.6213975
0.2125	1.215172616	-0.5712973	0.4750	0.754546402	-6.2415068
0.2250	1.207742963	-0.6179085	0.4875	0.657311693	-9.9377775
0.2375	1.199712550	-0.6674865	0.5000	0.450236075	-33.0818316
0.2500	1.191041608	-0.7204734			

Table. 5.5: Local heat transfer coefficients on Horizontal Bottom surface of the vertical cylinder

Local Heat Transfer Coefficient for Horizontal Bottom Surface, $h_{A,sat}$ W/(m^2.K) for Case Ans-Bns (D=L=32mm)				
Radius [mm]	ΔT_{sat} [K]			
	200	300	400	500
0	64.507	63.490	63.750	64.482
0.8	64.544	63.525	63.784	64.518
1.6	64.654	63.634	63.893	64.627
2.4	64.841	63.817	64.076	64.810
3.2	65.107	64.078	64.338	65.071
4.0	65.458	64.423	64.683	65.415
4.8	65.901	64.858	65.119	65.850
5.6	66.447	65.394	65.656	66.385
6.4	67.110	66.044	66.307	67.033
7.2	67.906	66.825	67.089	67.812
8.0	68.861	67.763	68.027	68.745
8.8	70.009	68.888	69.153	69.863
9.6	71.395	70.247	70.512	71.210
10.4	73.088	71.907	72.172	72.851
11.2	75.193	73.968	74.232	74.882
12.0	77.874	76.592	76.852	77.455
12.8	81.423	80.061	80.312	80.832
13.6	86.406	84.923	85.153	85.513
14.4	94.162	92.465	92.637	92.629
15.2	109.193	106.962	106.911	105.679
16.0	191.150	179.257	172.999	151.520

Table. 5.6: Local heat transfer coefficients at the vertical surface with smooth vapor-liquid interface of the vertical cylinder

Local Heat Transfer Coefficient for vertical Surface with smooth vapor-liquid interface, $h_{B1,sat}$ W/(m^2.K) for Case Ans-Bns (D=L=32mm)				
H [mm]	ΔT_{sat} [K]			
	200	300	400	500
0	243.063	228.292	219.903	215.840
0.32	234.33	220.366	212.577	208.818
0.64	226.985	213.649	206.328	202.807
0.96	220.658	207.845	200.902	197.572
1.28	215.124	202.753	196.122	192.951
1.6	210.222	198.229	191.861	188.823
1.92	205.831	194.169	188.027	185.103
2.24	201.864	190.493	184.547	181.722
2.56	198.252	187.141	181.367	178.630
2.88	194.942	184.064	178.444	175.783
3.2	191.890	181.225	175.742	173.150
3.52	189.064	178.592	173.232	170.703
3.84	186.434	176.139	170.893	168.420
4.16	183.977	173.847	168.703	166.281
4.48	181.675	171.697	166.647	164.272
5.12	179.509	169.673	164.710	162.379
5.44	177.467	167.763	162.88	160.590
5.76	175.535	165.956	161.149	158.895
6.08	173.705	164.242	159.505	157.286
6.40	171.966	162.613	157.942	155.756
6.72	170.311	161.478	156.843	154.297
7.04	168.732	159.582	155.031	152.904
7.36	167.225	158.168	153.672	151.572
7.68	165.782	156.814	152.370	150.296
8.00	164.399	155.516	151.121	149.071

Table. 5.7: Temperature distribution at the surface of the cylinder for Saturated Condition

Calculation Condition						
Average Heat Transfer Coefficient on each surface of the cylinder ΔT_{sub}=0K D=32mm, L=32mm M=20, L=20 Δr=0.8, Δz=1.6, Δt=0.001				Local Heat Transfer Coefficient at the bottom and lower vertical surface ΔT_{sub}=0K D=32mm, L=32mm M=20, L=20 Δr=0.8, Δz=1.6, Δt=0.001		
Time[sec]	Center Temp; [°C]	Lower Corner Temp; [°C]	Upper Corner Temp; [°C]	Center Temp; [°C]	Lower Corner Temp; [°C]	Upper Corner Temp; [°C]
0	600.000	600.000	600.000	600.000	600.000	600.000
5	571.172	569.211	567.938	566.693	563.188	563.861
10	542.749	540.915	539.728	534.170	530.927	531.553
15	515.934	514.218	513.111	503.771	500.766	501.349
20	490.630	489.022	487.989	475.353	472.567	473.110
25	466.756	465.248	464.284	448.784	446.198	446.705
30	444.224	442.810	441.908	423.945	421.544	422.018
35	422.964	421.637	420.794	400.722	398.490	398.932
40	402.900	401.654	400.866	379.010	376.935	377.349
45	383.967	382.797	382.059	358.714	356.782	357.170
50	366.104	365.004	364.313	339.738	337.940	338.303
55	349.247	348.213	347.566	322.005	320.332	320.672
60	333.344	332.371	331.766	305.434	303.875	304.193
65	318.344	317.429	316.862	289.949	288.496	288.795
70	304.194	303.334	302.802	275.488	274.135	274.416
75	290.849	290.040	289.542	261.986	260.725	260.988
80	278.269	277.508	277.042	249.380	248.206	248.452
85	266.412	265.696	265.259	237.619	236.526	236.757
90	255.237	254.563	254.154	226.654	225.635	225.853
95	244.707	244.073	243.690	216.433	215.485	215.689
100	234.793	234.196	233.838	206.911	206.029	206.220

Table. 5.8: Temperature distribution at the surface of the cylinder for Saturated Condition

Calculation Condition						
Local Heat Transfer Coefficient at the bottom and lower vertical surface ΔT_{sub}=0K D=32mm, L=32mm M=20, L=20 Δr=0.8, Δz=1.6, Δt=0.0001				Local Heat Transfer Coefficient at the bottom and lower vertical surface ΔT_{sub}=0K D=32mm, L=32mm M=40, L=40 Δr=0.4, Δz=0.8, Δt=0.0001		
Time[sec]	Center Temp; [°C]	Lower Corner Temp; [°C]	Upper Corner Temp; [°C]	Center Temp; [°C]	Lower Corner Temp; [°C]	Upper Corner Temp; [°C]
0	600.000	600.000	600.000	600.000	600.000	600.000
5	566.694	563.188	563.861	566.691	563.194	563.859
10	534.171	530.927	531.553	534.167	530.931	531.549
15	503.772	500.767	501.350	503.765	500.767	501.343
20	475.353	472.567	473.111	475.343	472.564	473.101
25	448.785	446.199	446.706	448.770	446.191	446.692
30	423.946	421.545	422.019	423.927	421.532	421.999
35	400.723	398.491	398.933	400.699	398.472	398.909
40	379.011	376.936	377.350	378.982	376.911	377.321
45	358.715	356.784	357.171	358.680	356.754	357.137
50	339.739	337.942	338.304	339.699	337.906	338.265
55	322.007	320.333	320.673	321.962	320.292	320.629
60	305.435	303.876	304.194	305.385	303.830	304.145
65	289.950	288.498	288.796	289.895	288.446	288.742
70	275.489	274.136	274.417	275.430	274.081	274.358
75	261.987	260.726	260.989	261.923	260.666	260.927
80	249.381	248.207	248.454	249.314	248.142	248.387
85	237.621	236.527	236.758	237.550	236.459	236.688
90	226.655	225.636	225.854	226.581	225.565	225.780
95	216.434	215.486	215.690	216.357	215.411	215.614
100	206.912	206.030	206.221	206.833	205.953	206.143

Table. 5.9: Comparison of temperature distribution at the surface of the cylinder with Average and Local heat transfer coefficient for Saturated Film Boiling

Calculation Condition						
Average Heat Transfer Coefficient on each surface of the cylinder ΔT_{sub}=0K D=32mm, L=32mm M=40, L=40 Δr=0.4, Δz=0.8, Δt=0.0001				Local Heat Transfer Coefficient at the bottom and lower vertical surface ΔT_{sub}=0K D=32mm, L=32mm M=40, L=40 Δr=0.4, Δz=0.8, Δt=0.0001		
Time[sec]	Center Temp; [°C]	Lower Corner Temp; [°C]	Upper Corner Temp; [°C]	Center Temp; [°C]	Lower Corner Temp; [°C]	Upper Corner Temp; [°C]
0	600.000	600.000	600.000	600.000	600.000	600.000
5	571.208	569.254	567.971	566.693	563.188	563.861
10	542.819	540.991	539.796	534.170	530.927	531.553
15	516.033	514.322	513.208	503.771	500.766	501.349
20	490.753	489.149	488.110	475.353	472.567	473.110
25	466.898	465.395	464.424	448.784	446.198	446.705
30	444.382	442.972	442.065	423.945	421.544	422.018
35	423.135	421.811	420.963	400.722	398.490	398.932
40	403.082	401.838	401.045	379.010	376.935	377.349
45	384.156	382.987	382.245	358.714	356.782	357.170
50	366.298	365.200	364.505	339.738	337.940	338.303
55	349.444	348.411	347.761	322.005	320.332	320.672
60	333.542	332.571	331.962	305.434	303.875	304.193
65	318.542	317.628	317.058	289.949	288.496	288.795
70	304.391	303.531	302.997	275.488	274.135	274.416
75	290.043	290.234	289.734	261.986	260.725	260.988
80	278.460	277.699	277.230	249.380	248.206	248.452
85	266.598	265.882	265.443	237.619	236.526	236.757
90	255.418	254.744	254.333	226.581	225.565	225.780
95	244.882	244.248	243.864	216.357	215.411	215.614
100	234.961	234.364	234.005	206.833	205.953	206.143

Table. 5.10: Comparison of temperature distribution at the surface of the cylinder with Average and Local heat transfer coefficient for Subcooled Film Boiling

Calculation Condition						
Average Heat Transfer Coefficient on each surface of the cylinder ΔT_{sub}=5K D=32mm, L=32mm M=40, L=40 Δr=0.4, Δz=0.8, Δt=0.0001				Local Heat Transfer Coefficient at the bottom and lower vertical surface ΔT_{sub}=5K D=32mm, L=32mm M=40, L=40 Δr=0.4, Δz=0.8, Δt=0.0001		
Time[sec]	Center Temp; [°C]	Lower Corner Temp; [°C]	Upper Corner Temp; [°C]	Center Temp; [°C]	Lower Corner Temp; [°C]	Upper Corner Temp; [°C]
0	600.000	600.000	600.000	600.000	600.000	600.000
5	567.173	564.418	564.605	561.392	556.046	558.917
10	535.548	532.495	532.793	523.548	518.492	521.324
15	505.216	502.283	502.685	488.060	483.265	486.065
20	476.504	473.681	474.181	454.771	450.211	452.987
25	449.321	446.599	447.191	423.532	419.185	421.941
30	423.582	420.951	421.632	394.204	390.047	392.792
35	399.201	396.654	397.419	366.662	362.676	365.416
40	376.105	373.633	374.480	340.779	336.947	339.687
45	354.218	351.815	352.740	316.451	312.755	315.503
50	333.471	331.130	332.131	293.563	289.987	292.750
55	313.803	311.517	312.593	272.023	268.553	271.338
60	295.146	292.908	294.059	251.730	248.348	251.166
65	277.477	275.253	274.477	232.594	229.288	232.146
70	260.650	258.492	259.790	214.530	211.281	214.193
75	244.695	242.568	243.941	197.441	194.230	197.213
80	229.540	227.437	228.887	181.241	178.050	181.121
85	215.132	213.047	214.576	165.828	162.626	165.817
90	201.417	199.342	200.956	151.071	147.815	151.174

Table. 5.11: Comparison of temperature distribution at the surface of the cylinder with Average and Local heat transfer coefficient for Subcooled Film Boiling

Calculation Condition						
Average Heat Transfer Coefficient on each surface of the cylinder ΔT_{sub}=10K D=32mm, L=32mm M=40, L=40 Δr=0.4, Δz=0.8, Δt=0.0001				Local Heat Transfer Coefficient at the bottom and lower vertical surface ΔT_{sub}=10K D=32mm, L=32mm M=40, L=40 Δr=0.4, Δz=0.8, Δt=0.0001		
Time[sec]	Center Temp; [°C]	Lower Corner Temp; [°C]	Upper Corner Temp; [°C]	Center Temp; [°C]	Lower Corner Temp; [°C]	Upper Corner Temp; [°C]
0	600.000	600.000	600.000	600.000	600.000	600.000
5	562.414	557.882	559.704	554.402	547.123	552.330
10	525.074	520.683	522.648	509.499	502.542	507.726
15	489.599	485.334	487.437	467.199	460.527	465.702
20	455.882	451.727	453.965	475.353	472.567	473.110
25	423.813	419.756	422.124	389.666	383.455	388.658
30	393.289	389.317	391.814	354.081	348.048	353.294
35	364.218	360.318	362.945	320.387	314.501	319.808
40	336.497	332.655	335.414	288.411	282.635	288.032
45	310.040	306.242	309.139	257.981	252.275	257.797
50	284.745	280.978	284.018	228.896	223.212	228.905
55	260.526	256.772	259.966	200.922	195.186	201.129
60	237.271	233.512	236.876	173.724	167.824	174.147

Table. 5.12: Comparison of temperature distribution at the surface of the cylinder with Average and Local heat transfer coefficient for Subcooled Film Boiling

Calculation Condition						
Average Heat Transfer Coefficient on each surface of the cylinder ΔT_{sub}=15K D=32mm, L=32mm M=40, L=40 Δr=0.4, Δz=0.8, Δt=0.0001				Local Heat Transfer Coefficient at the bottom and lower vertical surface ΔT_{sub}=15K D=32mm, L=32mm M=40, L=40 Δr=0.4, Δz=0.8, Δt=0.0001		
Time[sec]	Center Temp; [°C]	Lower Corner Temp; [°C]	Upper Corner Temp; [°C]	Center Temp; [°C]	Lower Corner Temp; [°C]	Upper Corner Temp; [°C]
0	600.000	600.000	600.000	600.000	600.000	600.000
5	556.564	550.732	554.124	546.872	537.755	545.173
10	513.241	507.558	511.132	494.304	485.538	492.959
15	471.911	466.357	470.110	444.529	436.059	443.510
20	432.439	426.992	430.926	397.306	389.076	396.590
25	394.695	389.332	393.451	352.385	344.338	351.957
30	358.543	353.242	357.556	309.502	301.573	309.352
35	323.838	318.576	323.096	268.347	260.458	268.471
40	290.429	285.173	289.924	228.523	220.553	228.930
45	258.145	252.855	257.874	189.408	181.139	190.131

Table. 5.13: Comparison of temperature distribution at the surface of the cylinder with Average and Local heat transfer coefficient for Subcooled Film Boiling

Calculation Condition						
Average Heat Transfer Coefficient on each surface of the cylinder ΔT_{sub}=20K D=32mm, L=32mm M=40, L=40 Δr=0.4, Δz=0.8, Δt=0.0001				Local Heat Transfer Coefficient at the bottom and lower vertical surface ΔT_{sub}=20K D=32mm, L=32mm M=40, L=40 Δr=0.4, Δz=0.8, Δt=0.0001		
Time[sec]	Center Temp; [°C]	Lower Corner Temp; [°C]	Upper Corner Temp; [°C]	Center Temp; [°C]	Lower Corner Temp; [°C]	Upper Corner Temp; [°C]
0	600.000	600.000	600.000	600.000	600.000	600.000
5	548.911	541.829	546.690	537.489	526.622	536.100
10	497.693	490.768	495.863	475.271	464.782	474.302
15	448.540	441.741	447.076	415.931	405.734	415.354
20	401.267	394.558	400.148	359.101	349.100	358.896
25	355.667	349.006	354.876	304.333	294.409	304.494
30	311.495	304.831	311.022	250.997	240.966	251.536
35	268.434	261.696	268.279	197.981	187.463	198.956

Table. 5.14: Comparison of temperature distribution at the surface of the cylinder with Average and Local heat transfer coefficient for Subcooled Film Boiling

Calculation Condition						
Average Heat Transfer Coefficient on each surface of the cylinder ΔT_{sub}=30K D=32mm, L=32mm M=40, L=40 Δr=0.4, Δz=0.8, Δt=0.0001				Local Heat Transfer Coefficient at the bottom and lower vertical surface ΔT_{sub}=30K D=32mm, L=32mm M=40, L=40 Δr=0.4, Δz=0.8, Δt=0.0001		
Time[sec]	Center Temp; [°C]	Lower Corner Temp; [°C]	Upper Corner Temp; [°C]	Center Temp; [°C]	Lower Corner Temp; [°C]	Upper Corner Temp; [°C]
0	600.000	600.000	600.000	600.000	600.000	600.000
5	533.216	524.039	531.113	518.895	504.999	517.746
10	465.576	456.558	463.987	437.116	423.645	436.555
15	399.807	390.869	398.702	357.826	344.531	357.796
20	335.420	326.457	334.783	279.818	266.367	280.333
25	271.631	262.460	271.466	200.527	186.032	201.699